PERFORMANCE STUDY OF MULTIPLE LINEAR FACET CONCENTRATOR SOLAR DISTILLATION SYSTEM

KOO LI SIN

MASTER OF ENVIRONMENTAL TECHNOLOGY

FACULTY OF ENGINEERING AND GREEN TECHNOLOGY
UNIVERSITI TUNKU ABDUL RAHMAN
APRIL 2023

PERFORMANCE STUDY OF MULTIPLE LINEAR FACET CONCENTRATOR SOLAR DISTILLATION SYSTEM

By

KOO LI SIN

A dissertation submitted to
Faculty of Engineering and Green Technology,
Universiti Tunku Abdul Rahman,
in partial fulfillment of the requirements for the degree of
Master of Environmental Technology
April 2023

ABSTRACT

PERFORMANCE STUDY OF MULTIPLE LINEAR FACET CONCENTRATOR SOLAR DISTILLATION SYSTEM

Koo Li Sin

Addressing water scarcity issues in rural area by solar distillation method is commonly used because of its simple process, fabrication and low energy cost. Low productivity of a conventional solar still encourages many modifications and novel design including pre-heating of inlet water to solar distillation system for higher water yield. This dissertation studies the enhanced performance of solar distillation system with multiple linear facet concentrator. The maximum inlet water temperature of the solar distillation system as pre-heated by multiple linear facet concentrator is up to 80.05^{o}C under the flow rate of 5LPH. It is concluded that the flow rate 5LPH has the highest water yield rate under the inlet water temperature of 70^{o}C to 80^{o}C. The highest water yield efficiency is found to be 45.59% at the flow rate of 3LPH. A mathematical model of the system is developed to simulate the solar distillation system which allows study of the system without on-site experiment, hence reduce the burden and cost of conducting experiment. Under steady state condition, the highest fresh water productivity of 10.45kg for 6 hours constant sun exposure is achieved at the flow rate 5LPH under ambient temperature of 30^{o}C and solar irradiance of 800W/m^{2}.

ACKNOWLEDGEMENTS

I would like to thank everyone who had contributed to the successful completion of this project. I would like to express my sincere gratitude to my project supervisor, Ts. Dr. Tan Ming Hui for his invaluable advice, guidance and his enormous patience throughout the development of the project. Besides, I would also like to express my gratitude to my research collaborator, TECHKEM GROUP and Ir. Dr. Chew Chun Ming for sponsoring this research with research grant project Number: HEAT-WES2535 and giving me an opportunity to conduct research for this project.

Other than that, I would like to thank ChM. Ts. Dr. Tan Kok Weng, the Head of Programme for Master of Environmental Technology who gave me full support on my project. Besides that, great appreciation to all the lecturers and laboratory officers who provide information and guidance through my whole process of developing the research model from data collection till performance analysis.

In addition, I would also like to thank my beloved parent and friends who had helped and given me encouragement, moral support and suggestions that are very helpful and valuable during the project carried out especially Ms. Cheong Phui Theng, Mr. Chin Ching Cheon, Ms. Kathrin and Ms. Woon Xuet Wei.

APPROVAL SHEET

This dissertation entitled "**PERFORMANCE STUDY OF MULTIPLE LINEAR FACET CONCENTRATOR SOLAR DISTILLATION SYSTEM**" was prepared by and submitted as partial fulfillment of the requirements for the degree of Master of Environmental Technology at Universiti Tunku Abdul Rahman.

Approved by:

(Ts. Dr. Tan Ming Hui)
Date: 25th April 2023
Supervisor
Department of Industrial Engineering
Faculty of Engineering and Green Technology
Universiti Tunku Abdul Rahman

FACULTY OF ENGINEERING AND GREEN TECHNOLOGY

UNIVERSITI TUNKU ABDUL RAHMAN

Date: 25th April 2023

SUBMISSION OF DISSERTATION

It is hereby certified that **Koo Li Sin** (ID No: **21AGM06086**) has completed this dissertation entitled "PERFORMANCE STUDY OF MULTIPLE LINEAR FACET CONCENTRATOR SOLAR DISTILLATION SYSTEM" under the supervision of Ts. Dr. Tan Ming Hui (Supervisor) from the Department of Industrial Engineering, Faculty of Engineering and Green Technology.

I understand that University will upload softcopy of my dissertation in pdf format into UTAR Institutional Repository, which may be made accessible to UTAR community and public.

Yours truly,

(*Koo Li Sin*)

DECLARATION

I hereby declare that the dissertation is based on my original work except for quotations and citations which have been duly acknowledged. I also declare that it has not been previously or concurrently submitted for any other degree at UTAR or other institutions.

Name: KOO LI SIN

Date: 25th April 2023

TABLE OF CONTENTS

LIST OF TABLES

LIST OF FIGURES

LIST OF SYMBOLS / ABBREVIATIONS

A_a	Aperture Area, m^2
A_r	Receiver Area, m^2
$c_{p,f}$	Average specific heat capacity of the working fluid
C_c	Geometric concentration
C_o	Optical concentration
ε	Emissivity
G	Solar radiation, W/m^2
G_a	Incident solar radiation to the areas of "aperture", W/m^2
G_r	Incident solar radiation to the areas of "receiver", W/m^2
h_{fg}	latent heat of vaporization
m_f	Working fluid mass flow rate, kg/s
m_p	Productivity or water yield, kg
η	Thermal efficiency, %
P_w	Partial vapor pressure of water at water film, N/m^2
P_{pc}	Partial vapor pressure of water at plastic cover, N/m2
Q	Thermal energy, W
T	Temperature
T_a	Ambient temperature, K
T_b	Temperature of black plate, K
T_m	Mean fluid temperature in the absorber, K
T_{pc}	Temperature of plastic cover, K
T_w	Temperature of water film, K
T_{sky}	Sky Temperature, K
$T_{MLFC,i}$	Water tank temperature, K
$T_{MLFC,o}$	MLFC outlet water temperature, K
$T_{w,in}$	REWART inlet water temperature, K
t	Time of data collection
U	Collector overall heat loss coefficient, $W/m^2.K$
w	Wind speed
θ'_i	Half acceptance angle
σ	Stefan Boltzmann constant

α	Absorptivity
ρ_{pc}	Reflectivity of the plastic cover
CPC	Compound Parabolic Concentrator
CR	Concentration Ratio
ED	Electrodialysis
EDR	Electrodialysis Reversal
ETC	Evacuated-Tube Collector
FPC	Flat Plate Collector
FWY	Freshwater Yield
GHI	Global Irradiance Index
GI	Galvanized Iron
H/D	Humidification-dehumidification
ICS	Integrated collector storage
Low-E	Low emissivity
LPH	Litres per hour
MD	Membrane Distillation
MED	Multi-Effect Distillation
MLFC	Multiple Linear Facet Concentrator
MSF	Multistage Flash Distillation
MVC	Mechanical Vapor Compression
PE	Percentage Error, %
PTC	Parabolic Trough Collector
PV	Photovoltaic
PV/T	Photovoltaic and Thermal Hybrid
REWART	Renewable Energy Water Refine Technology
RO	Reverse Osmosis
SS	Solar Stills
SWH	Solar Water Heater
TDS	Total Dissolved Solids
TEG	Thermoelectric Generator
TISS	Thickness Insensitive Spectrally Selective
TVC	Thermal Vapor Compression
UV	Ultra Violet

LIST OF APPENDICES

CHAPTER 1

INTRODUCTION

1.1 Background

Surface water as well as groundwater are overused due to the enormous water uses in the agricultural, industrial, and residential sectors. Together with the population growth and water contamination issues, this leads to water stress or scarcity which jeopardizes the environmental and ecological systems. To supply safe drinking water, distillation or desalination is employed for fresh water production. Distillation is a method of removing salts or contaminants from unclean water and produce clean freshwater by heating, evaporation, and condensation processes. The simplest example of distillation is the boiling of sea water to produce steam-purified vapor, and it has already been used for thousands year. The common water desalination methods are electro-dialysis, humidification-dehumification, multi-effect distillation, freezing, multistage flash distillation, reverse osmosis, and vapor compression distillation (Tuly et al., 2021). Most of these processes are using electricity from non-renewable energy sources. Solar distillation system is one of sustainable technology widely studied by researcher in order to use as a mean of meeting the water demand, especially in remote areas where there is limited access to freshwater. Solar distillation system uses solar energy to produce clean water from impure water such as salty or brackish water. This method reduces the use of conventional energy sources which also indirectly mitigates the global warming issue associated with fuel-driven energy.

The simplest type of design for solar distillation system is solar still (SS). Figure 1.1 demonstrates the basic structure of a passive solar still and how distilled water is obtained by solar heating, evaporation and condensation (Manchanda and Kumar, 2015). Solar stills are widely used to meet water demand because of its relatively simple technology, low energy consumption as well as experienced labour for maintenance work is not required (Tuly et al., 2021).

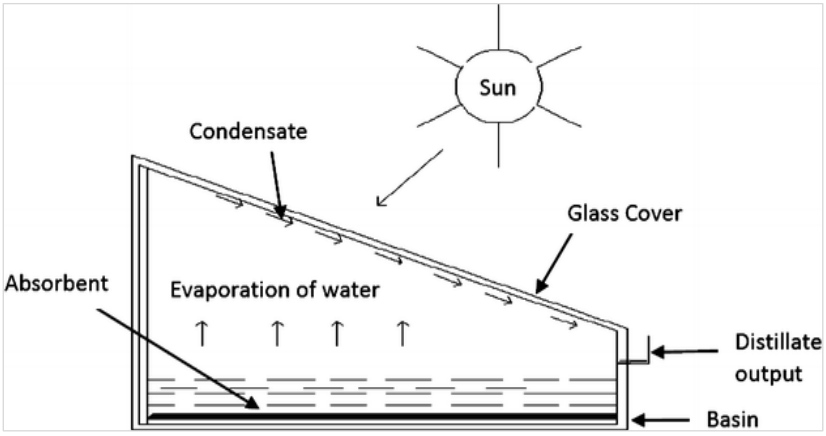

Figure 1.1: Basic structure of a passive solar still (Manchanda and Kumar, 2015)

Even though the solar distillation process is environment-friendly and clean, it is less productive than other conventional desalination methods (Velmurugan and Srithar, 2011). A conventional SS can provide a freshwater yield (FWY) of 2–7 L/m^2 per day with average global irradiance of 4–8 kWh/m^2 per day (Nomor et al., 2021). Extensive studies had been conducted for integration of SS with other processes and development of innovative design in order to achieve higher FWY. For instance, SS can be incorporated with reflectors, latent heat storage, nanofluids, solar collectors, photovoltaic thermal, solar ponds, humidification-dehumidification process. Whereas, the designs of SS are not limiting to active and passive SSs, pyramid SS, tubular SS, SS with condensers, inclined SS, wick type SS, and stepped SS (Tuly et al., 2021).

Concentrating solar collector, usually equipped with a group of mirrors, uses reflective surfaces to concentrate sun radiation into receivers, where the solar energy is absorbed and converted into heat energy. Concentrating solar collector is commonly used for water heating and power generation. When compared to a flat-plate system with the collecting surface of same solar energy, the working fluid in a concentrator system is capable of reaching higher temperatures. The combination of solar water heating process by concentrating solar collector with solar distillation system provides new solution to increase the vaporization rate of the salt water and yielding more fresh water.

1.2 Problem Statement

There are many advanced technologies in water desalination industry. However, the requirement of regular maintenance, electricity cost and professional to operate the system render the difficulty in small scale installation, especially in rural area which may have limited access to electricity and clean water. During solar distillation process, feed water in a still is evaporated and condensed on the transparent cover, which is tilted to promote downward flow, because of the temperature difference between the water vapor and transparent cover, which is then collected in a container. This leaves behind the brine which is composed of impurities. Most pathogens are rendered killed or inactive by ultraviolet rays from the sun, making the condensed water safe to drink. (Nomor et al., 2021). The major drawback of a SS is its low productivity of water because sunlight supply is intermittent. The investigation of design of these heat processes, evaporation or condensation to increase productivity of a SS is important to produce higher FWY.

TECHKEM Group is a leading developer of water treatment solutions in process and specialty chemicals, dedicated to assisting industries in solving treatment plant operating problems, not limiting to boiler, cooling tower, municipal, and industrial wastewater treatment systems. They had developed solar distillation system called Renewable Energy Water Refine Technology (REWART) system at Balingian, Sarawak which depicted in Figure 1.2. However, the REWART system has lower distillate yield rate due to the low inlet water temperature (27°C to 29.5°C) which causes the system need more solar energy to heat up the water to the vaporization temperature before it can distil the water. A solar water heater to preheat the water before the water flow into the inlet of the REWART system are proven to increase the water yield rate in many studies.

Figure 1.2: REWART system (Techkem Group, 2018)

Among the common solar water heater systems like flat plate, evacuated tube, and compound parabolic concentrator (CPC) collectors, CPC is able to accomplish concentration ratio greater than one (CR ≥ 1) and obtain higher temperature of water under good sun radiation. Nevertheless, because of its complex curvature design, CPC is known to have high geometry complexity, which causes problems when trying to construct CPC reflectors. Apart from that, it is difficult to manufacture CPC reflector, and its effectiveness may be reduced as a result of flaws in its symmetrical design that arise during the manufacturing process. In this dissertation, a multiple linear facet concentrator (MLFC) is introduced that emulate the concept of CPC but the several flat facets are used with designed tilted angle to concentrate the sunlight rather than continuous curvature geometry. This can make the fabrication process much simpler and easier. The performance and characterization of MLFC integrated with solar distillation system are studied as well as the mathematical model is developed to simulate the water yield of the system without performing on-site experiment in order to determine the maximum freshwater productivity.

1.3 Objectives

The objectives of this proposed study are:

1 To design and construct the Multiple Linear Facet Concentrator (MLFC) REWART Solar Distillation System

2 To evaluate the performance of the MLFC REWART Solar Distillation System

3 To develop the mathematical model of the MLFC REWART Solar Distillation System.

CHAPTER 2

LITERATURE REVIEW

2.1 Solar Distillation System

According to Belessiotis, Kalogirou and Delyannis, 2016, desalination is defined by "a physical procedure of separating the excess of dissolved salts from waters, brackish and seawater, or any aqueous salt solution in order to collect low-salt content water for any suitable use, such as drinking, industrial, pharmaceutical, municipal, or household water". Desalination is an industrial procedure which consumes a lot of energy independently of the process, leading to high energy cost. Distillation is an ancient desalination method involving a phase change process where the feedwater (mostly seawater or brackish water) is heated to form vapor and then condensed back to liquid (clean water). The condensed water (distillate) is subsequently separated leaving behind by-product known as brine during the process of evaporation and condensation (Isah et al., 2021). The main desalination processes are summarized in Table 2.1 according to the type of energy applied. Conventional desalination thermal methods are powered by steam or vapor pressure produced by fossil fuels whereas nonthermal by grid electrical energy.

Table 2.1: Type of desalination process

Thermally driven desalination methods	Electrically driven desalination methods
• Humidification-dehumidification (H/D) • Membrane distillation (MD) • Multiple effect distillation (MED) • Multiple humidification-dehumidification (MHD) • Multistage flash distillation (MSF) • Solar Distillation • Thermal vapor compression (TVC)	• Electrodialysis (ED), electrodialysis reversal (EDR) • Reverse osmosis (RO) • Mechanical vapor compression (MVC). • Crystallization – freezing & hydrates • Ion Exchange

From the methods mentioned above, MED, MSF, TVC, ED/EDR, RO, and MVC are technologically mature because most of their operational problems have been solved. The main challenge nowadays is to enhance efficiency, to reduce energy consumption, and to construct more compact units in order to minimize installation cost, transportation weight and eventually cost of producing fresh water. The remaining methods with the exception of H/D and MD, which are still in the industrial development stage, have found no wide practical use due to problem of operation and cost (Belessiotis, Kalogirou and Delyannis, 2016).

Solar distillation is the desalination process of evaporation of water by mean of solar energy and the simultaneous condensation of vapour to clean water. It is a simple process of humidification-dehumidification, works in one and the same device, known as “solar still” (SS). According to mode of

operation, they are divided into: a) **Active solar still**, uses a pump to circulate the water in the basin in a low flow rate, running either by connection to a solar collector which increases the feedwater temperature or by height difference from a storage tank; b) **Passive solar still,** operates without circulation of feed water. The basin is refilled every early morning around the sunrise hour. A conventional SS consists of a rectangular basin, a black liner at the basin's bottom (to increase absorption of sunlight and transform it into heat energy), insulation (covers the bottom and sides of the still), a top case (to hold the transparent cover), a transparent glazing cover (like glass or a durable plastic material), feeding and blow down pipes and pumps (feedwater circulation and brine blow down). The mechanism of SS basically involves simultaneous water evaporation and vapour condensation in the air tide space between the basin and cover. The vapour is condensing at the inner side of cooler transparent cover surface. Solar radiation strikes through the tilted transparent cover and airtight space. Then, it is partially absorbed by the basin water, the rest being absorbed by the black liner. The temperature of water in the basin is heated above that of the cover but below than its boiling point. The black liner surface changes wavelength in response to radiation and produces long-wave heat (Belessiotis, Kalogirou and Delyannis, 2016).

The still will operate more efficiently when the initial temperature is higher and the condensing surface is cooler. The efficiency can be maximized by using low emissivity glazing, a black surface, the collector inclined at an angle bigger than 15^{o} (preferably facing south in the northern hemisphere and north in the southern hemisphere, perpendicular to the midday sun), water depth

of a shallow 20 mm, and the collector located away from the shadows of trees or buildings. Moreover, the optimal time for SS to operate is in the early evening when the ambient temperature is falling but the feed water is still hot. A cool wind will also aid in reducing and keeping the temperature of the condensing cover. Poor maintenance can lead to issues when fittings create holes that allow cold air to enter. Cracking, algal growth, dirt or scratches on the transparent cover reduces the transmission of sun radiation (Belessiotis, Kalogirou and Delyannis, 2016). The parameters affecting the efficiency of SS are summarized in Table 2.2 (Jathar et al., 2022).

Table 2.2: Parameters affecting the performance of solar still

Climatic parameters	Design parameters	Operational parameters
✓ Intensity of solar radiation ✓ Wind speed ✓ Ambient temperature ✓ Dust & cloud cover ✓ Latitude & longitude of the location	✓ Area of absorber plate ✓ Gap distance ✓ Inclination of the cover plate ✓ Selection of material ✓ Sun tracking system ✓ Thermal energy storage materials ✓ Thickness of the cover plate ✓ Thickness of insulation & insulating material ✓ Use of internal/external reflectors ✓ Water depth	✓ Water salinity ✓ Water flow rate ✓ Use of dyes ✓ Others

Figure 2.1 illustrates an inclined SS which has a support frame with bottom of the basin exposing to the surrounding. The inclined SS consists of an absorber plate and a glass cover which forms a cavity. The absorber plate is covered by a black wick which distributes the water uniformly on the plate, increasing the thickness of the water film. The still is 30^{o} inclined with respect to horizontal ground. This inclination angle allows an incident of solar radiation to normal for most hours of the day and also smooth dripping of water. Solar energy heats the black wick and absorber plate. Part of the water on the absorber plate will evaporate and create water vapor, then the water vapor condenses when it touches the cool transparent cover. The remaining feed water passes into another collection channel while the distillate flows into a condensate channel (Aybar, 2006).

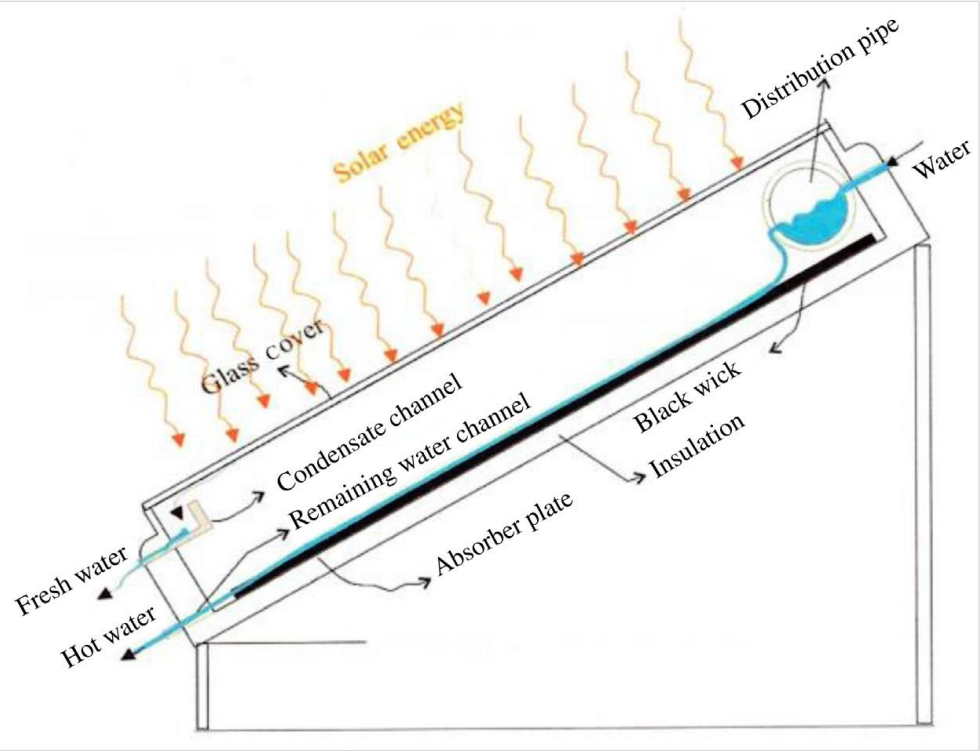

Figure 2.1: An inclined solar still (Aybar, 2006)

F Cubed invented the Carocell panel (as shown in Figure 2.2), which is a simple, portable, direct solar-powered desalination technology. The panel creates its natural water cycle to revitalize impure water including contaminated, polluted, industrial wastewater, brackish ground water, saline aquifers and sea water to drinking water quality. Carocell heats the feed water while operating at the ambient temperature, causing a vapor condensation change prohibiting all bacteria and pathogen, thus eliminating all water borne diseases. Exposure to extreme heat and ultraviolet (UV) light from solar energy through the advanced composite panel boosts up the process of germ-killing. The water yield from this system is purified to a level of 1-10ppm of total dissolved solids (TDS), which is much lower as compared to sea water measured at 35,000ppm. The Carocell panel is a flow through system. The feed water, which is not evaporated, continues down and out of the panel and can be used as UV treated hot water (depending on feedwater source) or be reprocessed through the Carocell panel (F Cubed Limited, n.d.).

Figure 2.2: Carocell (F Cubed Limited, n.d.)

2.2 Solar Water Heating System

Solar water heating system converts solar radiation into heat by transmitting the solar energy into a transfer medium which is water. This system is often used to replace fossil fuels and electricity for water heating. When the working fluid is flowing through a high absorptive blackened surface that is exposed to sunlight, which causes the fluid temperature to rise. A direct system refers to the solar thermal energy is transferred by heating the water directly, whereas indirect system is heating the heat transfer fluid (for example glycol) that is passed through some form of a heat exchanger. The types of solar water heater are summarized in Figure 2.3 (Jamar et al., 2016).

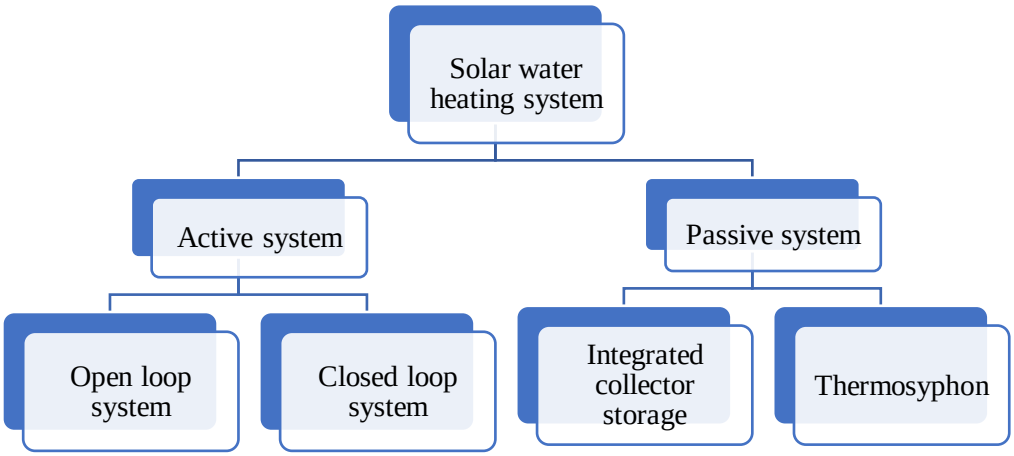

Figure 2.3: Solar water heating system (Jamar et al., 2016)

Active system stores solar energy in a storage unit and uses collectors to heat water in a controlled manner. It uses controller, electrical pump and valve to circulate working fluids through the collectors. Figure 2.4 demonstrates the mechanism of a pumped active solar water heating system (Open University, n.d.). An open loop (direct) system warms the household water in the solar collector. Upon heated, the water is pumped into a storage tank, then delivered to spouts for usage at home. Since this system uses household water in the

collectors, it should be utilised only in places without freezing conditions. A closed loop (indirect) system usually uses an antifreeze water mixture for heat transfer process and is commonly seen in areas with freezing condition. The heat transfer fluid is pumped into a storage tank after being heated in the solar collector, where a heat exchanger transfers the heat from the fluid for the household usage (Jamar et al., 2016).

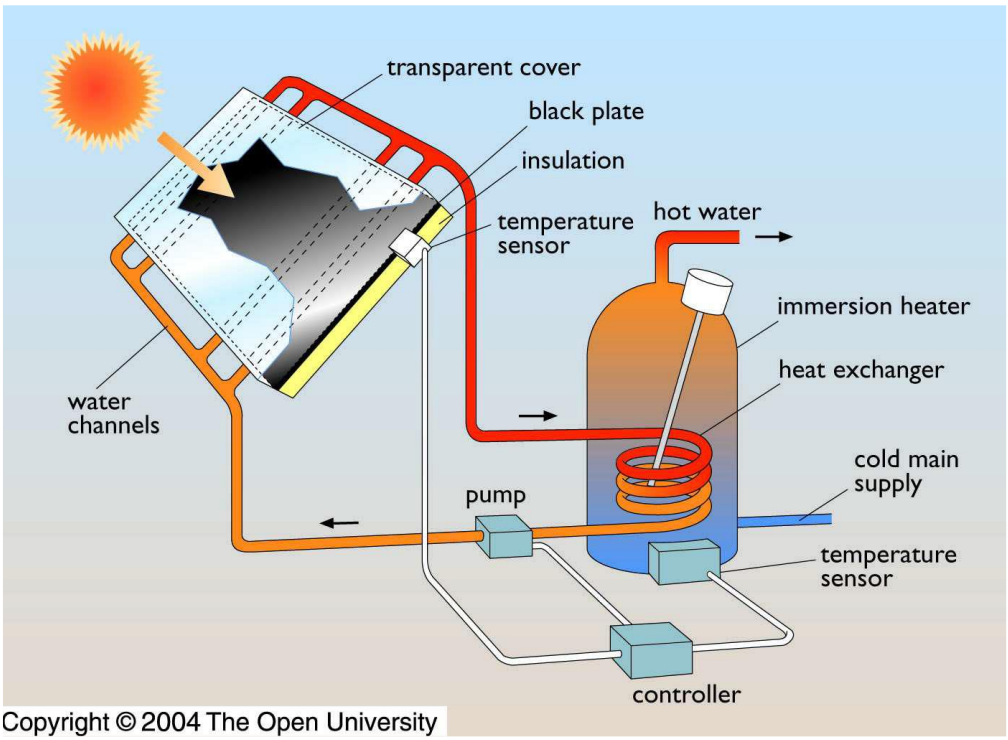

Figure 2.4: A pumped active solar water heating system

In contrast, a passive system uses natural convection to transfer heat and circulates working fluids between an elevated storage tank and a collector without mechanical devices. Starting with the collector, the system collects solar energy, the fluid in the collector will absorb heat, leading to a fall in fluid density and an upsurge of fluid to the collector's top, and then gushing into the storage tank. Subsequently, the fluid will cool down at the bottom of the storage tank.

Finally, the fluid will flow back to the collector. This phenomenon will continuous until the supply of solar energy stops (Jamar et al., 2016). The examples of passive system are thermosyphon (Figure 2.5) and the integrated collector storage (ICS) (Figure 2.6).

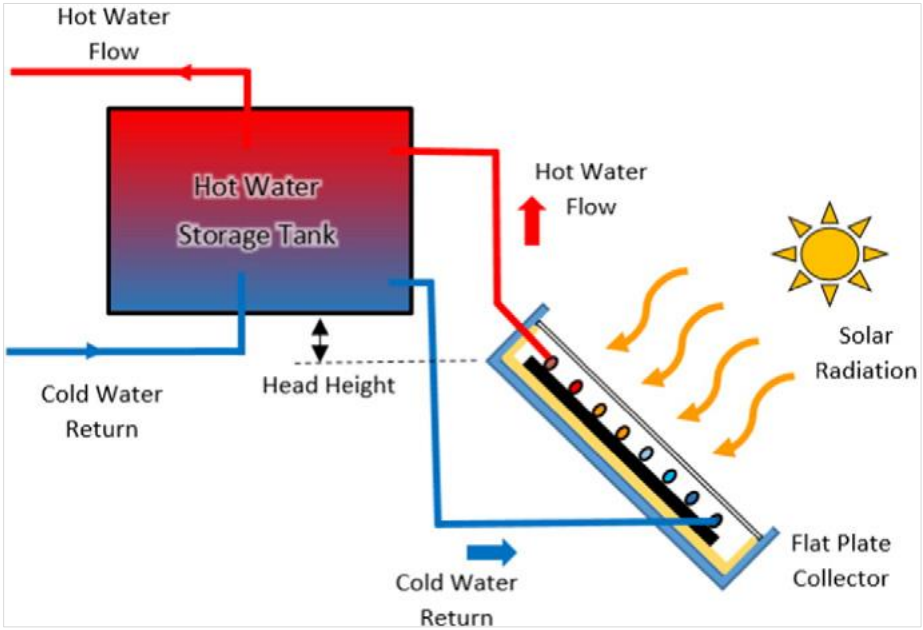

Figure 2.5: Schematic diagram of the thermosyphon hot water system (Jamar et al., 2016)

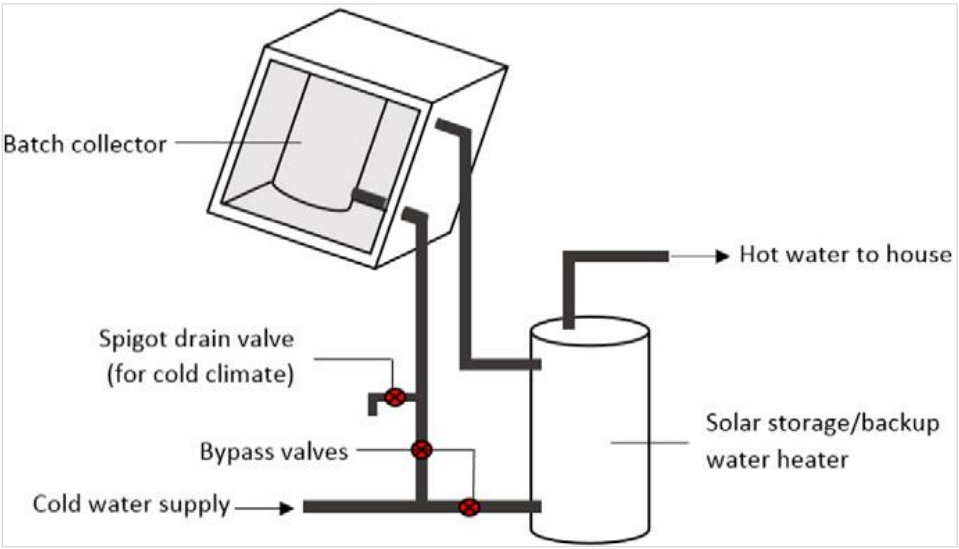

Figure 2.6: Integrated Collector Storage (Jamar et al., 2016)

2.1.1 Type of Solar Collector

Through the use of a heat transfer fluid, solar collectors transform solar energy into thermal energy that can either be used directly or stored for use at night or during cloudy conditions. The type of solar collectors is chosen based on the temperature requirement of the desalination system, and may categorised as flat plate, evacuated tube and concentrating collectors. Solar collectors usually consist of solar absorber, transparent cover and heating pipe. The absorber is selectively coated to absorb all the sun irradiance, whereby heat is transferred from the absorber to the flowing fluid inside the absorber by conduction. Selective coatings usually have the highest absorptivity which is more than 0.95 and negligible emissivity. Transparent cover is used to reduce heat losses due to convection as well as to protect the absorber from dust. Heat is transferred from the absorber to the fluid at the header using the heating pipe. (Kumar, Said and Bellos, 2021).

Flat plate collector (FPC) is the most common type of collector. They are selectively black coated absorbers whereby water flows in pipes, covered in insulated box except for the front which is covered with low emissivity transparent glass. Several FPCs can be connected together – either in parallel or in series. Figure 2.7 shows that how a FPC collects heat. In a solar collector, heat is transferred by conduction from the absorber to the fluid inside the absorber. Evacuated-tube collector (ETC) are made up of a row of glass tubes a long absorber painted with the black selective surface that prevents the infrared radiation re-emitting out. There is vacuum within the space between the glass tube and the absorber which prevents and reduces the convective heat loss. The

heat is circulated through a heat exchanger coil in the storage tank after being transported to a manifold at the top of the tube (Thorpe, 2011). Figure 2.8 illustrates the ETC (Supankanok et al., 2021).

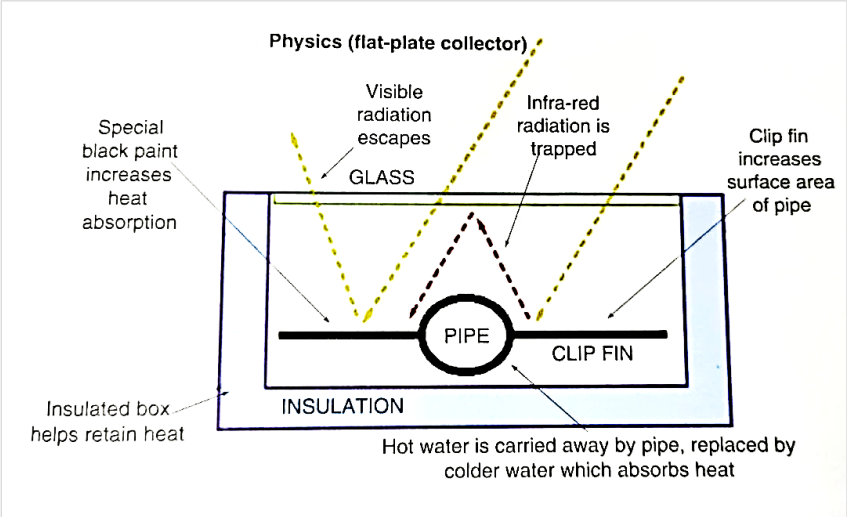

Figure 2.7: How a FPC collects heat. (Thorpe, 2011)

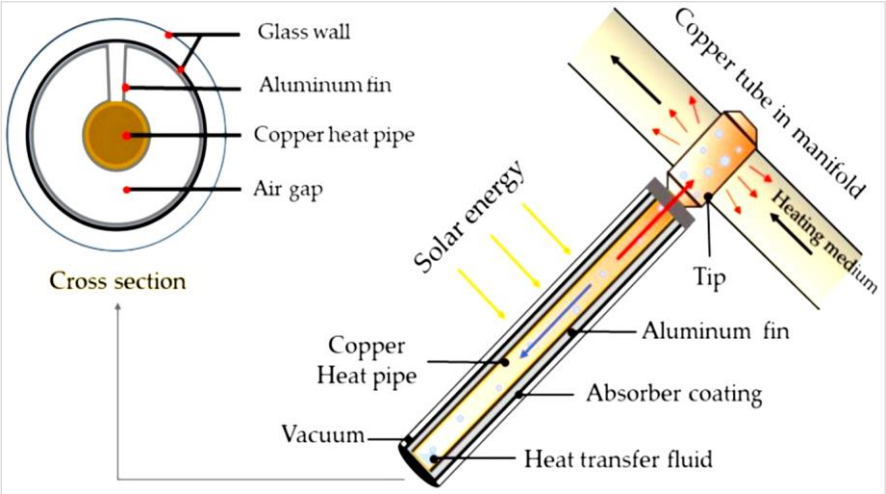

Figure 2.8: Principle of an ETC (Supankanok et al., 2021).

Concentrating collector is system that reflect or refract the sunlight from one reflective or refractive aperture surface A_a to an absorber or receiver surface, A_r, where $A_a > A_r$ applies. The optical concentration is $C_o = G_r/G_a$ while the

geometric concentration is $C_c=A_r/A_a$, where G_r and G_a are the intensities of sun irradiation to the areas of "aperture" and "absorber" respectively (Belessiotis, Kalogirou and Delyannis, 2016). The common types of concentrating solar collector used for solar distillation are shown in Figure 2.9, which include linear Fresnel reflector, central receiver, parabolic collector, and parabolic trough (HVAC/R and Solar Energy Engineering, n.d.).

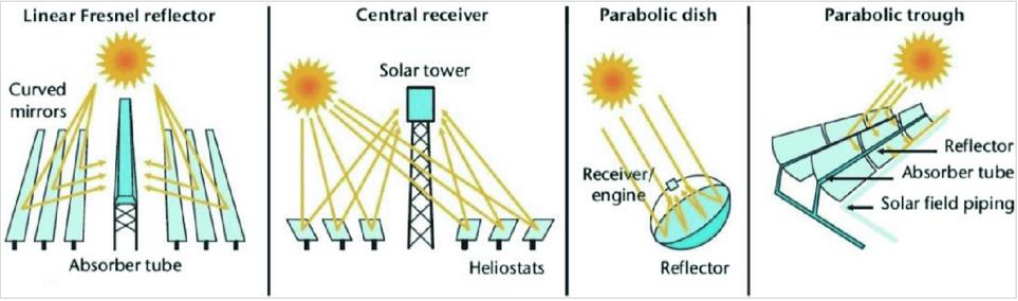

Figure 2.9: Tracking concentrating solar collectors
(HVAC/R and Solar Energy Engineering, n.d.)

Linear Fresnel reflector consists of smooth optical segmented surfaces. It reflects or refracts the sunlight depending on the type and location of reflector. This is also known as linear type focusing system. Central receiver system, also called solar towers) functions with a field of heliostats, which are large flat or slightly curved mirrors fitted on metallic structures. These dual axis sun tracking heliostats concentrate sunlight on a boiler (receiver or heat exchanger) located at the top of a tower where a steam of high temperature (at around 1000^{o}C) can be produced and used for the power generation. The generated electricity can be used in desalination system like reverse osmosis, electrodialysis and mechanical vapor compression, or for distillation systems if bleed steam of the right temperature is produced. Parabolic dish collector is point focusing concentrating system, consists of a set of parabolic dish-shaped mirrors, solar

receiver, sun tracking system and pipe work to carry the heat transfer fluid. It produces hot water under high-temperature steam or pressure. The temperatures gained are between 375ºC and 2000ºC. Parabolic trough collector (PTC) is concentrating system of linear focus with a set of concave mirrors and receiver tube at the center producing hot water or steam typically up to 375ºC. It can have a concentration factor of solar energy of 20 to 100 suns. Generally, they use single-axis tracking of the sun and have a higher performance at temperatures of 150-190ºC. PTC can be used for desalination, cooling, and power generation (Belessiotis, Kalogirou and Delyannis, 2016).

The compound parabolic concentrator (CPC) is a non-imaging concentrator that have the capability of reflecting all of the incident radiation to the absorber surface located at the bottom of the collector over a relatively wide range of angles by utilizing the principle of edge optics. The basic concept is that by using a trough with two parts of a parabola facing each other, shifting the concentrator to account for the apparent daily motion of the sun can be reduced. The configurations of absorber can be flat, bifacial, wedge or cylindrical as depicted in Figure 2.10. The gap between the reflector and the receiver is important to prevent the reflector from acting as a fin that conducts heat away from the absorber. CPC collector can be constructed either in one unit (one opening and one receiver) or a panel. The CPC collector looks like an FPC when it was constructed as a panel, as shown in Figure 2.11 (Kalogirou, 2014).

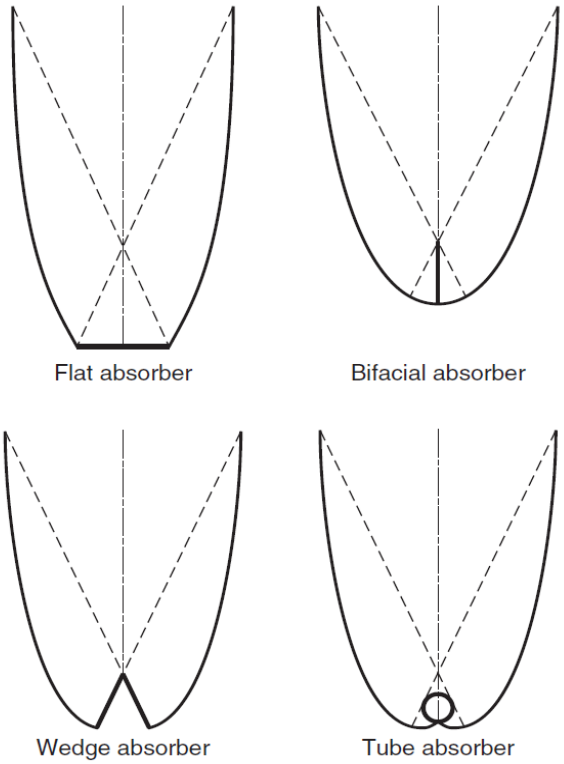

Figure 2.10: The types of CPC absorber

(a)

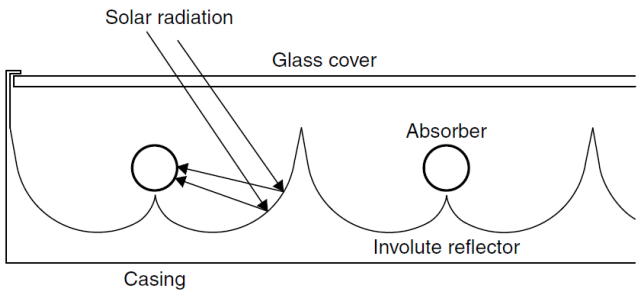

(b)

Figure 2.11: CPC panel collector with cylindrical absorbers: - (a) Schematic diagram (b) Photo

2.3 Enhanced Solar Distillation System with Solar Water Heater

Nowadays, solar distillation is generally used in rural and remote areas. Lack of electricity, the rise in the fuel price, and lack of technical operator hinder the people in rural areas to generate fresh water. A conventional SS has low productivity. Many researches are focused on minimizing energy consumption, fabrication price, environmental impact, maximizing productivity and thermal efficiency in solar distillation systems. Figure 2.12 lists down the improvement in design of a conventional SS (Chaurasiya et al., 2022). The distillation efficiency increases with the amount of heat energy trapped. The heating time of the water in the absorber and the inlet water temperature are the parameters that affect the amount of heat energy trapped. Therefore, increasing the inlet water temperature must be effective and at the same time, easy to manufacture, use, maintain, and low cost (Sambada et al., 2020). Table 2.3 summarizes the pre-heating effect of the feedwater by solar water heater on SS. From the papers on the hybrid system, it can be deducted that the pre-heating of the inlet water can increase the SS distillation efficiency. This study proposes a new method that is easier and simpler to increase the inlet water temperature.

Table 2.3: Pre-heating modification to solar distillation system

SS Types	Modification	Findings	References
Single slope basin SS	Integrated with evacuated tube collector	The daily yield obtained is 3.8 kg/m^2 for 0.03 m basin water depth. The water depth increases, the yield increases.	(Singh et al., 2013)
Basin SS	Integrated with flat-plate	Increases the distillate about 60% than that of the conventional SS for the	(Rajaseenivasan, Nelson Raja and Srithar, 2014)

	collector	same basin condition.	
Conical SS	Coupled with concentrating solar water heater	Increased system productivity by about 180%.	(Chaichan and Kazem, 2015)
Double basin SS	Vacuum tubes & granite gravel	Distillate is increased to 56% with adding vacuum tubes and 65% of adding vacuum tubes & black granite gravel.	(Panchal, 2015)
Single-slope SS & Pyramid SS	Coupled with compound parabolic concentrator	Productivity of a single slope SS & a pyramid SS were found as 6460 ml/day & 7770 ml/day, respectively.	(Arunkumar et al., 2016)
Triple basin SS including cover cooling technique	Integrated with parabolic dish concentrator	The temperature of lower basin water enhances up to 85% with a concentrator. The combined effect of the concentrator, cover cooling method, & charcoal in fins gives the productivity of 16.94 kg/m^2.day.	(Srithar et al., 2016)
Basin SS	Integrated with evacuated tubes & PV module	The maximum water production (4.77 $kg/m^2 \cdot day$) is achieved for the basin depth of 0.07 m & 30 numbers of tube.	(Yari, Mazareh and Mehr, 2016)
Single-slope SS	Coupled with Parabolic dish with conical tank	FWYs are 7.5 & 13.48 kg/day using 2 solar dishes and 5.54 & 8.8 kg/day with single solar dish at water depth of 20 mm & 10 mm respectively.	(Kabeel et al., 2019)
Triple basin SS	Integrated with evacuated heat pipes	The daily FWY is found 19 kg/m^2/day using granite gravels & evacuated heat pipes.	(Patel, Patel and Panchal, 2020)

Basin SS	Coupled with evacuated tubes & zig-zag shape air-cooled condenser	The maximum distillate output for conventional SS & modified SS was 2.26 kg/m^2 & 3.92 kg/m^2, respectively. It gives 73.45% of higher productivity than conventional SS.	(Mevada, Panchal and Sadasivuni, 2021)
Horizontal wick basin SS	Integrated with flat plate collector	The overall cumulative & day efficiency of the horizontal wick SS was found to be 16.6% & 12.1% higher than the conventional SS.	(Negi, Dhindsa and Sehgal, 2021)
Modified pyramid SS	Integrated with flat plate collector (FPC)	Modified pyramid still coupled with FPC gives 3100 ml of pure water which gives higher productivity of around 40% than pyramid SS without FPC for 2220 ml.	(Subramanian et al., 2021)
Single slope basin SS	Coupled with parabolic trough collector	The yield obtained at 5 cm, 10 cm & 15 cm water level was 4.1 L/m^2, 3.645 L/m^2, & 3.2 L/m^2, respectively.	(Kumar, Vyas and Nchelatebe Nkwetta, 2020)
Single slope basin SS	Combined with flat plate collector, parabolic trough & packed bed	The daily freshwater productivities recorded for conventional SS is 1.02 kg/m^2 (winter) & 1.988 kg/m^2 (summer); for modified SS is 2.775 kg/m^2 (winter) & 6.036 kg/m^2 (summer).	(Madiouli et al., 2020)
Inclined & tubular SS	Integrated with parabolic concentrator	The developed device productivity & efficiency are 7.82 L/day & 35.62%.	(Ahmed et al., 2022)

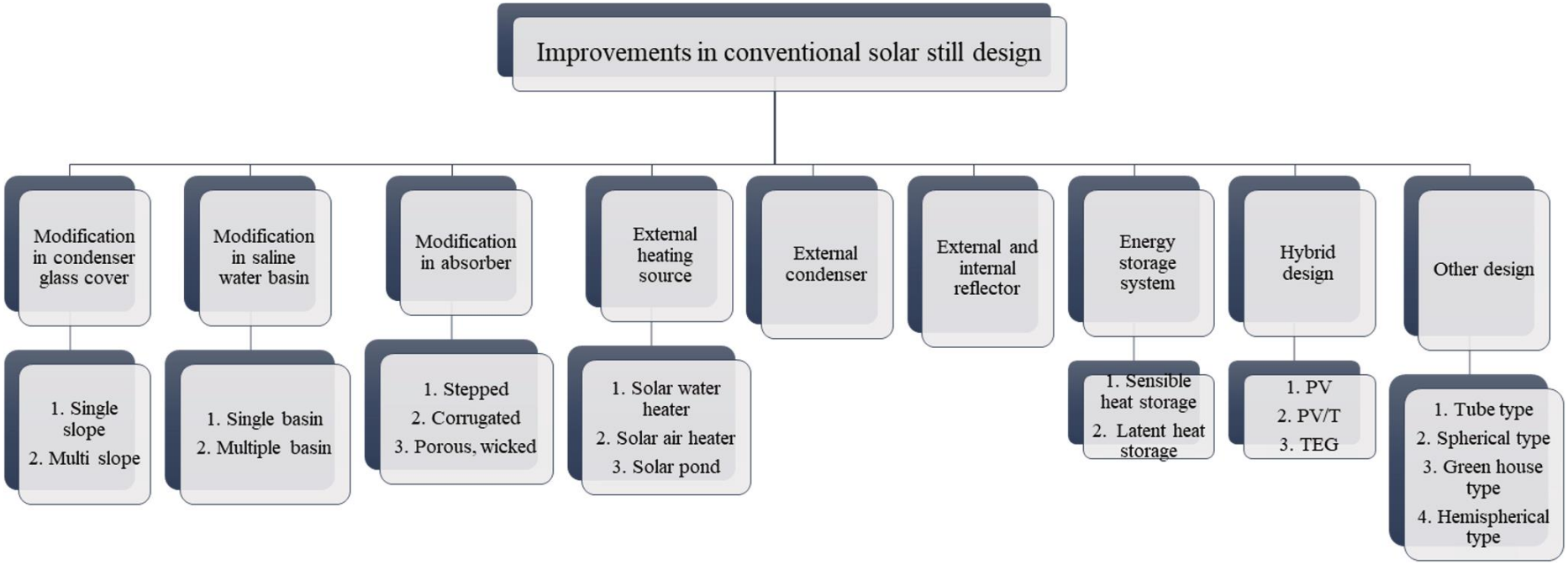

Figure 2.12: Improvement in solar still design (Chaurasiya et al., 2022)

2.4 Mathematical Transient Modelling

To make solar distillation systems technically and financially feasible, it is important to design it at higher energy efficiency reducing thermal losses and irreversibility in the component (Ranjan, Kaushik and Panwar, 2016). From the mathematical model, the energy flow from each component of the system, system efficiency and optimum condition of the system with the input of real-life data and simulation data can be determined.

2.4.1 Solar Water Heater – Flat Plate Solar Collector

According to Chekerovska and Filkoski (2015) , the working conditions of the solar collector on the fluid flow and heat transfer are non-uniform and unavoidably transient because of the nature of the sun radiation. Under steady-state condition, the overall energy balance is defined as "Heat energy delivered by the collector equals to heat energy absorbed by the plate and the pipes, deducts the heat losses to the surroundings". The heat transfer process includes conduction, convection, and radiation within solid and fluid area. The breakdown of the incident solar energy into useful energy gain, heat losses and optical losses are depicted in Figure 2.13. The geometrical and physical properties of the collector, climatic, and operation parameters are the input parameters of the model. Basic outcomes are thermal energy gain Q_u and collector efficiency. The useful gain from the collector is defined by:

$$Q_u = A_a[G - U(T_m - T_a)] \quad (1)$$

where A_a is the area of the collector glass cover, m^2; G is the insolation on the absorber plane, W/m^2; U is the overall heat loss coefficient of the collector, $W/m^2.K$; T_m is the mean fluid temperature in the absorber, K, and T_a is the

ambient temperature, K. This equation for calculating the efficiency of a solar collector is also known as Hottel-Whillier-Bliss equation (Kalair et al., 2022).

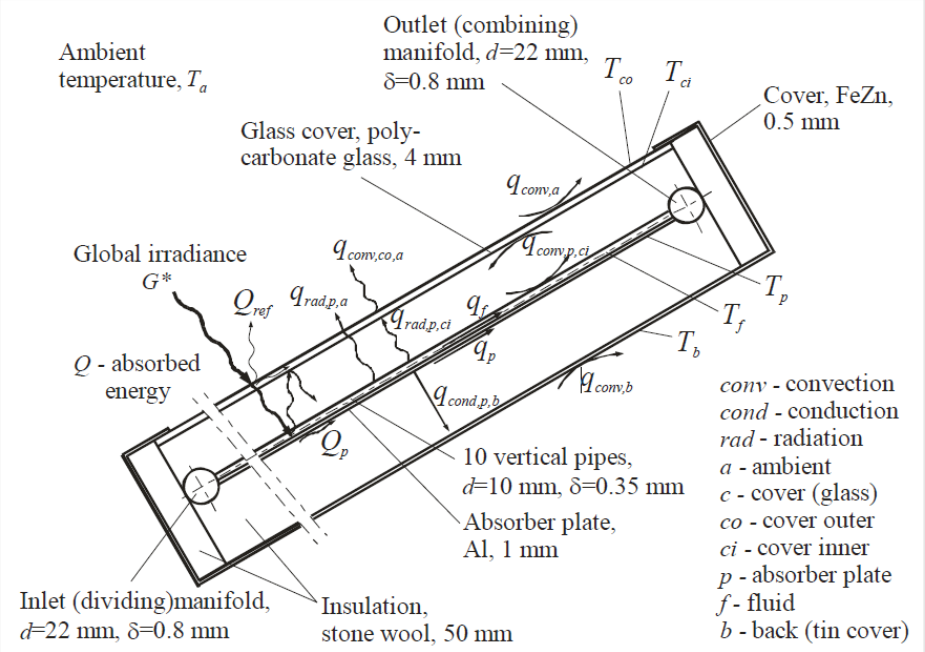

Figure 2.13: A schematic diagram of an energy balance of a typical liquid FPC (Chekerovska and Filkoski, 2015).

The collector thermal efficiency is the ratio of the useful heat energy gain to the incident solar energy on the plane of the absorber, over a predetermined time period, which is given by the following equation:

$$\eta_c = \frac{Q_u}{GA_a} \tag{2}$$

Using the main technical parameters, the efficiency is calculated by:

$$\eta_c = \frac{m_f c_{p,f}(T_{f,out} - T_{f,in})}{GA_a} \tag{3}$$

where m_f is the working fluid mass flow rate, kg/s; $c_{p,f}$ is the specific heat capacity of the working fluid, J/kg.K; $T_{f,out}$ is the working fluid outlet temperature, K; $T_{f,in}$ is the working fluid inlet temperature, K; G is the incident solar radiation, W/m^2; and A_a is the area of the collector aperture, m^2 (Chekerovska and Filkoski, 2015).

2.4.2 Solar Distillation System

A number of unpredictable factors, like the amount of solar energy, the ambient temperature, and the wind speed outside the clear cover, have an impact on an SS's productivity. Other crucial parameters that can be controlled or changed include the temperature difference between the water's surface and the transparent inner cover surface, the temperature difference between the water's surface and the black liner surface, the cover's angle of inclination, the temperature of the feed water, and the depth of the water in the basin. Figure 2.14 describes the thermal behaviour of a conventional SS. As incident solar radiation, G (W/m^2), i.e., direct and diffuse, falls onto the transparent cover, a portion of it ($G_{\alpha g}=q_{abs}$) is absorbed by the cover and the rest ($G_{\tau g}=q_{pen}$) penetrates into the air tide space of the SS. The water at the basin ($G_{\alpha w}\tau_g=q_{wab}$) absorbs energy and warms up. At temperature T_w, small portions of the water heat are reflected from the water surface back to the cover by radiation (q_{rwg}), by convection (q_{cwg}), and by evaporation (q_{ewg}). At the same time, heat fluxes are created from the cover surface to the surrounding by radiation (q_{rga}) and by convection (q_{cga}), which are in fact an energy loss. Despite the insulation, there are some heat losses from the bottom (q_b), and the sides of the SS (q_{sd}). Vapor leakage to the ambient (q_{leak}) may occur in non-air tide stills. Some energy is also lost as sensible heat (q_{sen}) with the distillate and brine blow down (Belessiotis, Kalogirou and Delyannis, 2016).

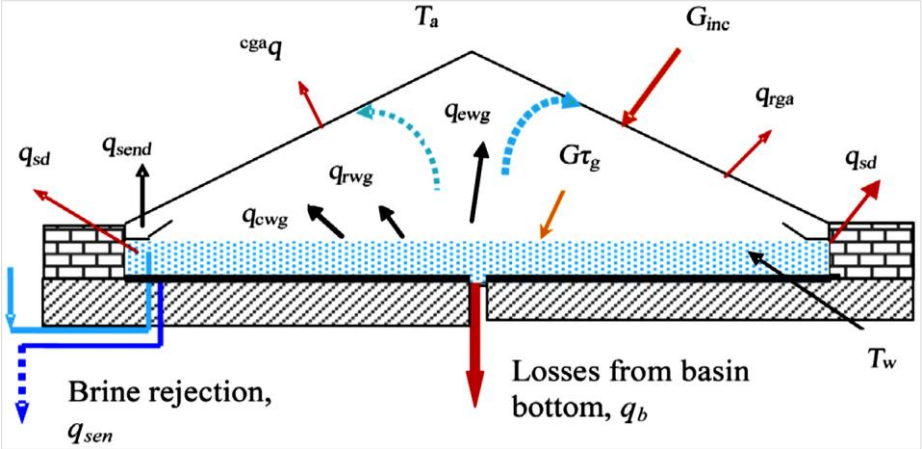

Figure 2.14: Schematic of heat transfer in a conventional symmetric SS (Belessiotis, Kalogirou and Delyannis, 2016)

For heat balance calculations, the SS may be divided into two sections: brine-liner and cover-distillate. It is assumed that in an idealised system, the SS has no leakage and operates without temperature gradients in the transparent cover and water. The SS efficiency could be usually calculated by the following equation:

$$\eta = \frac{\sum m h_{fg}}{\sum AG} \tag{4}$$

in which m, h_{fg}, G, and A are the productivity, latent heat of vaporization, solar intensity, and surface area exposed to the solar intensity, respectively (Ayoobi and Ramezanizadeh, 2021).

CHAPTER 3

METHODOLOGY

3.1 Overview of the project

The methodology for this project was demonstrated in a flowchart as shown in Figure 3.1. Firstly, the overall system of MLFC solar water heater was designed using 3D software and the MLFC structure was constructed with the aid of 3D printing machine. The MLFC solar water heater was fabricated and assembled with REWART solar distillation system. Subsequently, the performance and efficiency of the MLFC solar water heater were studied together with the REWART solar distillation system. Fresh water was allowed to flow through the MLFC solar water heater for pre-heating process. Once the water was heated, it was passaged to REWART solar distillation system investigating the water yield rate. Finally, a mathematical model of the REWART system has developed. The experiment result and simulated result from the mathematical model were compared and analyzed. The experiment was set up at Block J, Universiti Tunku Abdul Rahman, Kampar Campus. The parameters studied were listed as below:

Table 3.1: Experiment Parameters

Process Parameters	Result Parameters
✓ Time (minutes) ✓ Water Flow Rate (LPH) ✓ Inlet Water Temperature (^oC) ✓ Outlet Water Temperature (^oC) ✓ Ambient Temperature (^oC) ✓ Global Horizontal Irradiance (GHI)	✓ Water Yield (ml) ✓ System Efficiency (%)

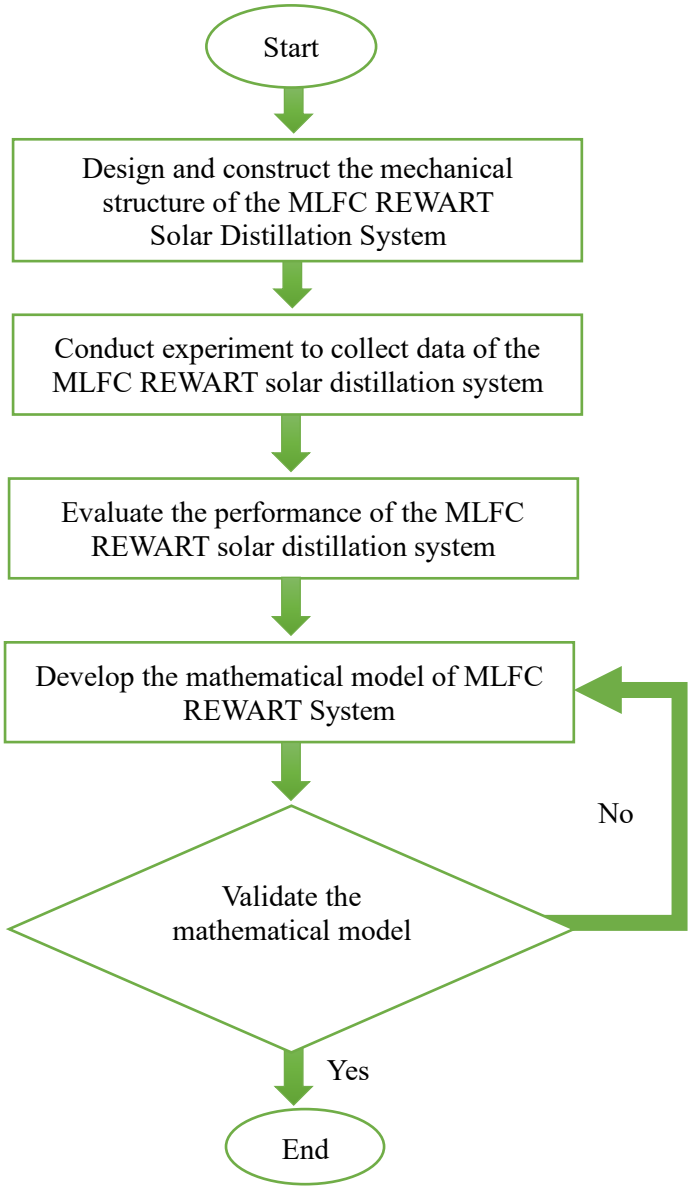

Figure 3.1: Flow chart of the proposed project

3.2 MLFC Design and Fabrication

The earth rotates in approximately 24 hours about its own polar axis, which is inclined to the ecliptic plane by 23.45 degrees (as shown in Figure 3.2), which is also referred to sun declination angle. Thus, the optical geometry design of the MLFC is crucial to ensure all the incident sunray reflect to the receiver.

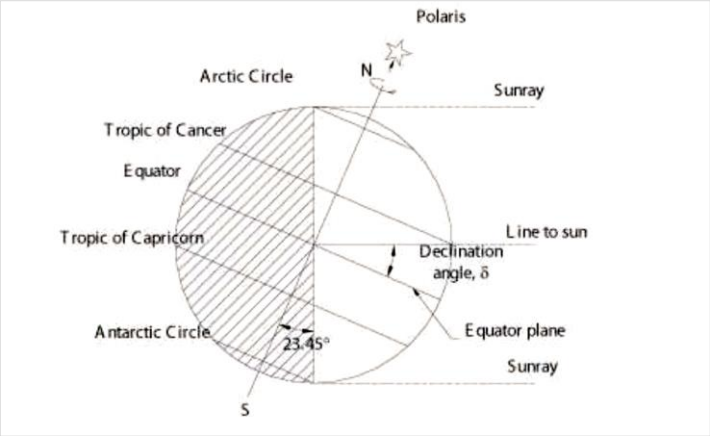

Figure 3.2 Illustration of declination angle and Earth rotation.

3.2.1 Solar Water Heating Concept of MLFC

The MLFC was built up of multiple linear facets with different tilted angle to ensure all the incident sunray can be reflected to the absorber pipe located at center of the concentrator as illustrated in Figure 3.3. It is a non-imaging stationery concentrator, heating the absorber pipe from the gathered solar energy without sun-tracking. According to Multi-Facet Trough Solar Concentrator design of Tan M.H, Fon C.Y. and Khong D., 2018, the tilted angle of each facet mirrors can be calculated (as demonstrated in Appendix I), which allows all the incident sunray are reflected by the MLFC toward the absorber pipe without any spillage losses.

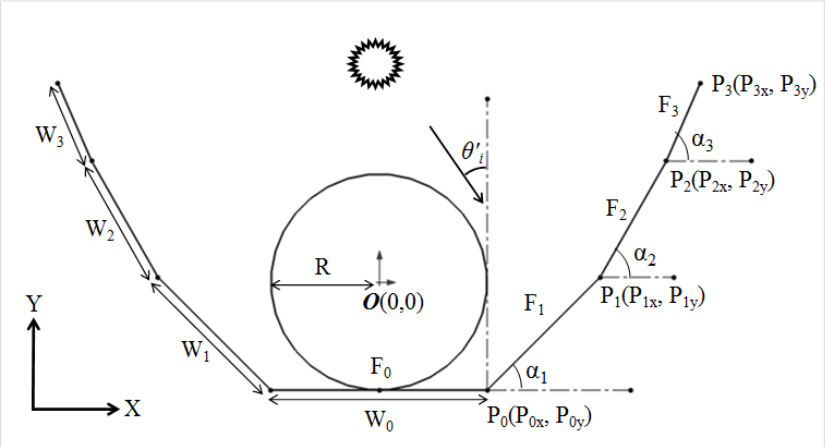

Figure 3.3: Parameter Symbol and Optical Geometry Design for MLFC.

In this experiment, the half acceptance angle and radius for the absorber pipe of the MLFC solar water heater system used are 24° and 21mm. The width and tilted angle for different flat facet mirrors are calculated as follows:

Table 3.2: The Width and Angle for Different Mirrors of the Collector

Mirror	Width, W_n (mm)	Tilted Angle, α_n (°)
1	42.00	0.00
2	33.89	45.00
3	29.92	60.77
4	20.05	64.24

3.2.2 Mechanical Structure of MLFC

The mechanical structure of MLFC was designed using *SolidWorks* as illustrated in Figure 3.4 and Figure 3.5. The MLFC solar water heater (SWH) system consists of a water tank, GI pipe, water pipe tap, transparent glass, galvanized iron plate, mirrors, plywood, and 3D printed support. The fabrication process of MLFC SWH was demonstrated in Figure 3.6. All the significant materials and equipment used were listed in Table 3.3 and Table 3.4.

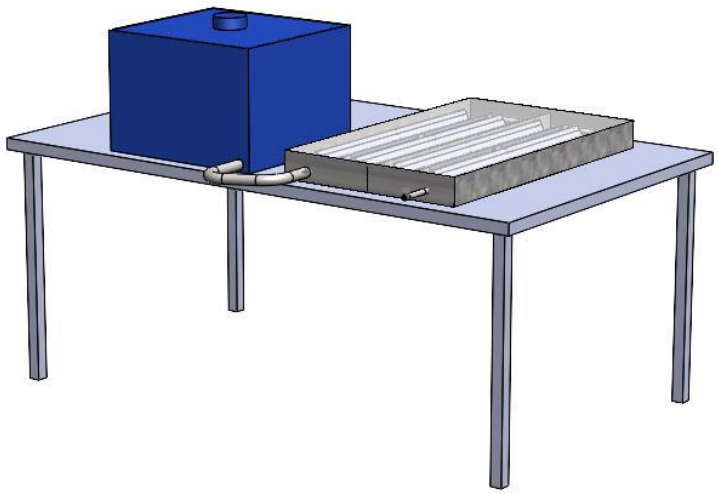

Figure 3.4: 3D Model of MLFC

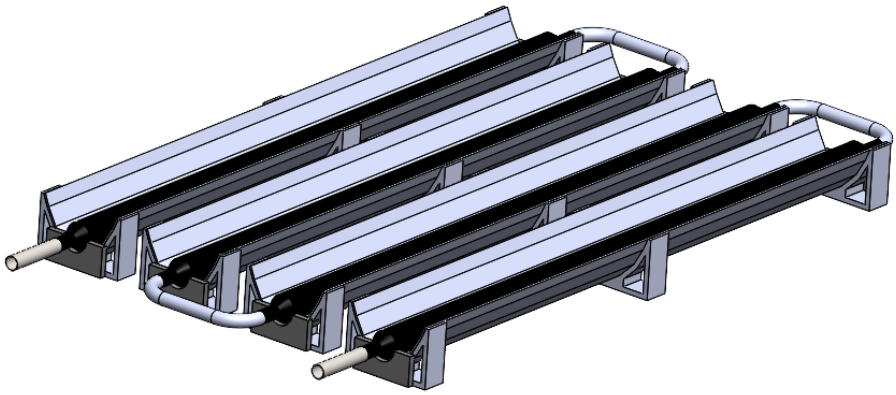

Figure 3.5: 3D Model of Collector and GI Pipe

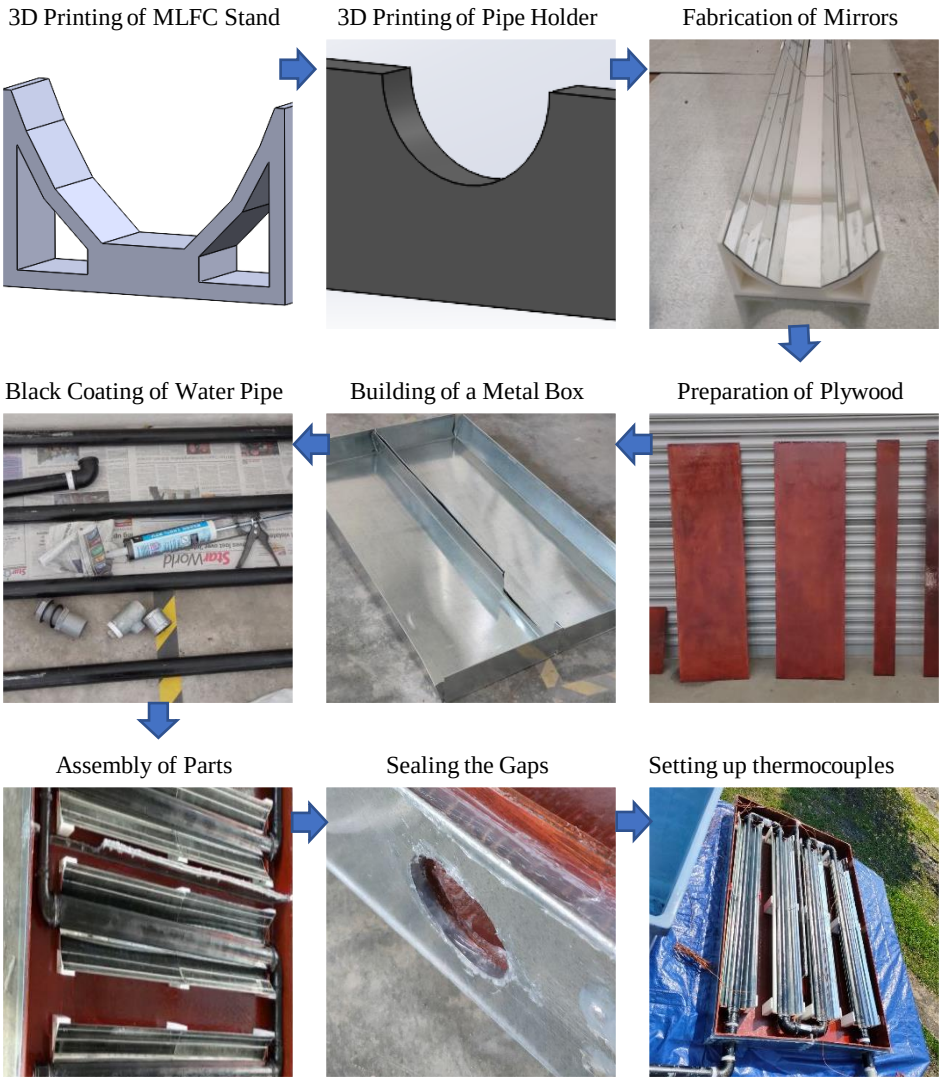

Figure 3.6: The fabrication process of MLFC SWH

Table 3.3: Materials for fabrication of MLFC REWART System

No	Items	Functions	Quantity
1	Polylactic acid	Raw material of 3D printing technology for the stand of the MLFC structure	1
2	Plywood	Act as insulator of the MLFC structure to prevent heat loss.	1 plate
3	Water pipe / Absorber	For the flow of water and heating process by solar energy	4 piles
4	Mirrors	Act as a reflective material of the sunlight	28 pieces
5	Silicone sealant	To fill up all the gaps of the structure.	4 bottles
6	Water valve	To control the flow rate of the water	4 valves
7	Carocell Panel	A solar distillation panel used in REWART system for evaluation of fresh water yield	2
8	Glazing Glass	To use as glazing of MLFC which allows most solar radiation to enter the system and reduces heat loss due to convection.	1plate
9	Galvanized Iron Plate	Used as outer most layer for the system in a box shape to support the design.	1 plate
10	Black Paint	To coat the water pipe and increase the absorptivity of the concentrator	2 bottles
11	Water Tank	A container used to store water	1
12	White Tape	To prevent water leaking from the pipe	2 rolls

Table 3.4: Equipment for fabrication of MLFC REWART System

No	Items	Functions	Quantity
1	3D Printing machine	To 3D-prints the stand of the MLFC structure	1
2	*Solidworks*	3D software used to design the MLFC solar water heater structure	1
3	Others	Drilling machine, scissors, rulers and pliers for measuring and cutting the materials	-

The heat absorber tube - GI pipe was designed in serpentine pattern, which was a single tube meanders across the absorber. The benefit is that the fluid only needs to pass through one tube, resulting in an even flow across the absorber. The main construction considerations are good collector efficiency factor, low material usage, and low production costs.

3.2.3 Specification of the MLFC REWART System

The specification of the system is divided into two parts as depicted in Table 3.5 and Table 3.6.

Table 3.5: Specification of a MLFC Solar Water Heater

No	Description	Feature / Value
1	Type of reflector	Normal mirror
2	Outer and inner diameter of pipe	42.50 mm, 32.00 mm
3	Overall Dimension*	800 mm (w) x 1290 mm (l) x 105 mm (h)
4	Dimension for each mirror*	42.00 mm (w) x 1030 mm (l) x 2 mm (t)
		33.89 mm (w) x 1030 mm (l) x 2 mm (t)
		29.92 mm (w) x 1030 mm (l) x 2 mm (t)
		20.05 mm (w) x 1030 mm (l) x 2 mm (t)
5	Dimension of glazing glass*	800 mm (w) x 1290 mm (l) x 4 mm (t)
6	Half acceptance angle	24^o
7	Number of concentrators	4
8	Orientation of the prototype	Along east-west direction
9	Aperture area, A_a	0.149 m^2
10	Absorber/Receiver area, A_r	0.801 m^2

*Dimension: width (w) x length (l) x height(h)/thickness (t)

Table 3.6: Specification of REWART Solar Distillation System*

No	Description	Feature / Value
1	Water Output	10 l/day + rainfall harvesting on daily average and may vary depending on availability of solar energy
2	Dimensions	1150 (w) x 2100(l) x 50 mm(t)
3	Surface Area	2.0 m^2
4	Weight	15 kg
5	Efficiency	55-65% solar energy to naturally purified water
6	Expected Life Span	10 – 20 years
7	Installation & Maintenance	10 – 15 minutes installation Zero/minimal maintenance

*Note: Extracted from (F Cubed Limited, n.d.)

3.3 Experimental Setup

The overall experiment setup was depicted in Figure 3.7 and 3.8. This setup was built up of one water tank, one MLFC solar water heater, one carocell, water pipe and hose. Carocell was connected to MLFC solar water heater via water tube. Eight thermocouples t_1, t_2, t_3, t_4, t_5, t_6, t_7 and t_8 were put at different locations in the system to measure the temperatures of the designated locations. A pyranometer was used to measure the global horizontal irradiance (GHI) of the sunlight. Thermocouples and pyranometer were connected to a data logger for data collection. During experiment, water was allowed to channel to the MLFC solar water heater and Carocell A at a fixed flow rate. The experiment ran from 11am to 5pm in sunny days. The final yield of the distillate in a day was measured to investigate the performance of the overall system. Different flow rates of 3 LPH, 5 LPH, 7 LPH and 9 LPH were evaluated in order to get the optimal flow rate of the system. The list of equipment used was shown in Table 3.7.

Figure 3.7: Picture of experimental setup

Table 3.7: Equipment used in the experiment

No	Items	Function	Quantity
1	Data Logger	A device used to record and monitor temperature and GHI.	1
2	Pyranometer	A device used to measure GHI	1
3	Thermocouple	A sensor for measuring temperature with the aid of thermopaste.	8
4	Measuring Cylinder	A glassware for measuring and controlling the flow rate of water	1

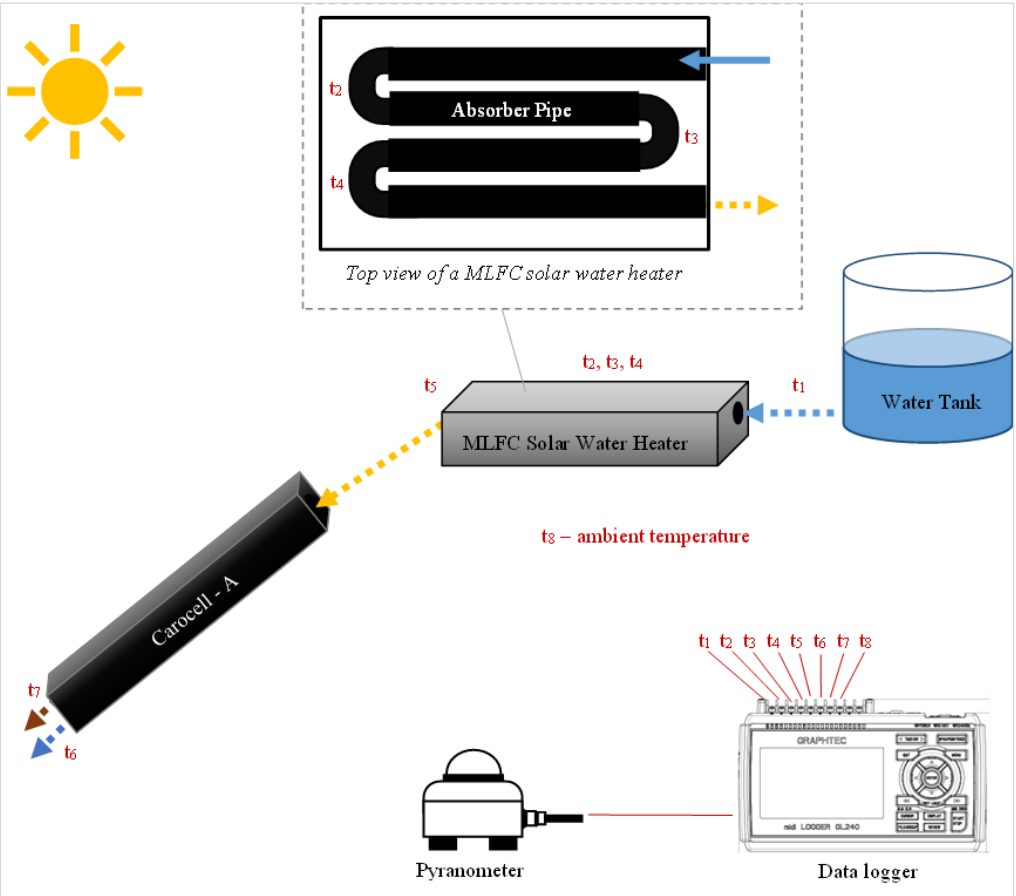

Figure 3.8: Schematic diagram of the experimental setup

3.4 Transient Mathematical Model

The transient mathematical model of solar distillation system is developed to simulate the water yield of the system without conducting the on-site experiment which is costly and time consuming. The test data are measured

every second. In an idealized system, the following assumptions were made:

i. The absorber pipe, the transparent glazing cover and water have a consistent temperature distribution.
ii. The ambient wind speed is constant throughout the simulation
iii. The MLFC REWART Solar Distillation System is in a steady state.
iv. There is no vapor leakage and the solar distillation system is air-tight
v. Same ambient temperature exists at the front and back of the MLFC REWART Solar Distillation System.
vi. No shading of MLFC REWART Solar Distillation System
vii. Dust effects on the cover are negligible.

The structure of the desalination unit - carocell used is depicted in Figure 3.9. It has an aluminium frame, galvanized steel legs and coated polycarbonate plastic sheet covers. There is a thin aluminium sheet underneath the absorber mat which helps to distribute the water across the absorber mat. When heated, the panel will distil the water on the absorber mat. The hot air will flow toward the panel's top, and then reverse its direction to flow to the panel's bottom. During this circulation process, the water vapor touches the cool transparent cover surfaces at the top and bottom of the unit, causing condensation. The condensed water flows down the panel and is then collected in the distillate channel (Mashaly and Alazba, 2017). According to Mousa and Arabi, 2009, the system can be modelled using energy balance and mass balance equations, and are solved the using 4th-order Runge–Kutta method.

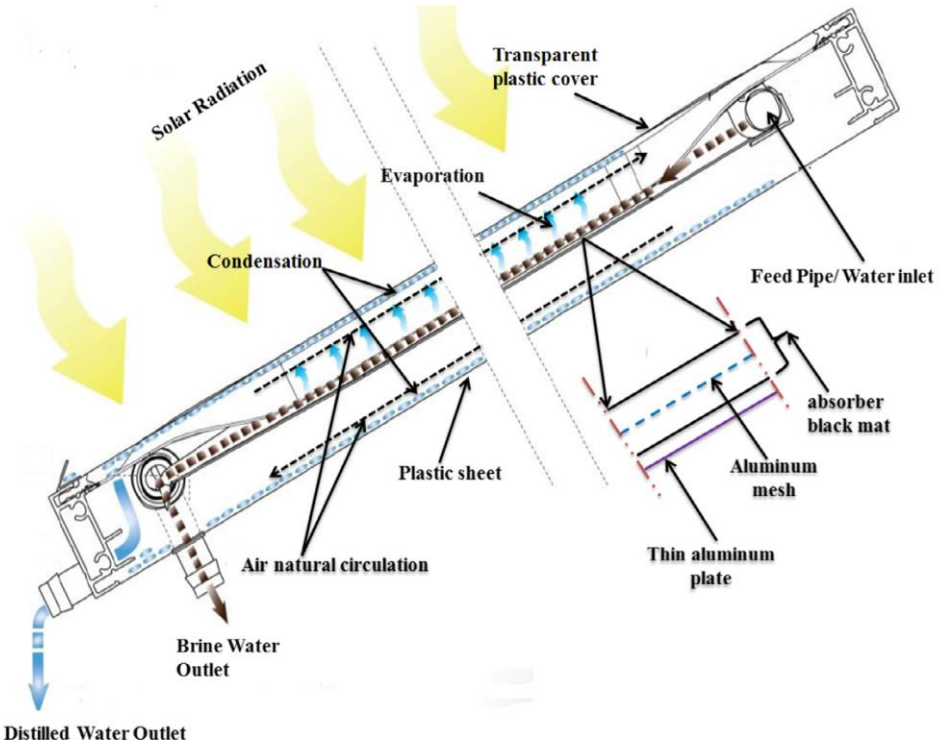

Figure 3.9: Schematic diagram of carocell (Mashaly and Alazba, 2017)

Energy balance can be performed on the black absorber mat, the plastic cover and the water film which gives:

Black Absorber Mat:

$$M_b C_b \frac{dT_b}{dt} = G(t)Aa_b - Q_{c,b-w} - Q_{loss} \quad (5)$$

Water Film:

$$M_w C_w \frac{dT_w}{dt} = G(t)Aa_w + Q_{c,b-w} - M_w C_w \frac{\partial T_w}{\partial x} dx - Q_{c,w-pc} - Q_{r,w-pc} - Q_{evap,w-pc} \quad (6)$$

Plastic Cover:

$$2M_{pc} C_{pc} \frac{dT_{pc}}{dt} = G(t)Aa_{pc} + Q_{c,w-pc} + Q_{r,w-pc} + Q_{evap,w-pc} - Q_{r,pc-sky} - 2Q_{c,pc-a} \quad (7)$$

Total water produced:

$$\frac{dM_p}{dt} = \frac{h_{evap,w-pc}(T_w - T_{pc})}{h_{evap}} \quad (8)$$

where all the abbreviations and symbols are defined as follows:

b = black absorber mat
pc = transparent plastic cover
w = water film
G = irradiation solar energy, W/m^2
A = aperture area of inclined solar still, m^2
t = time, s
M_p = mass of produced water, kg
M_b = mass of black absorber mat, kg
M_w = mass of water film, kg
M_{pc} = mass of plastic cover, kg
C_b = specific heat capacity of black absorber mat, J/kg.K
C_w = specific heat capacity of water, J/kg. K
C_{pc} = specific heat capacity of plastic cover, J/kg. K
T_b = temperature of black absorber mat, K
T_w = temperature of water film, K
T_{pc} = temperature of plastic cover, K
a_b = absorptance of black absorber mat
a_w = absorptance of water film
a_{pc} = absorptance of plastic cover
$Q_{c,b\text{-}w}$ = convective heat transfer between water film and black absorber mat, W
Q_{loss} = heat lost from the black absorber mat to the surrounding per unit area, W
$Q_{c,w\text{-}pc}$ = convective heat transfer between water film and plastic cover, W
$Q_{r,w\text{-}pc}$ = radiation heat transfer between water film and plastic cover, W
$Q_{evap,w\text{-}pc}$ = heat transfer due to evaporation from water film to plastic cover, W
$Q_{r,pc\text{-}sky}$ = radiation heat transfer between plastic cover and surrounding, W
$Q_{c,pc\text{-}a}$ = convective heat transfer between plastic cover and surrounding, W
$h_{evap,w\text{-}pc}$ = evaporation heat transfer coefficient between water film and plastic cover, W/m^2.K
$h_{evap,}$ = latent heat of vaporization of water, J/kg

As there are two plastic covers which allows condensation, the mass of the plastic cover and convective heat flux from the plastic cover to ambient are multiplied by two. The heat transfer between the black absorber mat, water film, plastic cover and surrounding are supported by:

$$Q_{c,b-w} = h_{c,b-w}A(T_b - T_w) \quad (9)$$

$$Q_{loss} = h_s A(T_b - T_a) \quad (10)$$

$$Q_{c,w-pc} = h_{c,w-pc}A(T_w - T_{pc}) \quad (11)$$

$$Q_{r,w-pc} = h_{r,w-pc}A(T_w - T_{pc}) \quad (12)$$

$$Q_{evap,w-pc} = h_{evap,w-pc}A(T_w - T_{pc}) \quad (13)$$

$$Q_{c,pc-a} = h_{c,pc-a}A(T_{pc} - T_a) \quad (14)$$

$$Q_{r,pc-sky} = h_{r,pc-sky}A(T_{pc} - T_{sky}) \quad (15)$$

where

h_s = heat loss coefficient from side to the surrounding, W/m^2.K
$h_{c,b\text{-}w}$ = convective heat transfer coefficient between black absorber mat and water film, W/m^2.K
$h_{c,w\text{-}pc}$ = convective heat transfer coefficient between water film and plastic cover, W/m^2.K
$h_{r,w\text{-}pc}$ = radiation heat transfer coefficient between water film and plastic cover, W/m^2.K
$h_{evap,w\text{-}pc}$ = evaporation heat transfer coefficient between water film and glass cover, W/m^2.K
$h_{c,pc\text{-}a}$ = convective heat transfer coefficient between plastic cover and surrounding, W/m^2.K
$h_{r,pc\text{-}sky}$ = radiation heat transfer coefficient between plastic cover and surrounding, W/m^2.K
T_a = ambient temperature, K
T_{sky} = sky temperature, K

The heat transfer coefficients are given by:

$$h_{r,w-pc} = \varepsilon_{eff}\sigma\left(T_w^2 + T_{pc}^2\right)\left(T_w + T_{pc}\right) \quad (16)$$

$$h_{evap,w-g} = 16.273\ x\ 10^{-3}h_{c,w-pc}\frac{(P_w - P_{pc})}{(T_w - T_{pc})} \quad (17)$$

$$h_{c,w-pc} = 0.884\ x\ (T_w - T_{pc} + \frac{(P_w - P_{pc})T_{wf}}{268900 - P_w})^{\frac{1}{3}} \quad (18)$$

$$h_{r,pc-sky} = \varepsilon_{eff}\sigma\left(T_{pc}^2 + T_{sky}^2\right)\left(T_{pc} + T_{sky}\right) \quad (19)$$

$h_{c,pc-a} = 2.8 + 3.0w$, $0<w<5ms^{-1}$ (Abdullah et al., 2022) (20)

$$\varepsilon_{eff} = (\frac{1}{\varepsilon_w} + \frac{1}{\varepsilon_{pc}} - 1)^{-1} \quad (21)$$

$$T_{sky} = (T_a - 6) \quad (22)$$

$\frac{1}{h_b} = \frac{\delta_i}{k_i} + \frac{1}{h_{cb}+h_{rb}}$ (Tiwari and Sahota, 2017) (23)

where
ε_w = emissivity of water film
ε_{pc} = emissivity of plastic cover
ε_{eff} = effective emissivity between water film and plastic cover
σ = Stefan-Boltzmann constant, W/m^2.K^4
P_w = partial vapor pressure of water at water film, N/m^2
P_{pc} = partial vapor pressure of water at plastic cover, N/m^2
w = wind speed, m/s
δ_i = thickness of the black plate insulation, m
k_i = thermal conductivity of the black plate insulation, W/m.K
h_{cb} = convective heat transfer coefficient between the bottom and ambient, W/m^2.K
h_{cb} = radiative heat transfer coefficient between the bottom and ambient, W/m^2.K

The absorptance of the black plate, water film and plastic cover are given by:

$$a_b = (1 - \rho_{pc} - a_w - a_{pc})\alpha_b \tag{24}$$

$$a_{wf} = (1 - \rho_{pc} - a_{pc})\alpha_w \tag{25}$$

$$a_{pc} = (1 - \rho_{pc})\alpha_{pc} \tag{26}$$

where ρ_{pc} is reflectivity of the plastic cover; α_b, α_w and α_{pc} is absorptivity of black absorber mat, water film and plastic cover respectively.

As discussed by Zurigat and Abu-Arabi, 2004, the variation of the flowing water temperature from inlet to outlet is assumed linear so that the term $\frac{\partial T_{wf}}{\partial x} dx$ is expressed in terms of the inlet water film temperatures as:

$$\frac{\partial T_w}{\partial x} dx = 2(T_w - T_{w,in}) \tag{27}$$

The partial pressure of water vapor at water and plastic cover temperatures can be obtained from the following expression (Abdullah et al., 2022).

$$P(T) = exp\left[25.317 - \frac{5144}{T+273}\right] \tag{28}$$

The latent heat of vaporization, h_{evap} (J/kg) is a function of temperature and can be expressed as (Tiwari and Sahota, 2017):

$$h_{evap} = 3161500\ (1 - 0.0007616T) \text{ for T} > 70^{o}\text{C} \quad (29)$$

$$h_{evap} = 2493500\ (1 - 0.0009477\ T + 0.0000001313\ T^2 - 0.000000004497\ T^3) \text{ for T} < 70^{o}C \quad (30)$$

Simulation parameters of MLFC REWART Distillation System are summarized in Table 3.8. The whole simulation was performed using EXCEL and was compared to the experiment result in graphs.

Table 3.8: Simulation Parameters of MLFC REWART Distillation System

Parameters	Symbol	Value
Mass of absorber plate	M_b	6.6 kg
Specific heat capacity of absorber plate*	C_b	473 J/kg.^{o}C
Absorptivity of absorber plate*	α_b	0.95
Reflectivity of absorber plate*	ρ_b	0.0735
Mass of plastic cover	M_{pc}	1.2 kg
Specific heat capacity of plastic cover	C_{pc}	1,200 J/kg.^{o}C
Absorptivity of plastic cover*	α_{pc}	0.0475
Reflectivity of plastic cover*	ρ_{pc}	0.0735
Emissivity of plastic cover*	ε_{pc}	0.88
Density of water	ρ_w	997 kg/m^3
Specific heat capacity of water	C_w	4,184 J/kg.^{o}C
Mass of water	M_w	9.97 kg
Absorptivity of water*	α_w	0.05
Emissivity of water*	ε_g	0.96
Latent heat of vaporization	h_{fg}	2,260 kJ/kg
Convective heat transfer coefficient from black plate to water film*	$h_{c,b\text{-}w}$	135 W/m^2.^{o}C
Wind speed	w	1 m/s
Stefan Boltzmann constant	σ	5.6697x10^{-8} W/m^2.K^4

*Note: value cited from Mousa and Arabi, 2009

3.5 Performance Analysis and Validation

Firstly, the time series graphs of GHI, ambient temperature, MLFC inlet water temperature and outlet water temperature were plotted to study the thermal process of MLFC. Subsequently, the following relationships of MLFC REWART Distillation System were plotted and studied:

- Effect of Water Flow Rate on the Water Yield
- Effect of GHI and Inlet Temperature on the Water Yield
- A comparison of system efficiency between different flow rates for MLFC heating system and water yield
- A comparison of water yield between experiment result and theoretical result from mathematical model.
- A study of steady state condition using the mathematical model

The hourly yield rate (l/m^2/h) of freshwater, m_p is described by:

$$Yield\ Rate = \frac{Average\ \ hourly\ Water\ Generated}{Aperture\ Area\ x\ Time\ (hour)} \tag{31}$$

The system efficiency of MLFC heating system is the energy lost to heating the water divided by the energy absorbed by MLFC, which is given by:

$$\eta = \frac{Q_u}{Q_{in}} = \frac{\sum M_w C_w (T_{MLFC,o} - T_{MLFC,i}) + M_f C_w\ (T_{m,f} - T_{m,i})}{\sum G A_{a,MLFC}} x100 \tag{32}$$

where Q_u is the useful heat energy gained, Q_{inc} is the incident solar energy, M_w is the mass of water in the MLFC, M_f is the mass of flowing water, C_w is the specific heat capacity of water, $T_{MLFC,o}$ is the outlet water temperature of MLFC, $T_{MLFC,i}$ is the inlet water temperature of MLFC and $A_{a,MLFC}$ is the aperture area of MLFC. $T_{m,f}$ and $T_{m,i}$ is the mean temperature of the outlet and inlet water

temperature, respectively.

The system efficiency of water yield is given by the energy used for the water evaporation divided by the amount of incident solar radiation collected.

$$\eta = \frac{Q_{ev}}{Q_{in}} = \frac{\sum \dot{m}\, x\, h_{fg}}{\sum GA_{a,MLFC\ REWART}} x100 \quad (33)$$

where Q_{ev} is heat energy used for evaporation, $\dot{m}$ is water yield from SS, h_{fg} is the latent heat of vaporization and $A_{a,\ MLFC\ REWART}$ is the total aperture area of both MLFC and carocell.

CHAPTER 4

RESULT

4.1 Performance analysis of Solar Distillation System

The performance of the MLFC REWART Solar Distillation System was analyzed for different inlet water flow rate 3LPH, 5LPH, 7LPH, and 9LPH. The raw data and time series graphs of the each data collection were presented in Appendix II. The details of experiment data were summarized in Table 4.1. The water temperature at the outlet of the MLFC ($T_{MLFC,o}$ or $T_{w,in}$) can be pre-heated up to approximately 80ºC by MLFC for lower flow rate 3LPH and 5LPH. The ranges of maximum irradiance, ambient temperature (T_a), water tank temperature ($T_{MLFC,\,i}$) and water yield (FWY) recorded are approximately 950 W/m^2 to 1,150 W/m^2, 36 ºC to 40ºC, 40ºC to 44ºC and 1.6 l/h to 2.4 l/h.

Table 4.1: Information of experiment data

Flow Rate	3 LPH	5 LPH	7 LPH	9 LPH
Date of data collection	2022-07-14 2022-07-15 2022-07-16 2022-07-17 2022-07-14	2022-07-20 2022-07-21 2022-07-22 2022-07-27	2022-07-30 2022-07-31 2022-08-01 2022-08-05 2022-09-16 2022-09-22 2022-09-23	2022-09-07 2022-09-09 2022-09-15
Max. irradiance or GHI	980.97 W/m^2	1,150.81 W/m^2	1,093.06 W/m^2	951.77 W/m^2
Max. FWY	2.27 l/h	1.99 l/h	2.35 l/h	1.59 l/h
Max. $T_{MLFC,o}$ or $T_{w,in}$	79.38ºC	80.05ºC	74.47ºC	70.29ºC
Max. T_a	39.80ºC	40.79ºC	36.79ºC	40.30ºC
Max. $T_{MLFC,i}$	44.00ºC	42.14ºC	40.29ºC	38.48ºC

The pattern of irradiance, MLFC water temperature and ambient temperature for 3LPH, 5LPH, 7LPH and 9LPH are studied and plotted in Figures 4.1, 4.2, 4.3 and 4.4 respectively. It is observed that the ambient temperature and water tank temperature changed slightly following the trend of irradiance.

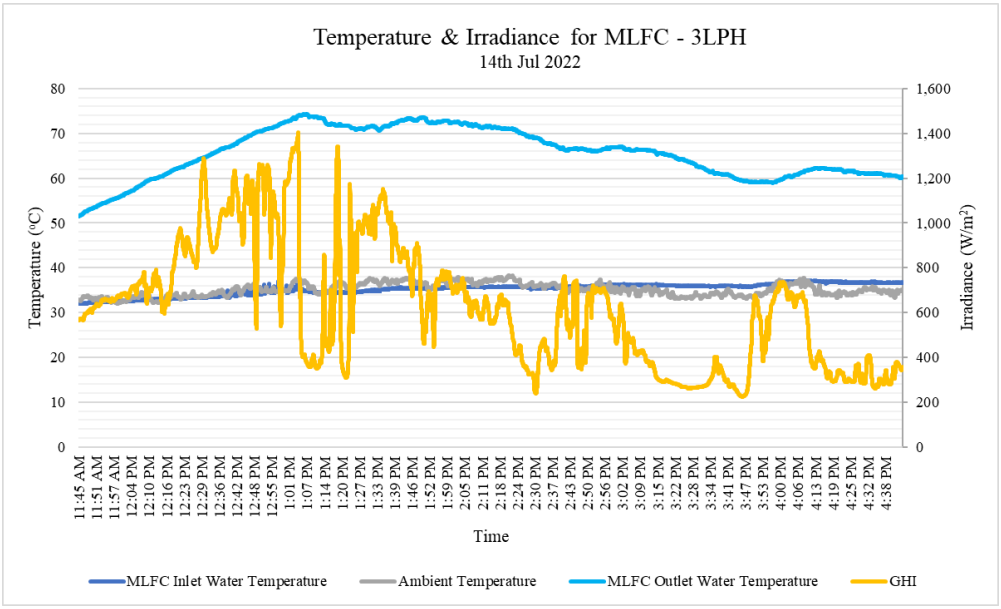

(a)

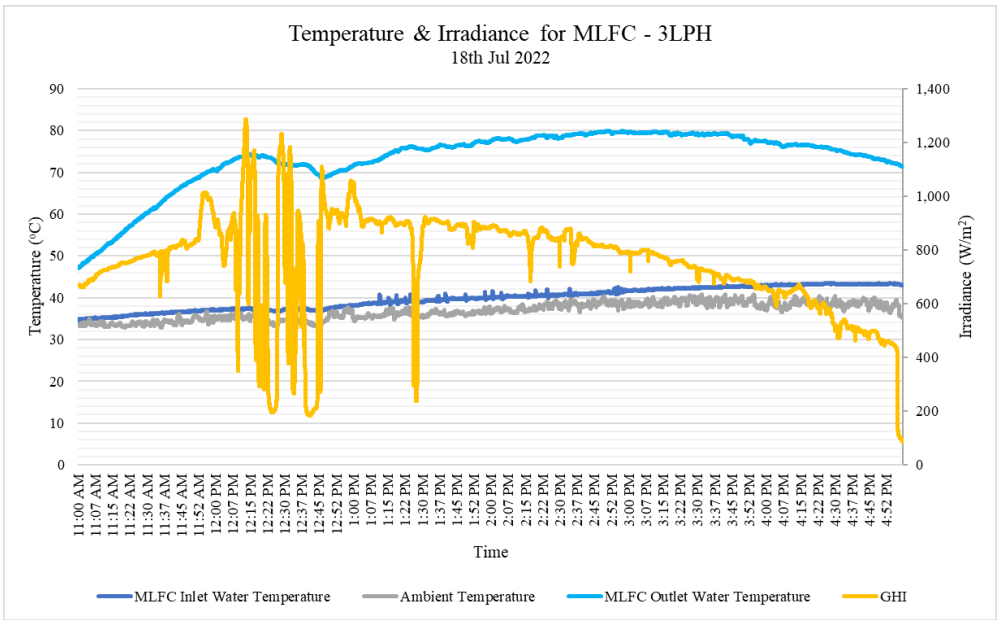

(b)

Figure 4.1: The graph of GHI, ambient temperature, MLFC's water inlet and outlet temperature vs time for flow rate 3LPH (a) 14-07-2022 (b) 18-07-2022

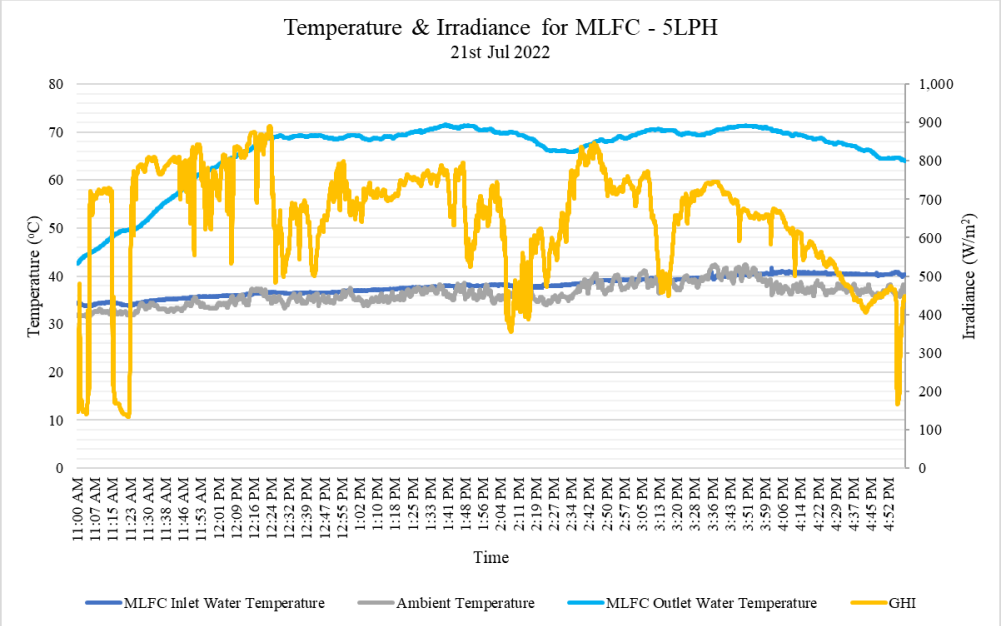

(a)

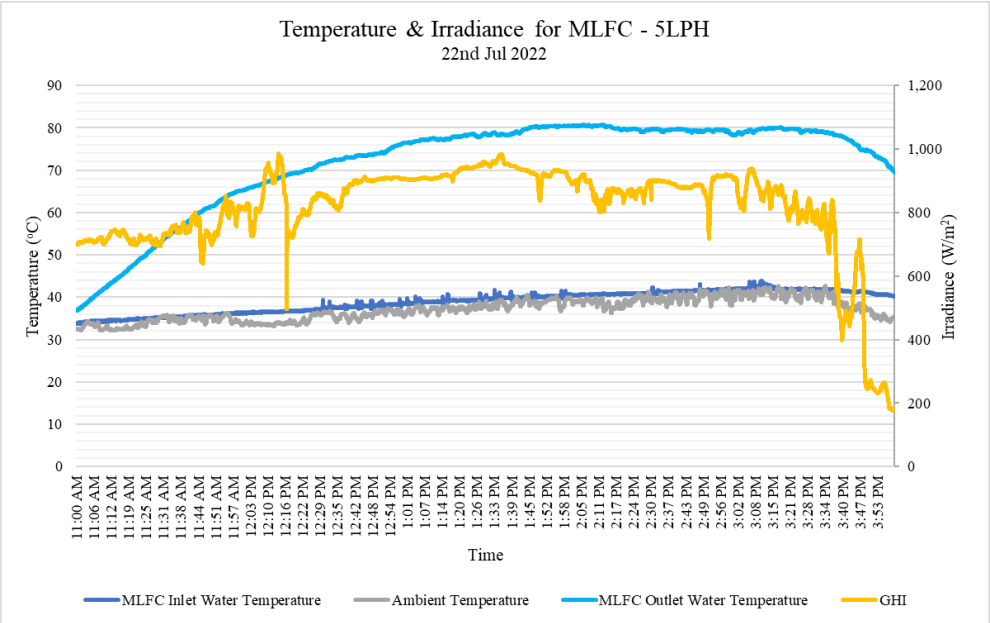

(b)

Figure 4.2: The graph of GHI, ambient temperature, MLFC's water inlet and outlet temperature vs time for flow rate 5LPH (a) 21-07-2022 (b) 22-07-2022

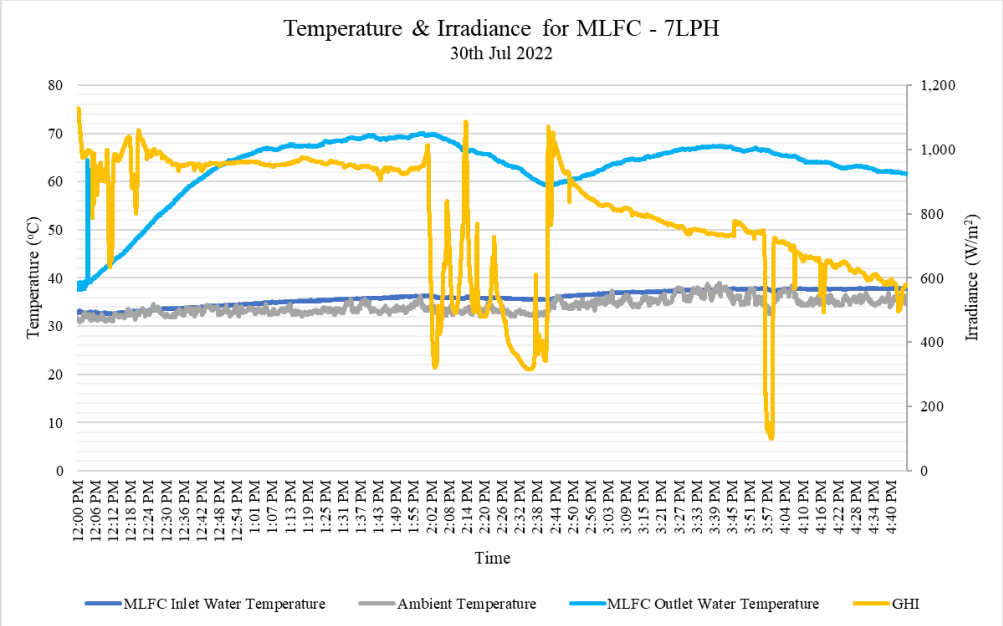

(a)

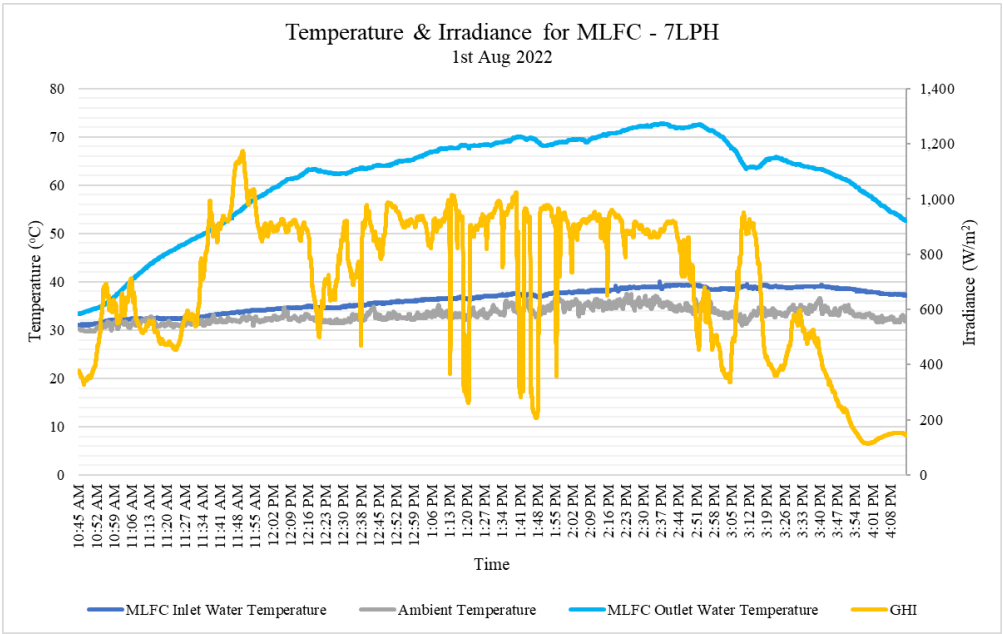

(b)

Figure 4.3: The graph of GHI, ambient temperature, MLFC's water inlet and outlet temperature vs time for flow rate 7LPH (a) 30-07-2022 (b) 01-08-2022

It can be concluded from Figure 4.1 to 4.4 that water take time to gain sufficient energy in order to rise the temperature. Once the saturated water temperature is reached, $T_{MLFC,o}$ will stop rising even with continuous same level of irradiance. The reason is the MLFC heating system has reached its maximum level where energy gained is the same as energy loss.

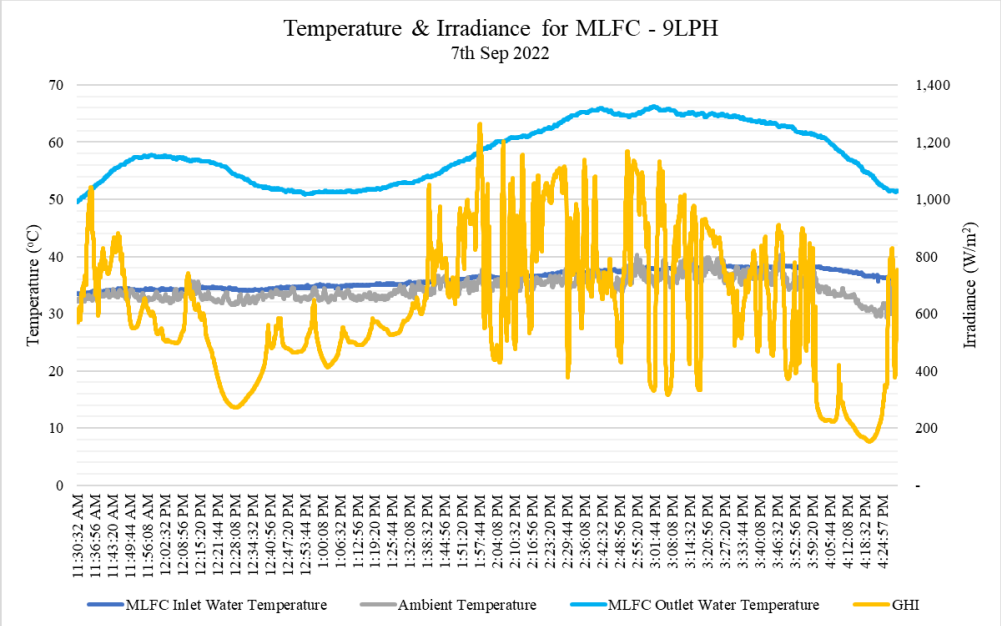

(a)

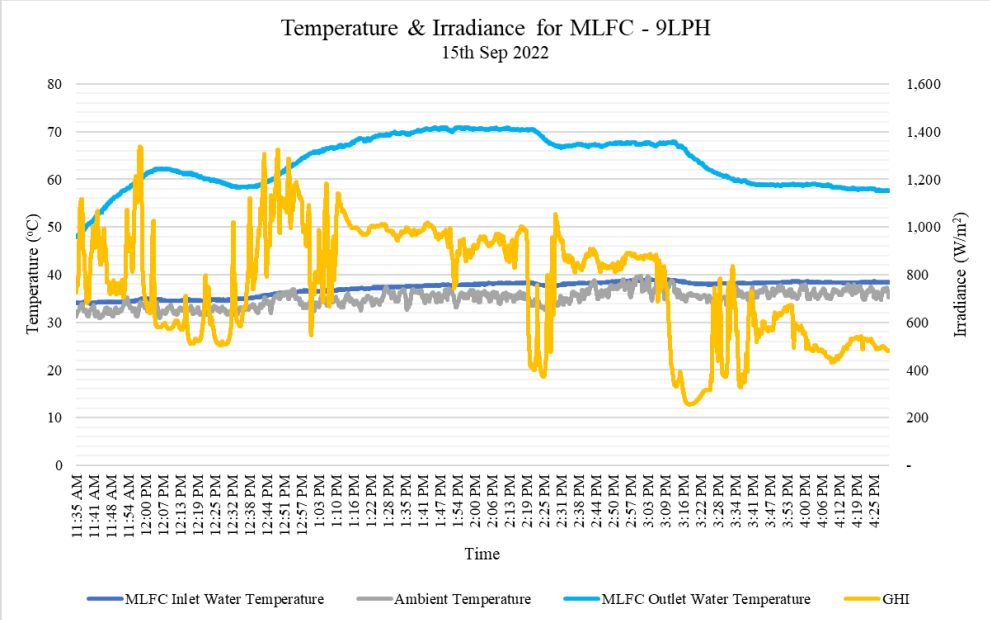

(b)

Figure 4.4: The graph of GHI, ambient temperature, MLFC's water inlet and outlet temperature vs time for flow rate 7LPH (a) 07-09-2022 (b) 15-09-2022

Furthermore, the effect of REWART's inlet water temperature, $T_{w,in}$ which was pre-heated by MLFC, on the water yield was studied as shown in Figure 4.5, 4.6, 4.7, 4.8 and 4.9. The data collected were categorized into 3 inlet water temperature groups: 50°C~60°C, 60°C~70°C and 70°C~80°C.

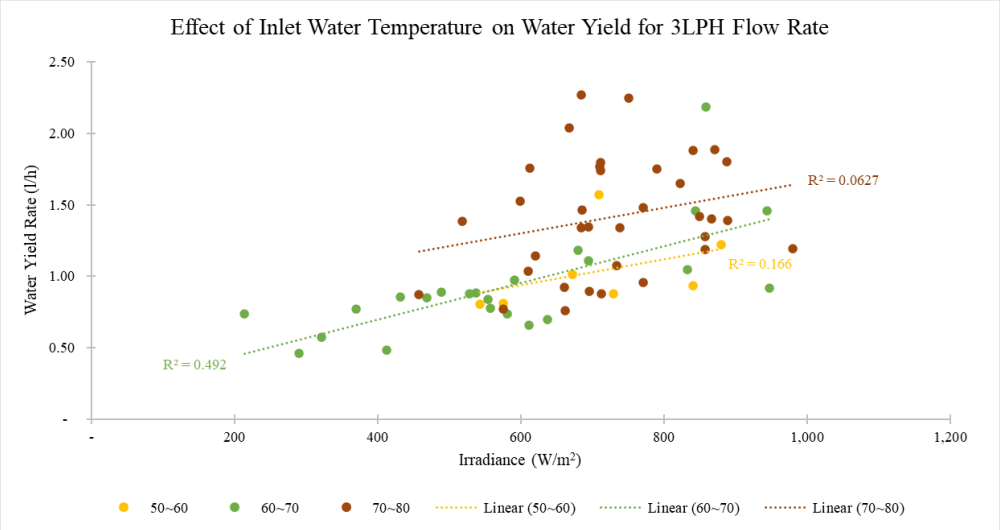

Figure 4.5: Graph of water yield rate against irradiance for 3LPH

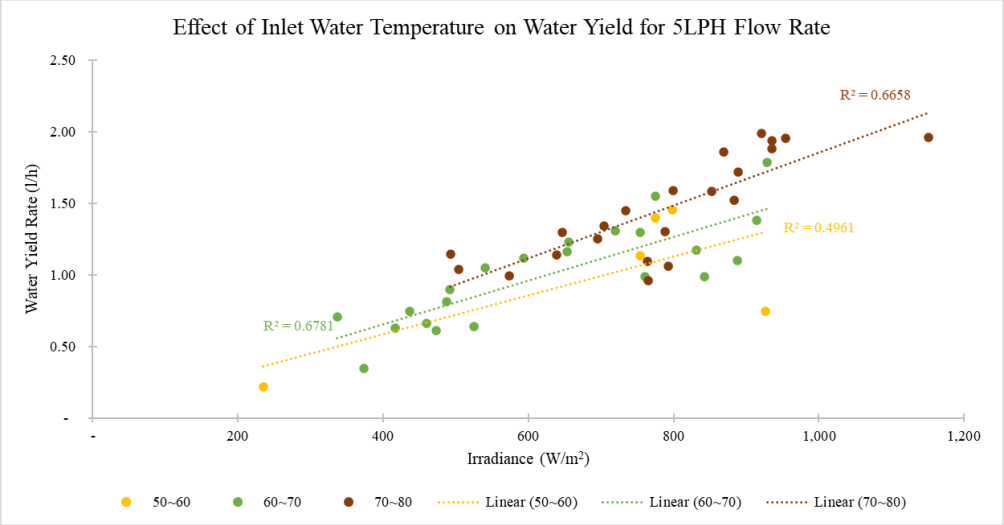

Figure 4.6: Graph of water yield rate against irradiance for 5LPH

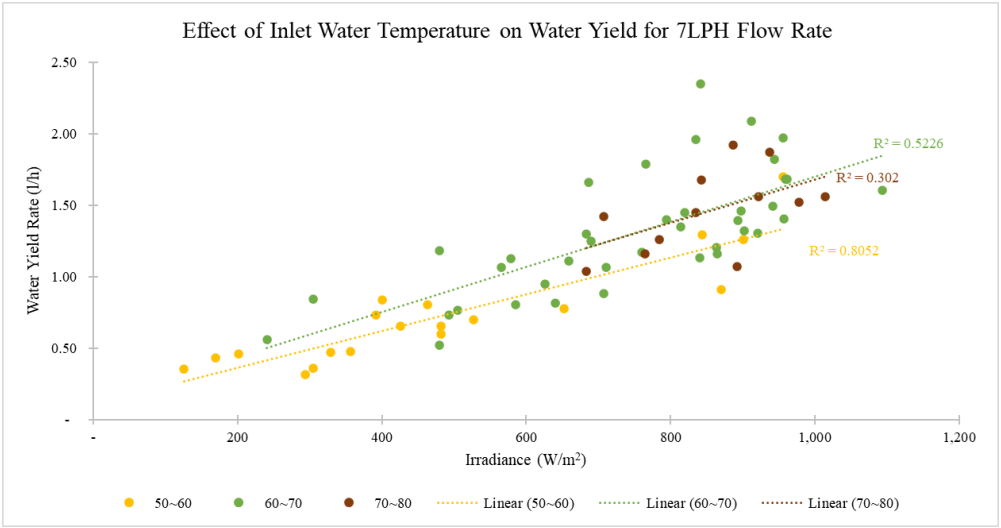

Figure 4.7: Graph of water yield rate against irradiance for 7LPH

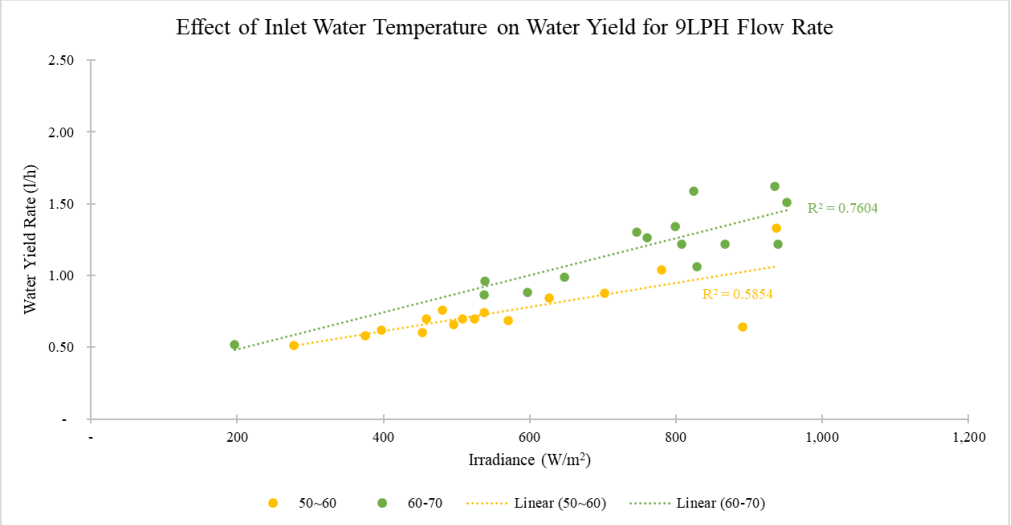

Figure 4.8: Graph of water yield rate against irradiance for 9LPH flow rate

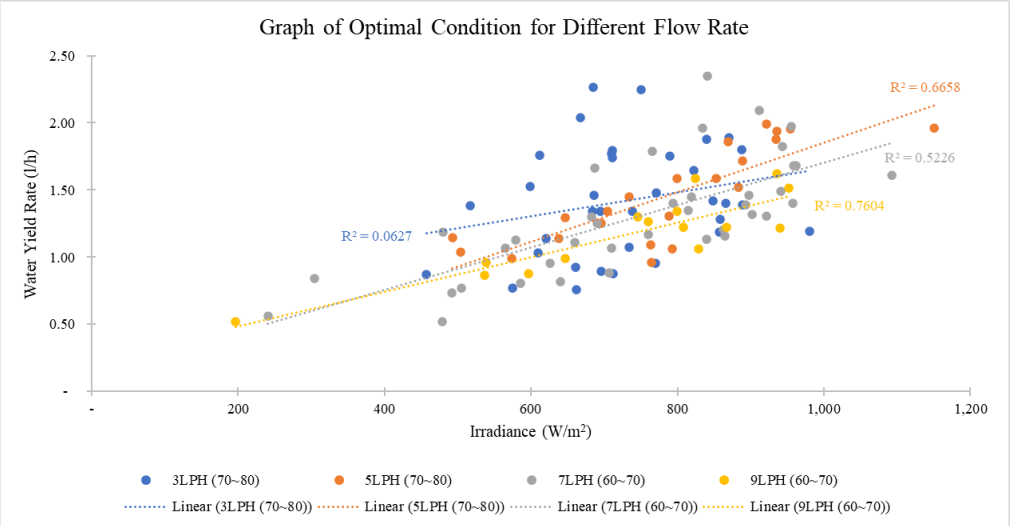

Figure 4.9: Graph of optimal condition for different flow rates

It can be deduced from Figure 4.5 to 4.9 that for each flow rate, the higher the irradiance, the greater the water yield. Figure 4.5 and 4.6 are showing that the flow rates 3LPH and 5LPH can yield more clean water at water inlet temperature 70ºC~80ºC respectively. Whereas for flow rates 7LPH and 9LPH, the water inlet temperature 60ºC~70ºC allows more production of clean water as depicted in Figure 4.7 and 4.8. It can be obviously observed that the high flow rate 9LPH has lowest FWY (up to 1.5 l/h) as compared to other flow rates

(up to 2.5 l/h). The optimal condition of each flow rate was compared and plotted in Figure 4.9. It is observed that 3LPH (70°C-80°C) can produce more volume of clean water when the irradiance is less than 800 W/m^2, whereas 5LPH (70°C-80°C) produce more volume of clean water when the irradiance is more than 800 W/m^2.

On top of that, the effect of flow rate on water yield for different categories of inlet water temperature was studied. Figure 4.10 is showing FWY at inlet water temperature 50°C~60°C can be up to 1.5 l/h which is lower than groups 60°C~70°C and 70°C~80°C. At this group, the influence of flow rate is not significant. When the inlet water temperature is at 60°C~70°C (Figure 4.11), the FWY of flow rate 7LPH is relatively high as compared to other flow rates. When it comes to 70°C~80°C (Figure 4.12), it is observed that 3LPH can produce more clean water when the irradiance is less than 800 W/m^2, whereas 5LPH produce more clean water when the irradiance is greater than 800 W/m^2.

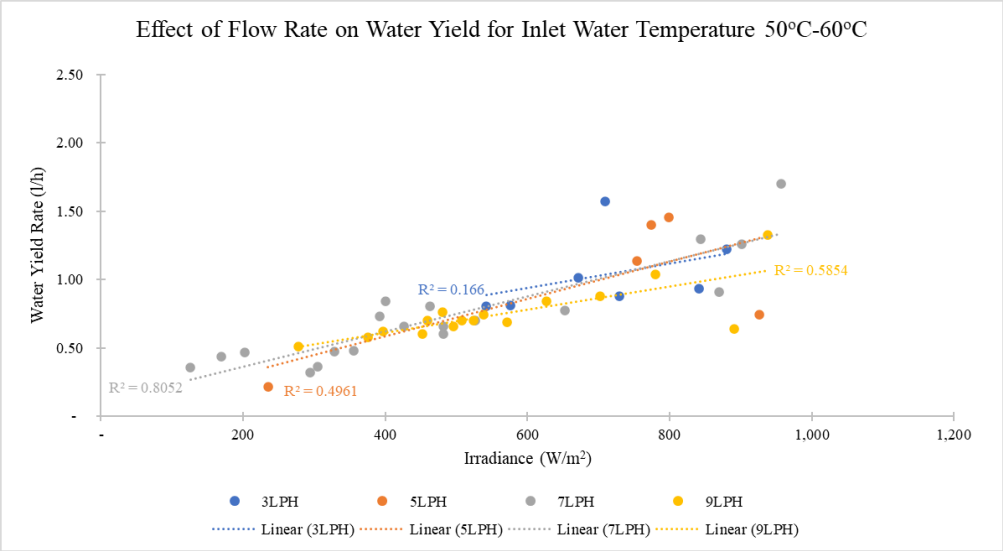

Figure 4.10: Graph of water yield against irradiance for inlet water temperature 50°C~60°C

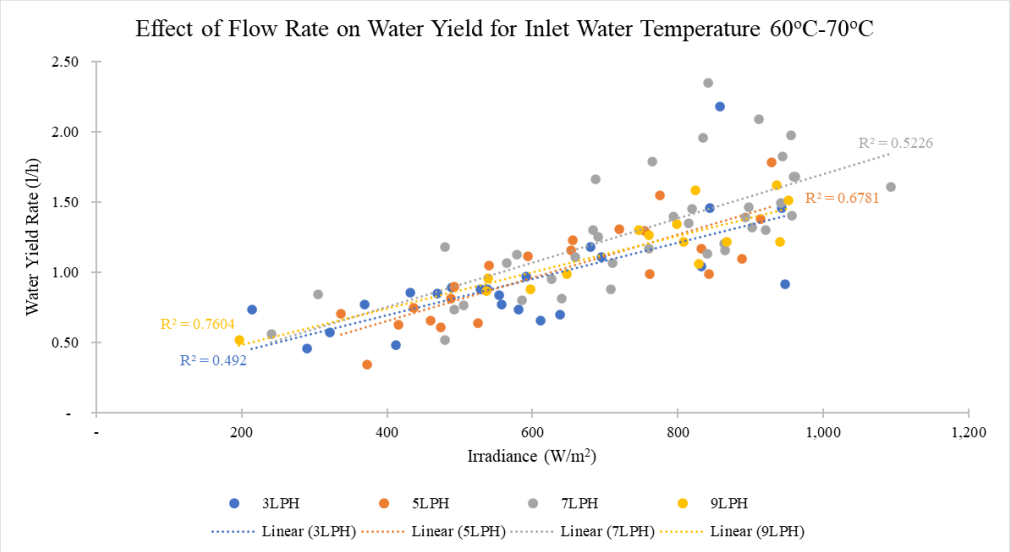

Figure 4.11: Graph of water yield against irradiance for inlet water temperature 60ºC~70ºC

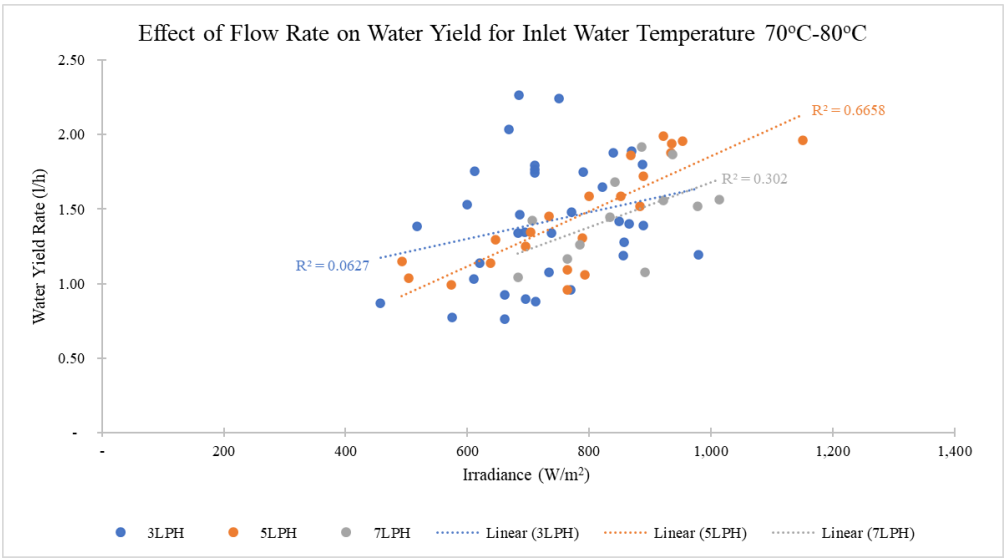

Figure 4.12: Graph of water yield against irradiance for inlet water temperature 70ºC~80ºC

4.2 System Efficiency

4.2.1 System Efficiency for MLFC Solar Water Heater System

The average efficiency for MLFC Solar Water Heater System for different flow rates was tabulated in Table 4.2. The time interval used is 10 minutes. The

average efficiency increases when the flow rate increases. The higher the flow rate, the lower the change of water temperature in the system. Thus, the energy loss to the ambient is lower which eventually leads to higher useful energy for heating the water.

Table 4.2: System Efficiency for MLFC Solar Water Heater System

Flow Rate	**3LPH**		**5LPH**		**7LPH**		**9LPH**	
	Date	η (%)	Date	η (%)	Date	η (%)	Date	η (%)
MLFC heating efficiency per collection date	07-14	32.47%	07-20	45.18%	07-30	51.73%	09-07	66.48%
	07-15	34.73%	07-21	45.68%	07-31	62.75%	09-09	67.82%
	07-16	34.18%	07-22	43.89%	08-01	56.37%	09-15	65.07%
	07-17	28.83%	07-27	44.67%	08-05	55.04%		
	07-18	29.49%			09-16	56.38%		
					09-22	56.90%		
					09-23	57.27%		
Average Efficiency		**31.94%**		**44.86%**		**56.63%**		**66.46%**

4.2.2 System Efficiency for Water Yield

The time interval used to calculate the average efficiency for water yield is 30 minutes. The result is tabulated in Table 4.3. It is observed that the 3LPH has achieved the highest water yield efficiency with value of 45.59% as compared to other flow rates. When the flow rate is lower, the evaporation rate is higher for the same solar intensity because less inlet water enters the system. The residence time is bigger and the amount of water on the surface of absorber mat is lesser leading to a higher water film temperature. As a result, the vapor pressure is higher and therefore more evaporation occurs (Mousa and Arabi, 2009).

Table 4.3: System efficiency for Water Yield

Flow Rate	3 LPH		5 LPH		7 LPH		9 LPH	
	Date	η (%)	Date	η (%)	Date	η (%)	Date	η (%)
Water yield efficiency per collection date	07-14	41.19%	07-20	43.58%	07-30	43.02%	09-07	35.71%
	07-15	38.55%	07-21	43.07%	07-31	48.02%	09-09	35.68%
	07-16	59.77%	07-22	43.07%	08-01	47.88%	09-15	34.12%
	07-17	47.81%	07-27	36.15%	08-05	34.77%		
	07-14	40.64%			09-16	38.10%		
					09-22	33.66%		
					09-23	37.86%		
Average Efficiency		**45.59%**		**41.47%**		**40.47%**		**35.17%**

4.3 Mathematical Modelling

Experiment data are used to validate the mathematical modelling developed for this dissertation. The experiment data of GHI, T_a, and $T_{w,in}$ for each date were inserted into simulation. The initial temperature of plastic cover, T_{pc} is assumed to be the initial T_a, whereas the initial temperature of black plate, T_b and water film, T_w are assumed to be the initial $T_{w,in}$. Temperature $T_{pc,}$ T_b and T_w are the 3 key factors calculated from energy balance equations which contribute to find the simulated water yield. Accumulated water produced was recorded to compare the theoretical and experimental results. The examples of the comparison theoretical and experimental result for different flow rates are given in Figure 4.13, 4.14, 4.15 and 4.16. The picture of running the model in EXCEL was captured and shown in APPENDIX III.

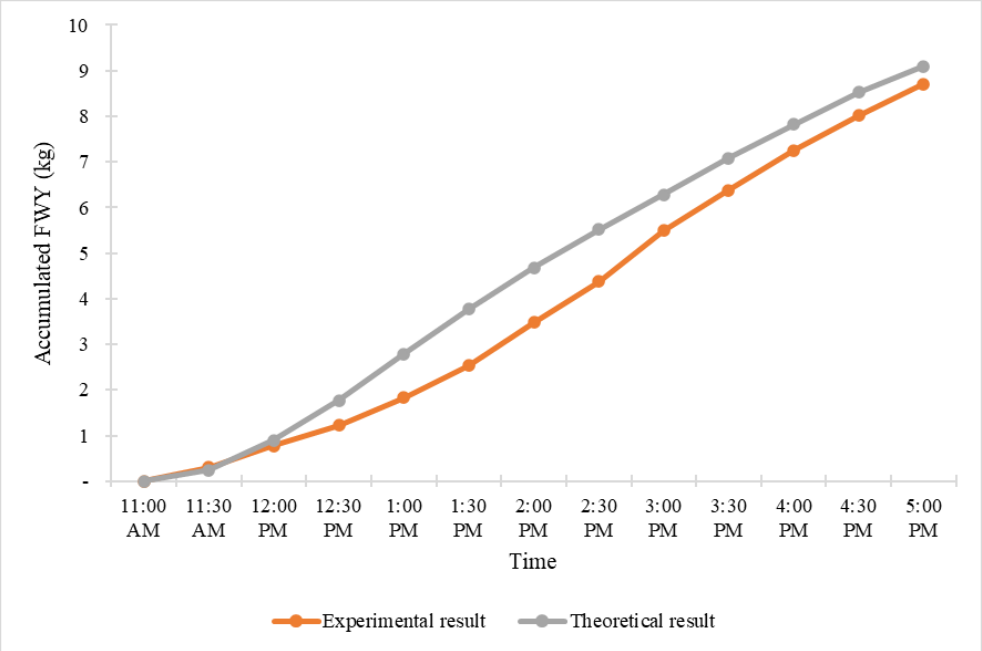

Figure 4.13: Accumulated water yield between theoretical and experimental result for 3LPH on 2022.07.17

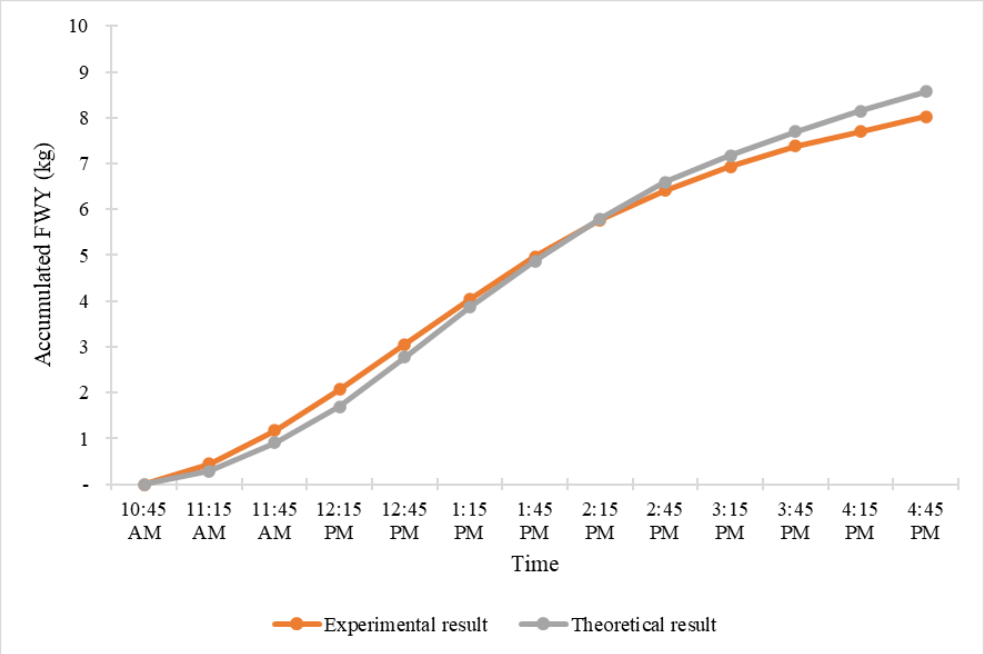

Figure 4.14: Accumulated water yield between theoretical and experimental result for 5LPH on 2022.07.20

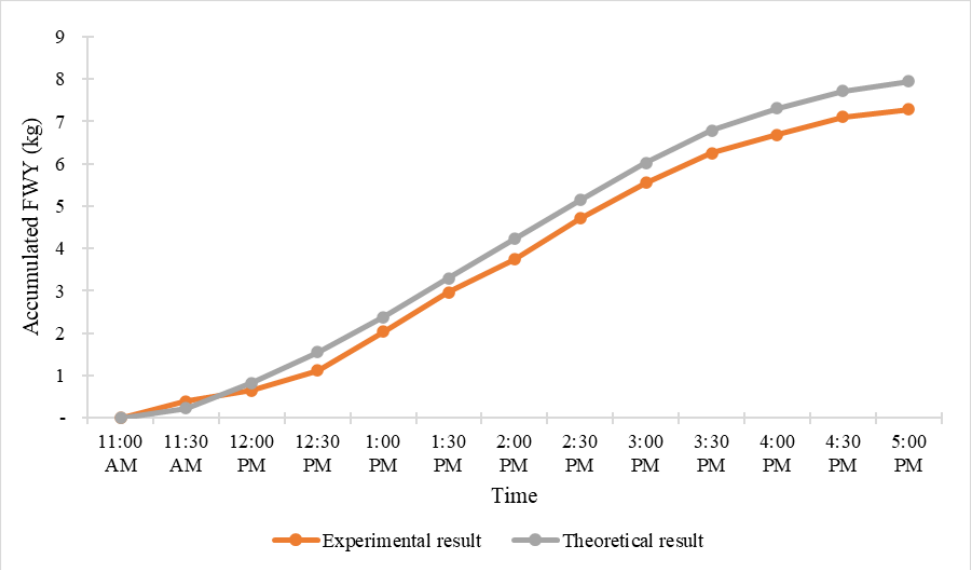

Figure 4.15: Accumulated water yield between theoretical and experimental result for 7LPH on 2022.07.31

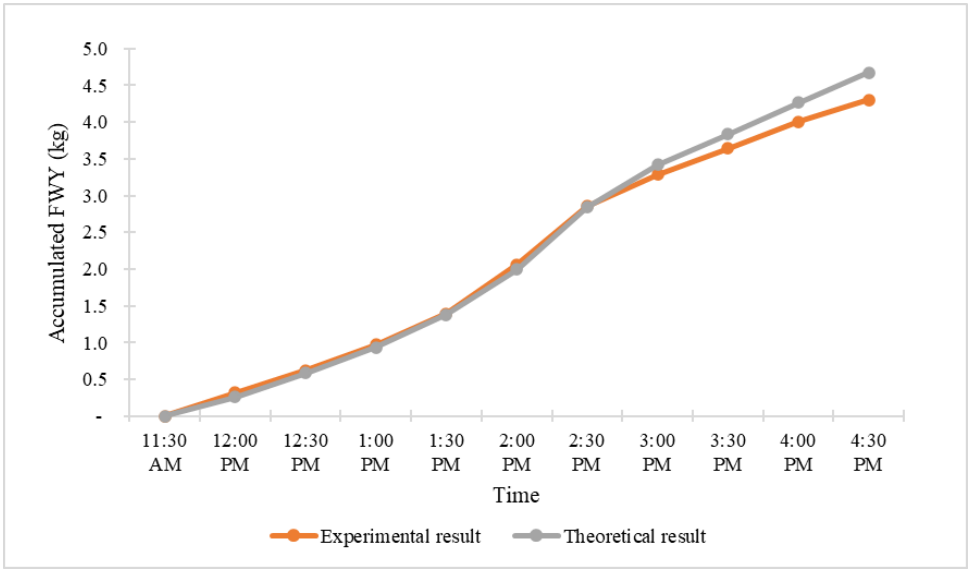

Figure 4.16: Accumulated water yield between theoretical and experimental result for 9LPH on 2022.09.09

Besides, percentage error (PE) is calculated to show the difference between experiment results and theoretical results from mathematical modelling. It is expressed by:

$$PE = \frac{|Simulated\ Value - Experiment\ Value|}{Experiment\ Value}\ x\ 100\% \qquad (34)$$

The PE for 19 data collection days is showing in Table 4.4. The average PE obtained is 13.03%. The variation between theoretical and experimental results might be due to different wind speed and heat transfer coefficient from black plate to water film which are assumed constant in simulation. Bigger wind velocity over the transparent cover increases the convective heat loss, which in turn reduces the temperature of the transparent cover. Eventually, the temperature difference between the inner surface of the transparent cover and evaporative surface increases; hence, this significantly increases the SS productivity (Tiwari and Sahota, 2017). In addition, the flow rate is measured manually using measuring cylinder instead of water flow meter which leads to accuracy problem and contributes to the variance.

Furthermore, the 27 steady-state conditions for different combinations of flow rate (3LPH, 5LPH, 7LPH), GHI (600W/m^2, 700 W/m^2, 800 W/m^2) and $T_{w,in}$ (60^{o}C, 70^{o}C, 80^{o}C) were assessed to study the optimal condition of the system via simulation. T_a and time interval were fixed at 30^{o}C and 6 hours, respectively. The effect of GHI, flow rate and $T_{w,in}$ on the MLFC REWART system were plotted in Figure 4.17. From the graph, it can be deduced that:

- When the flow rate and $T_{w,in}$ are fixed at certain level, the greater the solar irradiation received by SS, the greater the volume of FWY and vice versa. For example, the accumulated FWY for 3LPH and 60^{o}C increases from 6.52kg to 8.92kg when the irradiance increases from 600W/m^2 to 800W/m^2. This is agreed with study from Nguyen in 2018 on factors affecting the yield of solar distillation systems

- When the flow rate and irradiance are fixed at certain level, the higher the inlet water temperature, the greater the volume of FWY and vice versa. Taking example of 3LPH and 600W/m^2, the accumulated FWY increases from 6.52kg to 7.82kg when the $T_{w,in}$ increases from 60^{o}C to 80^{o}C.

- The effect of flow rates is different when the $T_{w,in}$ is at different level. Regardless of the irradiance, the accumulated FWY decreases with the increasing flow rates when $T_{w,in}$ is 60^{o}C, whereas the accumulated FWY increases with the increasing flow rates when $T_{w,in}$ is 80^{o}C. At $T_{w,in}$ = 70^{o}C, the accumulated FWY increases flow rates at GHI of 600W/m^2, does not change with flow rates at GHI of 700W/m^2, and decreases with flow rates at GHI of 800 W/m^2. When the $T_{w,in}$ is at 70^{o}C, the saturated temperature is reached and hence, there no much changes in accumulated FWY.

Moreover, the optimal conditions for the highest FWY per day are 10.28kg for 3LPH, 10.45kg for 5LPH and 10.59kg for 7LPH at GHI of 800 W/m^2 and $T_{w,in}$ of 80^{o}C. Based on the real-life experiment data, the maximum outlet water temperature achieved by MLFC for 3LPH and 5LPH is around 80^{o}C, whereas it turns out to be around 70^{o}C for 7LPH. This is because the residence time for water film temperature to heat up until 80^{o}C at the 7LPH is insufficient. Thus, 5LPH for highest productivity is assumed achievable.

Table 4.4: Percentage errors for each collection date

Flow Rate	**3LPH**				**5LPH**				**7LPH**				**9LPH**			
	Date	FWY (E)	FWY (M)	PE (%)	Date	FWY (E)	FWY (M)	PE (%)	Date	FWY (E)	FWY (M)	PE (%)	Date	FWY (E)	FWY (M)	PE (%)
Percentage Error (PE) per collection date	07-14	5.29	5.97	12.92%	07-20	8.03	8.38	4.42%	07-30	6.99	6.42	8.09%	09-07	4.53	5.03	11.09%
	07-15	4.98	5.68	14.01%	07-21	7.00	7.17	2.40%	07-31	7.28	7.76	6.54%	09-09	4.30	4.52	5.16%
	07-16	9.42	7.39	21.51%	07-22	7.28	7.82	7.50%	08-01	7.54	6.71	10.96%	09-15	5.33	6.38	19.72%
	07-17	8.71	8.90	2.25%	07-27	4.14	5.27	27.43%	08-05	4.85	5.21	7.51%				
	07-18	7.55	9.05	19.81%					09-16	5.40	6.32	17.01%				
									09-22	5.44	6.97	28.14%				
									09-23	4.69	5.67	21.08%				
Average PE				**14.10%**				**10.44%**				**14.19%**				**11.99%**
Total average PE																**13.03%**

*Note: FWY (E) is freshwater yield from experiment, FWY (M) is freshwater yield from mathematical modelling

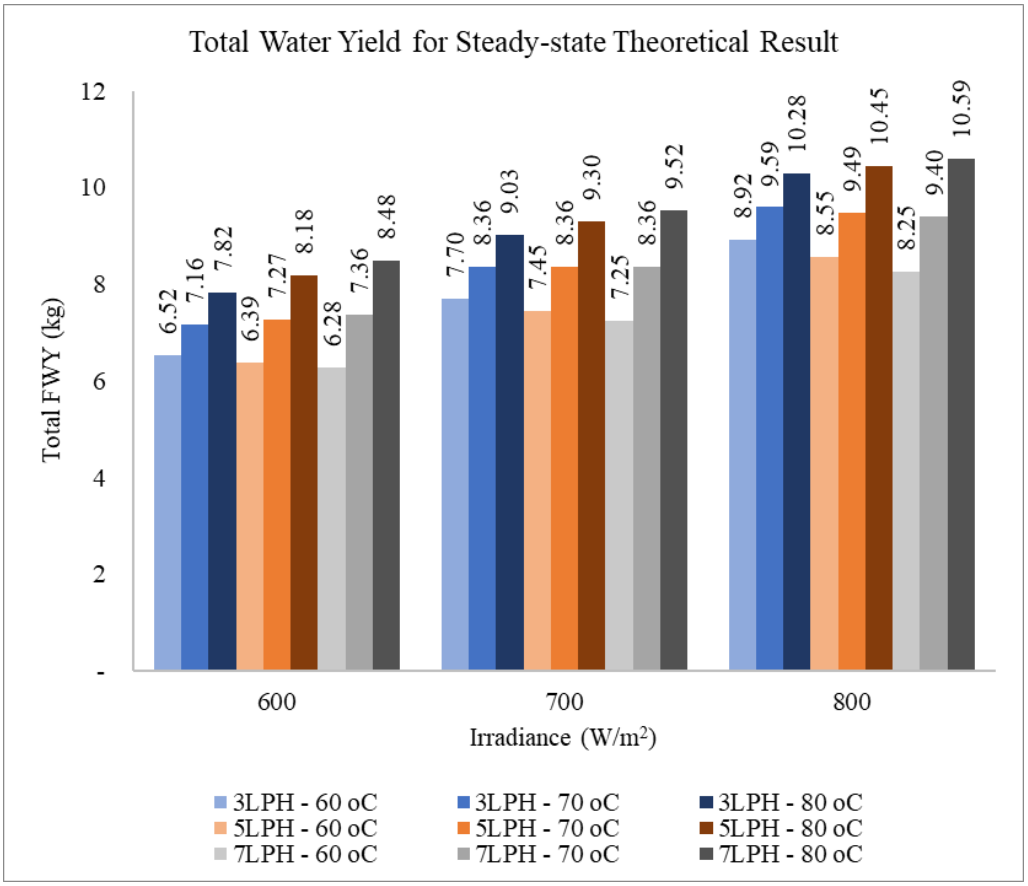

Figure 4.17: Total Water Yield for Steady-state Theoretical Results

CHAPTER 5

CONCLUSION

From the study, the maximum inlet water temperature of REWART solar distillation system as pre-heated by the multiple linear facet concentrator is 80.05ºC which is achieved under the flow rate of 5LPH. The MLFC REWART solar distillation system can generate more clean water when the irradiance is getting higher regardless the level of flow rates. The optimal water inlet temperature for the flow rate 3LPH and 5LPH to produce highest volume of clean water is 70ºC-80ºC, whereas it turns to 60ºC~70ºC for flow rate 7LPH and 9LPH. Among the optimal condition for highest water yield rate of different flow rates, it can be concluded that 3LPH (70ºC-80ºC) can produce more volume of clean water when the irradiance is less than 800 W/m^2, whereas 5LPH (70ºC-80ºC) produce more volume of clean water when the irradiance is more than 800 W/m^2. Besides, the highest flow rate 9LPH is observed to have the lowest water yield rate. Based on the study of optimal water yield of different flow rates, it is deduced that the flow rate 5LPH can be used for higher production of clean water at the inlet water temperature of 70ºC to 80ºC as compared to other flow rates. The average thermal efficiency for MLFC heating function is increasing with the flow rate. The higher the flow rate, the higher the change in water temperature which leads to more energy is absorbed to heat up the water. The average water yield efficiency is found to be highest for 3LPH at 45.59%.

Mathematical model is developed for the MLFC REWART solar distillation system in order to simulate the water yield from uncontrollable parameters such as ambient temperature, wind speed and solar irradiance in order to get optimal operating parameters. The average percentage error between theoretical and experimental results for 19 collection days is 13.03%. The reason for the variance is the constant wind speed and heat transfer coefficient from absorber plate to water film is used. From the steady state study using the mathematical model, it is concluded that the 5LPH at solar irradiance of 800 W/m^2 and inlet water temperature of 80^oC performs the best for highest productivity, i.e.10.45kg, under constant ambient temperature of 30^oC and time interval of 6 hours.

With sufficient equipment, running 4 carocells together with flow rate 3LPH, 5LPH, 7LPH and 9LPH at the same time is recommended to ensure a more accurate comparison between performance of different flow rates. The number of days for data collection for each flow rate should be fixed to ensure the consistency and accuracy of performance analysis. Wind speed and wind direction are other factors to study for a sound performance analysis of the system. Moreover, the total water yield per day (24 hours) should be assessed for better understanding of the economic study, so the system cost and efficiency can be taken in account for installation advice or improvement.

REFERENCE

Abdullah, A.S., Omara, Z.M., Essa, F.A., Alqsair, U.F., Aljaghtham, M., Mansir, I.B., Shanmugan, S. and Alawee, W.H., 2022. Enhancing trays solar still performance using wick finned absorber, nano- enhanced PCM. *Alexandria Engineering Journal*, 61(12), pp.12417–12430. https://doi.org/10.1016/j.aej.2022.06.033.

Ahmed, M.M.Z., Alshammari, F., Alatawi, I., Alhadri, M. and Elashmawy, M., 2022. A novel solar desalination system integrating inclined and tubular solar still with parabolic concentrator. *Applied Thermal Engineering*, 213. https://doi.org/10.1016/j.applthermaleng.2022.118665.

Arunkumar, T., Velraj, R., Denkenberger, D.C., Sathyamurthy, R., Kumar, K.V. and Ahsan, A., 2016. Productivity enhancements of compound parabolic concentrator tubular solar stills. *Renewable Energy*, 88, pp.391–400. https://doi.org/10.1016/j.renene.2015.11.051.

Aybar, H.Ş., 2006. Mathematical modeling of an inclined solar water distillation system. *Desalination*, 190(1–3), pp.63–70. https://doi.org/10.1016/j.desal.2005.07.015.

Ayoobi, A. and Ramezanizadeh, M., 2021. *An Exhaustive Review on a Solar Still Coupled with a Flat Plate Collector*. *International Journal of Photoenergy*, https://doi.org/10.1155/2021/9744219.

Belessiotis, V., Kalogirou, S. and Delyannis, E., 2016. *Thermal Solar Desalination : Methods and Systems*. Elsevier.

Chaichan, M.T. and Kazem, H.A., 2015. Water solar distiller productivity enhancement using concentrating solar water heater and phase change material (PCM). *Case Studies in Thermal Engineering*, 5, pp.151–159. https://doi.org/10.1016/j.csite.2015.03.009.

Chaurasiya, P.K., Rajak, U., Singh, S.K., Nath Verma, T., Sharma, V.K., Kumar, A. and Shende, V., 2022. A review of techniques for increasing the productivity of passive solar stills. *Sustainable Energy Technologies and Assessments*, 52. https://doi.org/10.1016/j.seta.2022.102033.

Chekerovska, M. and Filkoski, R.V., 2015. Efficiency of liquid flat-plate solar energy collector with solar tracking system. *Thermal Science*, 19(5), pp.1673–1684. https://doi.org/10.2298/TSCI150427099C.

F Cubed Limited, n.d. *Carocell Panel*. [online] Available at: <http://www.fcubed.com.au/aspx/carocell-panels.aspx> [Accessed 28 June 2022].

HVAC/R and Solar Energy Engineering, 2022. *Solar Collectors Technologies*. [online] Available at: <https://hvac-eng.com/solar-collectors-technologies/> [Accessed 26 June 2022].

Isah, A.S., Takaijudin, H., Singh, B. and Singh, M., 2021. Principles and Modes of Distillation in Desalination Process. [online] IntechOpen. https://doi.org/http://dx.doi.org/10.5772/intechopen.100855.

Jamar, A., Majid, Z.A.A., Azmi, W.H., Norhafana, M. and Razak, A.A., 2016. A review of water heating system for solar energy applications. *International Communications in Heat and Mass Transfer*, 76, pp.178–187. https://doi.org/10.1016/j.icheatmasstransfer.2016.05.028.

Jathar, L.D., Ganesan, S., Shahapurkar, K., Soudagar, M.E.M., Mujtaba, M.A., Anqi, A.E., Farooq, M., Khidmatgar, A., Goodarzi, M. and Safaei, M.R., 2022. Effect of Various Factors and Diverse Approaches to Enhance the Performance of Solar Stills: A Comprehensive Review. *Journal of Thermal Analysis and Calorimetry*, 147(7), pp.4491–4522. https://doi.org/10.1007/s10973-021-10826-y.

Kabeel, A.E., Khairat Dawood, M.M., Ramzy, K., Nabil, T., Elnaghi, B. and elkassar, A., 2019. Enhancement of single solar still integrated with solar dishes: An experimental approach. *Energy Conversion and Management*, 196, pp.165–174. https://doi.org/10.1016/j.enconman.2019.05.112.

Kalair, A.R., Seyedmahmoudian, M., Saleem, M.S., Abas, N., Rauf, S. and Stojcevski, A., 2022. A Comparative Thermal Performance Assessment of Various Solar Collectors for Domestic Water Heating. *International Journal of Photoenergy*, 2022, pp.1–17. https://doi.org/10.1155/2022/9536772.

Kalogirou, S.A., 2014. *Solar Energy Engineering Processes and Systems*. 2nd ed. Elsevier.

Kumar, A., Said, Z. and Bellos, E., 2021. *An up-to-date review on evacuated tube solar collectors*. *Journal of Thermal Analysis and Calorimetry*, https://doi.org/10.1007/s10973-020-09953-9.

Kumar, A., Vyas, S. and Nchelatebe Nkwetta, D., 2020. Experimental study of single slope solar still coupled with parabolic trough collector. *Materials Science for Energy Technologies*, 3, pp.700–708. https://doi.org/10.1016/j.mset.2020.07.005.

Madiouli, J., Lashin, A., Shigidi, I., Badruddin, I.A. and Kessentini, A., 2020. Experimental study and evaluation of single slope solar still combined with flat plate collector, parabolic trough and packed bed. *Solar Energy*, 196, pp.358–366. https://doi.org/10.1016/j.solener.2019.12.027.

Manchanda, H. and Kumar, M., 2015. A Comprehensive Decade Review and Analysis on Designs and Performance Parameters of Passive Solar Still. *Renewables: Wind, Water, and Solar*, 2(1). https://doi.org/10.1186/s40807-015-0019-8.

Mashaly, A.F. and Alazba, A.A., 2017. Thermal performance analysis of an inclined passive solar still using agricultural drainage water and artificial neural network in arid climate. *Solar Energy*, 153, pp.383–395.

https://doi.org/10.1016/j.solener.2017.05.083.

Mevada, D., Panchal, H. and Sadasivuni, K.K., 2021. Investigation on evacuated tubes coupled solar still with condenser and fins: Experimental, exergo-economic and exergo-environment analysis. *Case Studies in Thermal Engineering*, 27. https://doi.org/10.1016/j.csite.2021.101217.

Mousa, H. and Arabi, M.A., 2009. Theoretical study of water desalination by a falling film solar unit. *Desalination and Water Treatment*, 12(1–3), pp.331–336. https://doi.org/10.5004/dwt.2009.966.

Negi, A., Dhindsa, G.S. and Sehgal, S.S., 2021. Experimental investigation on single basin tilted wick solar still integrated with flat plate collector. In: *Materials Today: Proceedings*. Elsevier Ltd. pp.1439–1446. https://doi.org/10.1016/j.matpr.2021.09.210.

Nguyen, B.T., 2018. Factors Affecting the Yield of Solar Distillation Systems and Measures to Improve Productivities. In: *Desalination and Water Treatment*. InTech. https://doi.org/10.5772/intechopen.75593.

Nomor, E., Islam, R., Alim, M.A. and Rahman, A., 2021. Production of Fresh Water by A Solar Still: An Experimental Case Study in Australia. *Water (Switzerland)*, 13(23). https://doi.org/10.3390/w13233373.

Open University, 2022. *Can renewable energy sources power the world?* [online] Available at: <https://www.open.edu/openlearn/mod/oucontent/view.php?id=73759&section=6> [Accessed 29 June 2022].

Panchal, H.N., 2015. Enhancement of distillate output of double basin solar still with vacuum tubes. *Journal of King Saud University - Engineering Sciences*, 27(2), pp.170–175. https://doi.org/10.1016/j.jksues.2013.06.007.

Patel, M., Patel, C. and Panchal, H., 2020. Performance analysis of conventional triple basin solar still with evacuated heat pipes, corrugated sheets and storage materials. *Groundwater for Sustainable Development*, 11. https://doi.org/10.1016/j.gsd.2020.100387.

Rajaseenivasan, T., Nelson Raja, P. and Srithar, K., 2014. An experimental investigation on a solar still with an integrated flat plate collector. *Desalination*, 347, pp.131–137. https://doi.org/10.1016/j.desal.2014.05.029.

Ranjan, K.R., Kaushik, S.C. and Panwar, N.L., 2016. Energy and exergy analysis of passive solar distillation systems. *International Journal of Low-Carbon Technologies*, 11(2), pp.211–221. https://doi.org/10.1093/ijlct/ctt069.

Singh, R.V., Kumar, S., Hasan, M.M., Khan, M.E. and Tiwari, G.N., 2013. Performance of a solar still integrated with evacuated tube collector in natural mode. *Desalination*, 318, pp.25–33. https://doi.org/10.1016/j.desal.2013.03.012.

Srithar, K., Rajaseenivasan, T., Karthik, N., Periyannan, M. and Gowtham, M.,

2016. Stand alone triple basin solar desalination system with cover cooling and parabolic dish concentrator. *Renewable Energy*, 90, pp.157–165. https://doi.org/10.1016/j.renene.2015.12.063.

Subramanian, R.S., Kumaresan, G., Ajith, R., Sabarivasan, U., Gowthamaan, K.K. and Anudeep, S., 2021. Performance analysis of modified solar still integrated with flat plate collector. In: *Materials Today: Proceedings*. Elsevier Ltd. pp.1382–1387. https://doi.org/10.1016/j.matpr.2020.06.409.

Supankanok, R., Sriwong, S., Ponpo, P., Wu, W., Chandra-Ambhorn, W. and Anantpinijwatna, A., 2021. Modification of a solar thermal collector to promote heat transfer inside an evacuated tube solar thermal absorbe. *Applied Sciences (Switzerland)*, 11(9). https://doi.org/10.3390/app11094100.

Tan M.H, Fon C.Y. and Khong D., 2018. *Solar Water Heating System with a Multi-Facet Trough Solar Concentrator*. PI 2018002614.

Thorpe, D., 2011. *Solar Technology*. Earthscan.

Tiwari, G.N. and Sahota, L., 2017. *Green Energy and Technology Advanced Solar-Distillation Systems Basic Principles, Thermal Modeling, and Its Application*. [online] Springer. https://doi.org/10.1007/978-981-10-4672-8.

Tuly, S.S., Sarker, M.R.I., Das, B.K. and Rahman, M.S., 2021. Effects of Design and Operational Parameters On The Performance of A Solar Distillation System: A Comprehensive Review. *Groundwater for Sustainable Development*, 14. https://doi.org/10.1016/j.gsd.2021.100599.

Velmurugan, V. and Srithar, K., 2011. *Performance analysis of solar stills based on various factors affecting the productivity - A review*. *Renewable and Sustainable Energy Reviews*, https://doi.org/10.1016/j.rser.2010.10.012.

Yari, M., Mazareh, A.E. and Mehr, A.S., 2016. A novel cogeneration system for sustainable water and power production by integration of a solar still and PV module. *Desalination*, 398, pp.1–11. https://doi.org/10.1016/j.desal.2016.07.004.

Zurigat, Y.H. and Abu-Arabi, M.K., 2004. Modelling and performance analysis of a regenerative solar desalination unit. *Applied Thermal Engineering*, 24(7), pp.1061–1072. https://doi.org/10.1016/j.applthermaleng.2003.11.010.

APPENDIX I

OPTICAL GEOMETRY DESIGN AND ANALYSIS OF MLFC

The earth rotates in approximately 24 hours about its own polar axis, which is inclined to the ecliptic plane by 23.45 degrees (as shown in Figure AI.1). This angle is known as sun declination angle, which is the angle between the horizontal line to the sun and the earth equatorial plane. The earth's rotation about its polar axis produces days and nights, while the tilt of this axis relative to the ecliptic plane produces four seasons in some countries as the earth rotates about the sun. Thus, the optical geometry design of the MLFC is crucial to ensure all the incident sunray reflect to the receiver. The design parameters must be pre-determined in order to obtain an optimal geometry of the MLFC.

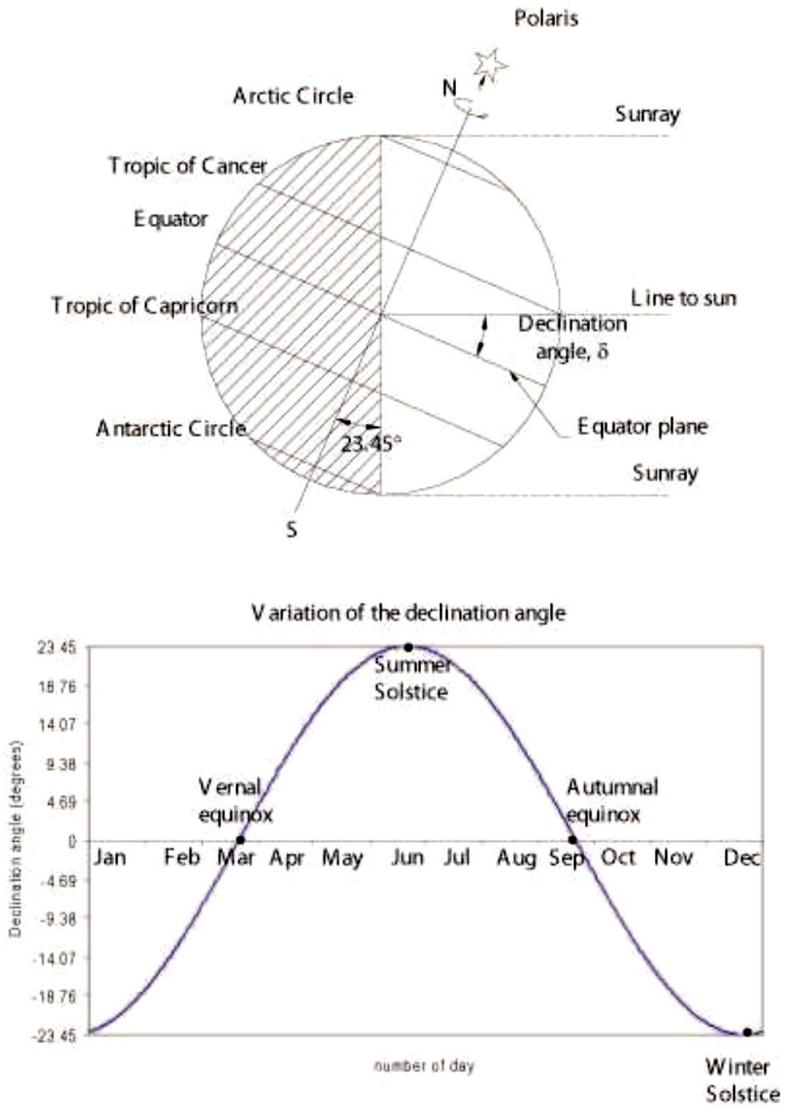

Figure AI.1: Solar Declination Angle

A. Determine the MLFC Geometry by Using Formula

MLFC is a two-dimensional concentrator consisting of multiple linear facets, the axes of which are inclined at angles $+\theta'_i$ with respect to the optical axis of the collector. The angle θ'_i, called the collector half acceptance angle, is defined as the angle through which a source of light can be moved and still converge at the absorber. According to the design of Solar Water Heating System with a Multi-Facet Trough Solar Concentrator by Tan and Khong in 2018, the MLFC consists of multiple linear facets with different tilted angles, which ensure all the incident sunray can be reflected to the receiver located at the centre of the concentrator. The tilted angle of each facet mirrors F_n can be calculated using formula as shown in equation (AI.1),

$$\alpha_n = \frac{a_n+\beta_n+90}{2} \tag{AI.1}$$

where,

$$\beta_n = \tan^{-1}\left(\frac{P_{(n-1)y}}{P_{(n-1)x}}\right) \tag{AI.2}$$

$$a_n = \sin^{-1}\left(\frac{R}{\sqrt{P^2_{(n-1)x}+P^2_{(n-1)y}}}\right) \tag{AI.3}$$

n is the number of flat facets, R is the radius of the absorber pipe, P_n is the coordinates of the top edge of the flat facet F_n, and P_{n-1} is the coordinates of the bottom edge of the flat facet F_n.

The x coordinate, P_{nx} of the top edge of flat facet n may be determined using the equation:

$$P_{nx} = \frac{R(\cos\sigma_n+\tan\sigma_n\sin\sigma_n)-(P_{(n-1)y}-\tan\alpha_n\, x\, P_{(n-1)x})}{\tan\alpha_n+\tan\sigma_n} \tag{AI.4}$$

The y coordinate, P_{ny} of the top edge of flat facet n may be determined using the equation:

$$P_{ny} = R\cos\sigma_n + R\tan\sigma_n\sin\sigma_n - \tan\sigma_n\, x\, P_{nx} \tag{AI.5}$$

where θ'_i is half acceptance angle of the MLFC.

Lastly, the width W_n of the mirror n are determined by the equation below:

$$W_n = \sqrt{(P_{nx}-P_{(n-1)x})^2+(P_{ny}-P_{(n-1)y})^2}\ ,\ n \geq 1 \tag{AI.6}$$

The optical geometry design is determined by these formulas, the number of mirrors on each side of concentrator is 3 due to the width of mirror number 4, F_4 is too small and difficult to cut. The parameter and optical geometry design are shown in Figure AI.2.

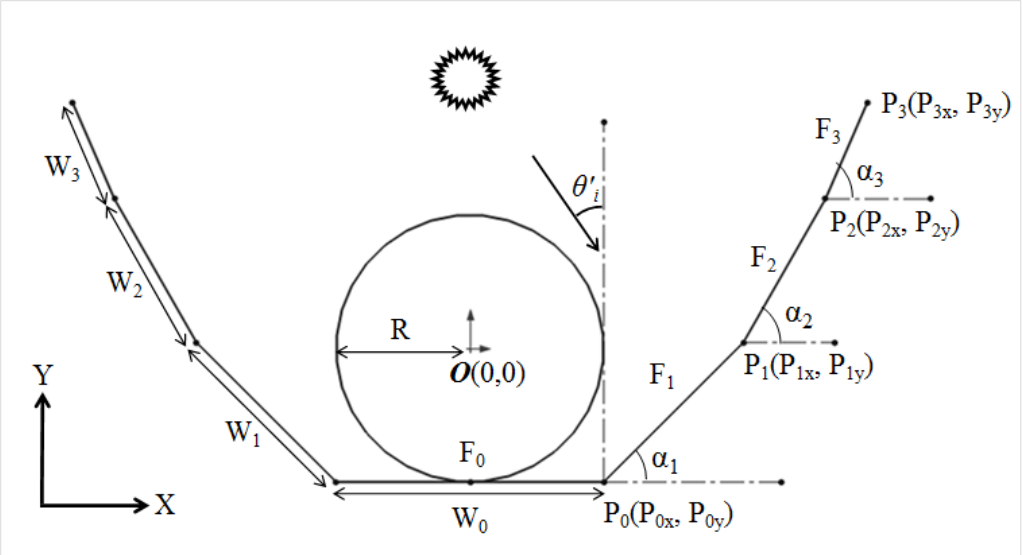

Figure AI.2: Parameter Symbol and Optical Geometry Design for MLFC.

MLFC is a non-imaging concentrator with a concentration ratio approaching the upper limit permitted by the second law of thermodynamics. This MLFC is covered with glass to avoid dust and other materials entering the collector and reducing the reflectivity of its walls. Since it is stationary, the radiation will be received only during the hours when the sun is within the collector acceptance angle. When the concentrator is oriented with its long axis along the east–west direction, with a little seasonal adjustment in tilt angle, the collector is able to catch the sun's rays effectively through its wide acceptance angle along its long axis. The minimum acceptance angle in this case should be equal to the maximum incidence angle projected in a north–south vertical plane during the times when output is needed from the collector. For stationary MLFC collectors mounted in this mode, the minimum acceptance angle is equal to 47°. This angle covers the declination of the sun from summer to winter solstices (2 x 23.5°). In practice, bigger angles are used to enable the collector to collect diffuse radiation at the expense of a lower concentration ratio. Smaller (less than 3) concentration ratio are of greatest practical interest.

Finally, the required frequency of collector adjustment is related to the collector concentration ratio. Thus, for $C < 3$ the collector needs only biannual adjustment, while for $C > 10$ the collector requires almost daily adjustment; these systems are also called *quasi-static*.

B. Ray Tracing Simulation of the MLFC

The *SolidWorks* files containing the MLFC SWH's optical geometry designs are then exported to *LightTools*, which is a ray tracing software used to simulate and validate the optical geometry design. A 2D ray-tracing simulation will be used instead of 3D because 2D is sufficient for the MLFC SWH system. The

2D ray-tracing simulation is performed on the MLFC optical geometry design to verify whether the sun rays able to completely reflected to the absorber pipe located at the centre without any loss of sun rays.

Moreover, three different incident angles are simulated to validate and ensure all the incident sunray are reflected by the MLFC toward the absorber pipe without any spillage losses. The aforementioned incident angles are 0°, 20° and 28°. Figure AI.3 depicts the optical design's ray tracing simulation at various incident angles. The ray-tracing simulation shows an excellent result that all the sunrays are fully reflected to the pipe. The highest solar concentration ratio (CR) can be achieved by the MLFC is 2.8 suns while the sun incident angle is 20°.

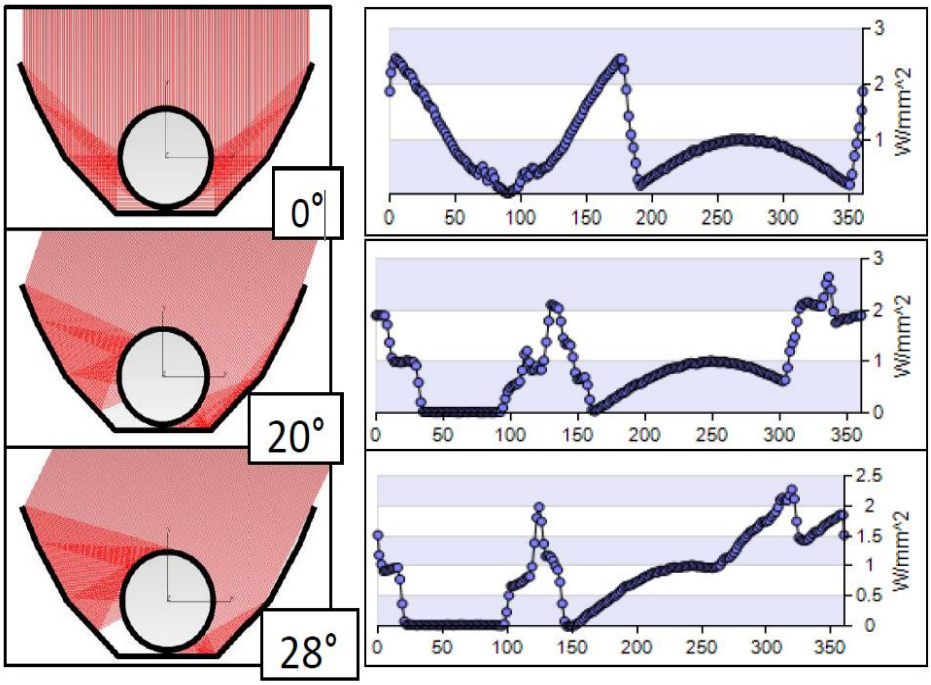

Figure AI.3: Ray Tracing simulation of the Optical Geometry Design

APPENDIX II:

RAW DATA AND TIME SERIES GRAPH OF MLFC

The experiment data is denoted by following:

- $T_{MLFC,i}$ = MLFC Inlet Water Temperature
- $T_{MLFC,o}$ = MLFC Outlet Water Temperature
- T_a = Ambient Temperature
- GHI = Global Horizontal Irradiance
- FWY = Fresh Water Yield

A. Flow Rate 3LPH

Date	Time Interval (30 mins)		GHI (W/m^2)	$T_{MLFC,i}$ (°C)	$T_{MLFC,o}$ (°C)	T_a (°C)	FWY (ml)	FWY (l/h)
07-14	11:45 AM	12:15 PM	671.82	32.53	56.12	33.06	506	1.01
	12:15 PM	12:45 PM	943.27	33.45	64.52	33.99	730	1.46
	12:45 PM	1:15 PM	888.11	34.77	72.14	35.53	900	1.80
	1:15 PM	1:45 PM	857.79	34.87	71.76	36.50	640	1.28
	1:45 PM	2:15 PM	683.86	35.54	72.42	36.77	670	1.34
	2:15 PM	2:45 PM	488.73	35.62	69.07	36.46	446	0.89
	2:45 PM	3:15 PM	528.48	36.08	66.44	35.27	440	0.88
	3:15 PM	3:45 PM	290.26	35.93	62.86	33.92	230	0.46
	3:45 PM	4:15 PM	537.65	36.49	60.16	35.31	442	0.88
	4:15 PM	4:45 PM	320.91	36.75	61.27	34.55	286	0.57
	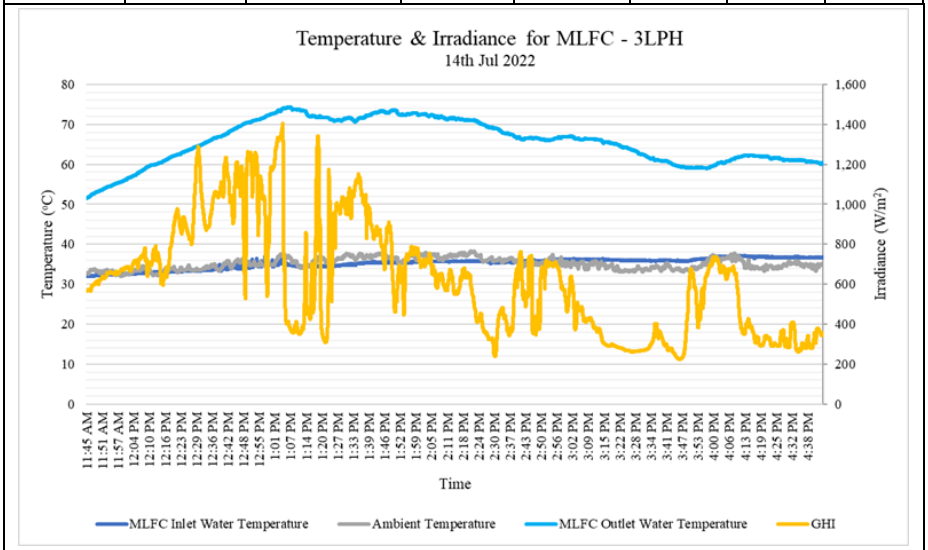							
07-15	11:15 AM	11:45 AM	542.30	33.24	53.18	31.07	402	0.80
	11:45 AM	12:15 PM	575.76	33.97	59.92	31.80	404	0.81
	12:15 PM	12:45 PM	431.40	34.24	62.78	32.63	428	0.86
	12:45 PM	1:15 PM	580.89	34.75	62.33	32.92	368	0.74
	1:15 PM	1:45 PM	591.16	35.77	64.37	32.81	487	0.97
	1:45 PM	2:15 PM	679.73	36.67	67.17	33.62	590	1.18
	2:15 PM	2:45 PM	554.33	37.05	68.16	33.47	420	0.84
	2:45 PM	3:15 PM	468.55	37.62	68.62	34.22	426	0.85
	3:15 PM	3:45 PM	557.87	38.01	65.47	33.55	387	0.77
	3:45 PM	4:15 PM	694.64	39.22	67.89	35.36	555	1.11
	4:15 PM	4:45 PM	610.07	40.01	70.71	36.64	517	1.03

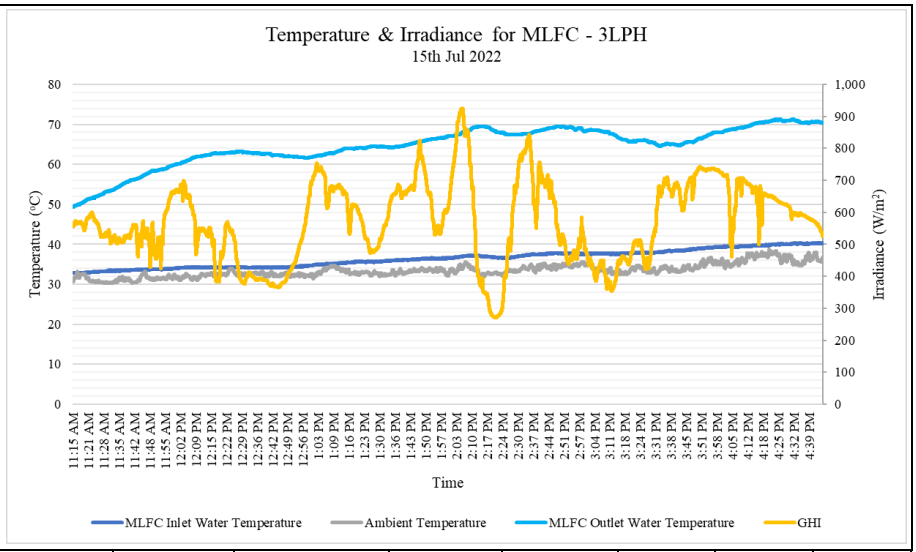

07-16	11:00 AM	11:30 AM	666.54	31.56	40.01	31.93	742	1.48
	11:30 AM	12:00 PM	709.10	34.34	54.27	32.32	786	1.57
	12:00 PM	12:30 PM	858.23	35.67	65.20	33.52	1,091	2.18
	12:30 PM	1:00 PM	789.93	37.00	73.33	34.11	876	1.75
	1:00 PM	1:30 PM	870.50	38.33	75.49	33.94	944	1.89
	1:30 PM	2:00 PM	667.96	38.60	74.73	33.86	1,019	2.04
	2:00 PM	2:30 PM	684.50	39.19	73.49	35.22	1,134	2.27
	2:30 PM	3:00 PM	612.00	39.90	73.35	35.49	878	1.76
	3:00 PM	3:30 PM	685.74	40.53	72.03	35.74	731	1.46
	3:30 PM	4:00 PM	660.90	41.68	73.70	36.34	462	0.92
	4:00 PM	4:30 PM	369.45	41.09	69.61	34.65	385	0.77
	4:30 PM	5:00 PM	213.89	41.60	67.04	36.15	368	0.74

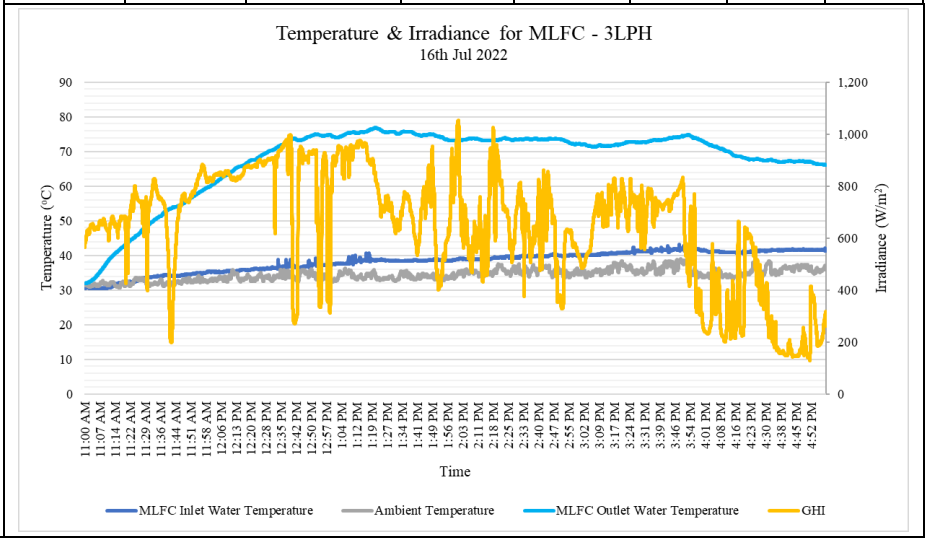

07-17	11:00 AM	11:30 AM	728.00	34.08	44.44	34.06	305	0.61
	11:30 AM	12:00 PM	840.85	35.79	59.30	34.55	467	0.93
	12:00 PM	12:30 PM	947.07	37.25	69.17	35.02	459	0.92
	12:30 PM	1:00 PM	980.07	38.70	75.41	36.38	597	1.19
	1:00 PM	1:30 PM	848.95	39.97	78.64	36.68	709	1.42
	1:30 PM	2:00 PM	840.18	41.16	78.22	36.32	940	1.88
	2:00 PM	2:30 PM	711.22	41.86	77.57	36.30	897	1.79
	2:30 PM	3:00 PM	750.04	42.37	76.03	37.38	1,123	2.25
	3:00 PM	3:30 PM	710.12	43.23	77.50	38.35	884	1.77
	3:30 PM	4:00 PM	710.78	43.69	77.08	39.12	871	1.74
	4:00 PM	4:30 PM	599.04	44.00	76.14	38.91	764	1.53

	4:30 PM	5:00 PM	517.51	43.93	73.82	39.80	692	1.38
	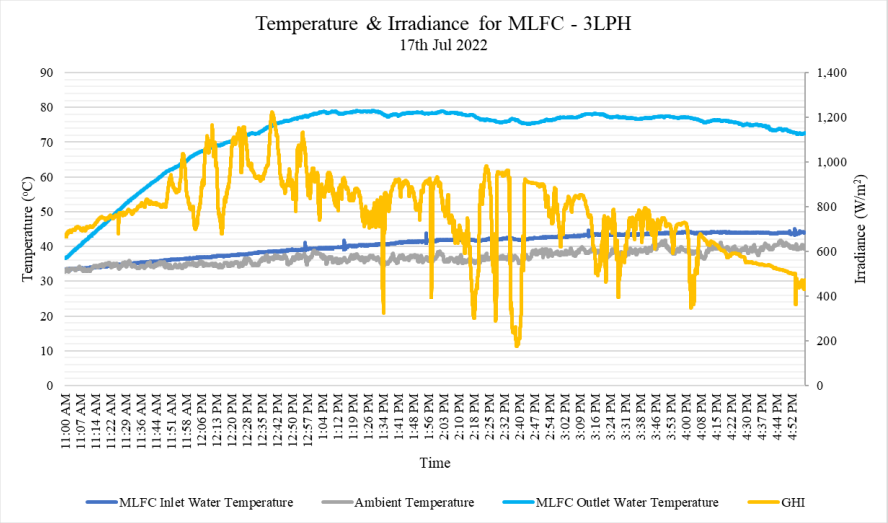							
07-18	11:00 AM	11:30 AM	728.70	35.34	53.64	33.63	440	0.88
	11:30 AM	12:00 PM	843.72	36.61	66.08	34.48	730	1.46
	12:00 PM	12:30 PM	770.24	37.17	73.03	35.06	478	0.96
	12:30 PM	1:00 PM	738.40	37.41	70.67	34.99	670	1.34
	1:00 PM	1:30 PM	866.31	38.84	74.07	35.88	702	1.40
	1:30 PM	2:00 PM	889.22	39.69	76.42	36.33	696	1.39
	2:00 PM	2:30 PM	856.74	40.43	78.17	37.46	594	1.19
	2:30 PM	3:00 PM	822.27	41.13	79.30	38.53	824	1.65
	3:00 PM	3:30 PM	770.57	42.03	79.38	38.94	740	1.48
	3:30 PM	4:00 PM	694.35	42.64	78.53	39.01	672	1.34
	4:00 PM	4:30 PM	620.26	43.17	76.44	38.57	570	1.14
	4:30 PM	5:00 PM	457.46	43.27	73.61	38.24	435	0.87
	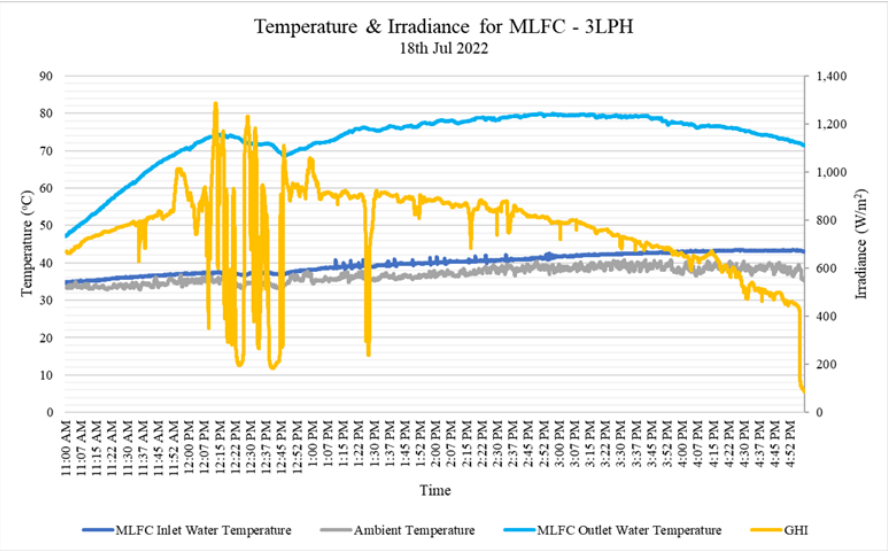							

B. Flow Rate 5LPH

Date	Time Interval (30 mins)		GHI (W/m^2)	$T_{MLFC,i}$ (°C)	$T_{MLFC,o}$ (°C)	T_a (°C)	FWY (ml)	FWY (l/h)
07-20	10:45 AM	11:15 AM	701.43	33.06	46.45	31.48	452	0.90
	11:15 AM	11:45 AM	798.71	34.52	59.55	32.03	728	1.46
	11:45 AM	12:15 PM	928.82	35.54	67.76	33.20	893	1.79
	12:15 PM	12:45 PM	1,150.81	36.64	73.98	34.73	980	1.96

	12:45 PM	1:15 PM	953.84	37.65	77.16	35.25	978	1.96
	1:15 PM	1:45 PM	934.94	38.75	78.03	34.89	940	1.88
	1:45 PM	2:15 PM	799.37	39.13	78.23	36.17	794	1.59
	2:15 PM	2:45 PM	646.34	39.61	75.50	35.75	648	1.30
	2:45 PM	3:15 PM	504.08	39.49	70.33	35.85	519	1.04
	3:15 PM	3:45 PM	491.99	39.85	66.72	36.03	449	0.90
	3:45 PM	4:15 PM	416.14	40.09	64.56	35.93	315	0.63
	4:15 PM	4:45 PM	459.47	40.40	62.87	36.48	330	0.66

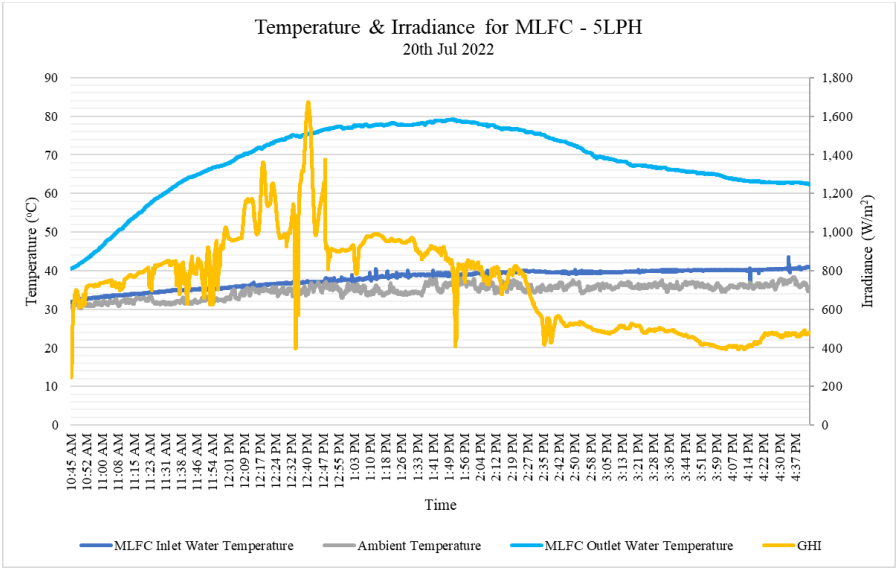

07-21	11:00 AM	11:30 AM	487.44	34.20	47.52	32.49	277	0.55
	11:30 AM	12:00 PM	774.65	35.31	57.72	33.63	700	1.40
	12:00 PM	12:30 PM	774.79	36.23	66.44	35.27	776	1.55
	12:30 PM	1:00 PM	655.79	36.57	69.03	35.36	614	1.23
	1:00 PM	1:30 PM	719.43	37.25	69.18	35.60	653	1.31
	1:30 PM	2:00 PM	704.23	37.92	70.89	36.67	672	1.34
	2:00 PM	2:30 PM	540.63	37.97	68.49	35.47	525	1.05
	2:30 PM	3:00 PM	754.43	38.78	67.49	37.68	648	1.30
	3:00 PM	3:30 PM	653.10	39.36	69.97	38.76	580	1.16
	3:30 PM	4:00 PM	695.45	40.16	70.67	40.43	625	1.25
	4:00 PM	4:30 PM	593.95	40.66	69.18	37.33	559	1.12
	4:30 PM	5:00 PM	436.60	40.40	65.84	36.98	374	0.75

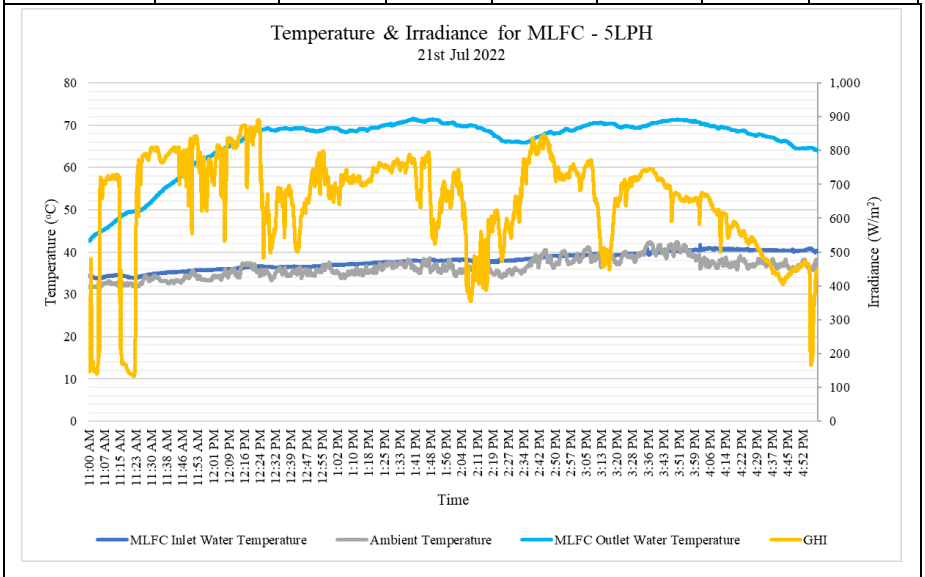

07-22	11:00 AM	11:30 AM	716.82	34.47	44.48	33.13	241	0.48
	11:30 AM	12:00 PM	753.46	35.63	59.43	35.00	568	1.14
	12:00 PM	12:30 PM	831.80	36.62	68.20	34.13	586	1.17
	12:30 PM	1:00 PM	883.13	37.89	73.58	35.93	760	1.52
	1:00 PM	1:30 PM	921.35	38.99	77.52	37.21	996	1.99
	1:30 PM	2:00 PM	935.52	40.01	79.48	38.62	970	1.94
	2:00 PM	2:30 PM	869.15	40.70	80.05	38.87	930	1.86
	2:30 PM	3:00 PM	888.73	41.51	79.40	39.99	860	1.72
	3:00 PM	3:30 PM	852.62	42.14	79.40	40.79	792	1.58
	3:30 PM	4:00 PM	492.62	41.29	75.92	37.80	574	1.15
	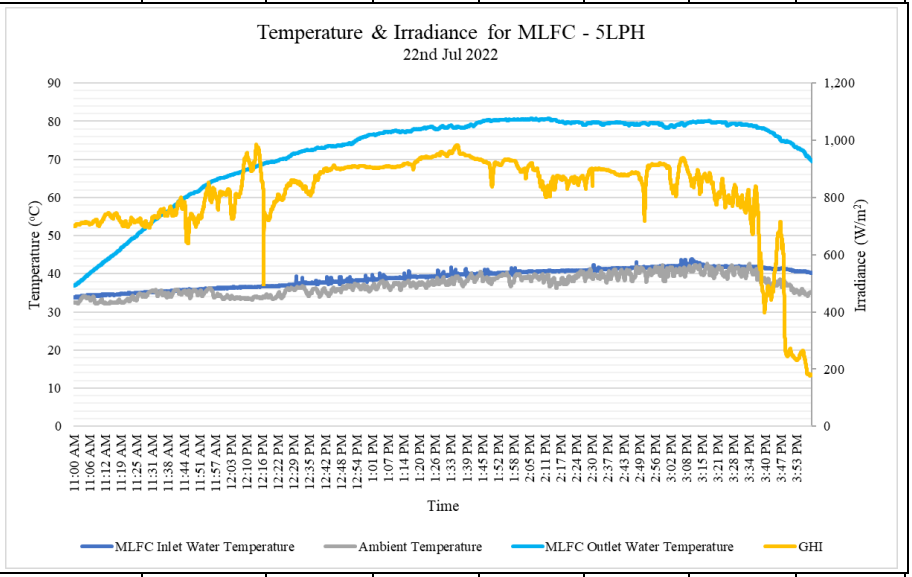							
07-27	11:00 AM	11:30 AM	799.03	32.79	46.60	31.47	406	0.81
	11:30 AM	12:00 PM	887.56	34.23	61.19	32.61	550	1.10
	12:00 PM	12:30 PM	914.10	35.46	69.15	32.31	690	1.38
	12:30 PM	1:00 PM	792.53	36.17	71.50	32.61	530	1.06
	1:00 PM	1:30 PM	763.97	37.10	72.04	33.09	546	1.09
	1:30 PM	2:00 PM	788.25	37.46	70.32	33.44	652	1.30
	2:00 PM	2:30 PM	487.44	37.69	69.22	33.12	407	0.81
	2:30 PM	3:00 PM	336.73	37.41	64.00	32.62	354	0.71
	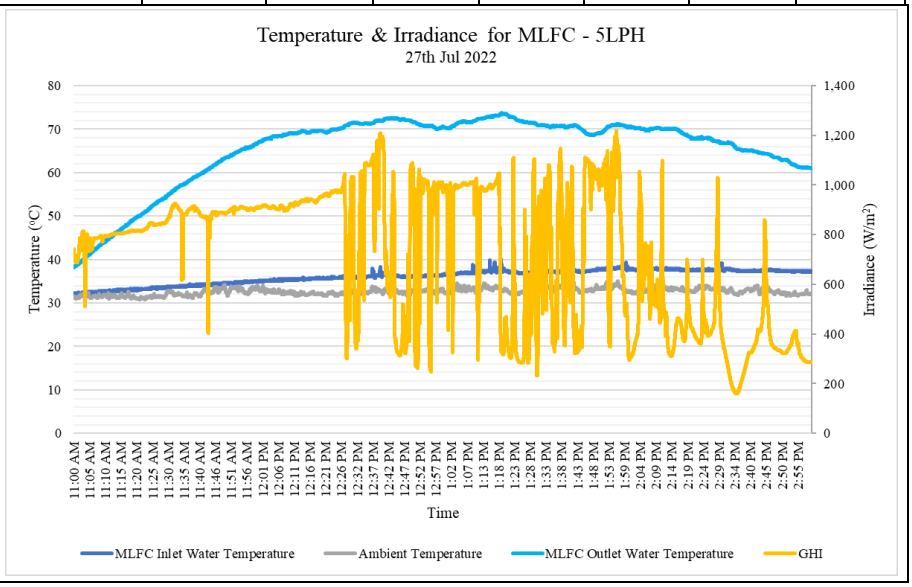							

C. Flow Rate 7LPH

Date	Time Interval (30 mins)		GHI (W/m^2)	$T_{MLFC,i}$ (°C)	$T_{MLFC,o}$ (°C)	T_a (°C)	FWY (ml)	FWY (l/h)
07-30	12:00 PM	12:30 PM	962.98	32.93	45.22	32.29	914	1.83
	12:30 PM	1:00 PM	955.51	34.06	61.02	33.11	987	1.97
	1:00 PM	1:30 PM	958.99	35.09	67.29	33.09	842	1.68
	1:30 PM	2:00 PM	941.39	35.86	69.15	33.86	746	1.49
	2:00 PM	2:30 PM	578.75	35.90	66.75	33.23	563	1.13
	2:30 PM	3:00 PM	682.90	35.96	60.80	33.75	650	1.30
	3:00 PM	3:30 PM	794.17	37.07	64.86	35.52	700	1.40
	3:30 PM	4:00 PM	689.96	37.61	66.84	36.19	626	1.25
	4:00 PM	4:30 PM	659.37	37.67	64.15	35.59	556	1.11
	4:30 PM	5:00 PM	585.38	37.79	62.28	35.42	402	0.80
	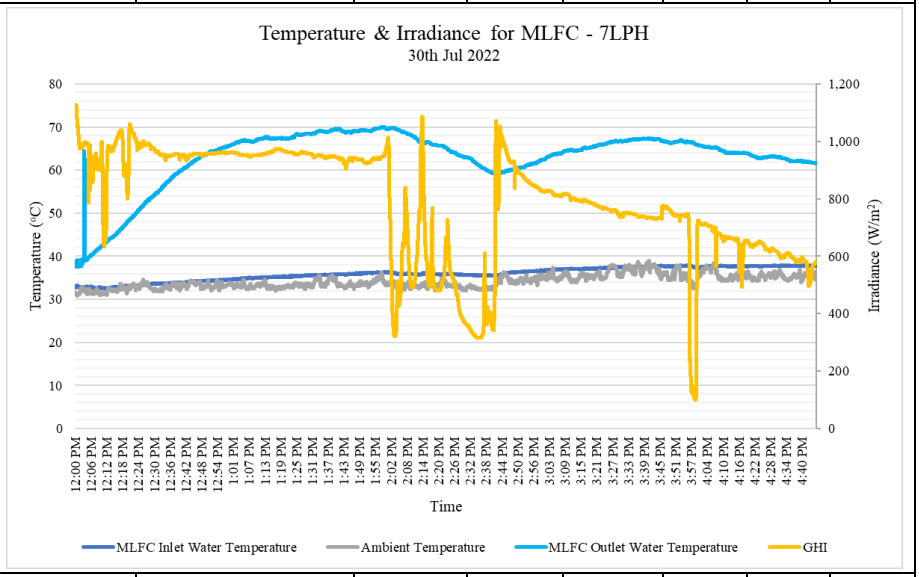							
07-31	11:00 AM	11:30 AM	744.70	32.74	40.26	31.65	394	0.79
	11:30 AM	12:00 PM	843.28	33.90	55.34	32.46	646	1.29
	12:00 PM	12:30 PM	818.96	35.03	63.78	32.56	725	1.45
	12:30 PM	1:00 PM	943.75	36.00	67.05	33.12	912	1.82
	1:00 PM	1:30 PM	937.45	37.18	70.49	33.23	935	1.87
	1:30 PM	2:00 PM	921.89	38.17	72.66	34.36	780	1.56
	2:00 PM	2:30 PM	886.47	39.29	73.75	34.98	960	1.92
	2:30 PM	3:00 PM	842.40	40.00	73.15	34.73	840	1.68
	3:00 PM	3:30 PM	706.93	40.29	71.43	35.18	712	1.42
	3:30 PM	4:00 PM	304.95	40.01	65.96	33.65	422	0.84
	4:00 PM	4:30 PM	400.43	40.08	59.99	33.30	420	0.84
	4:30 PM	5:00 PM	127.42	38.65	55.82	32.52	179	0.36

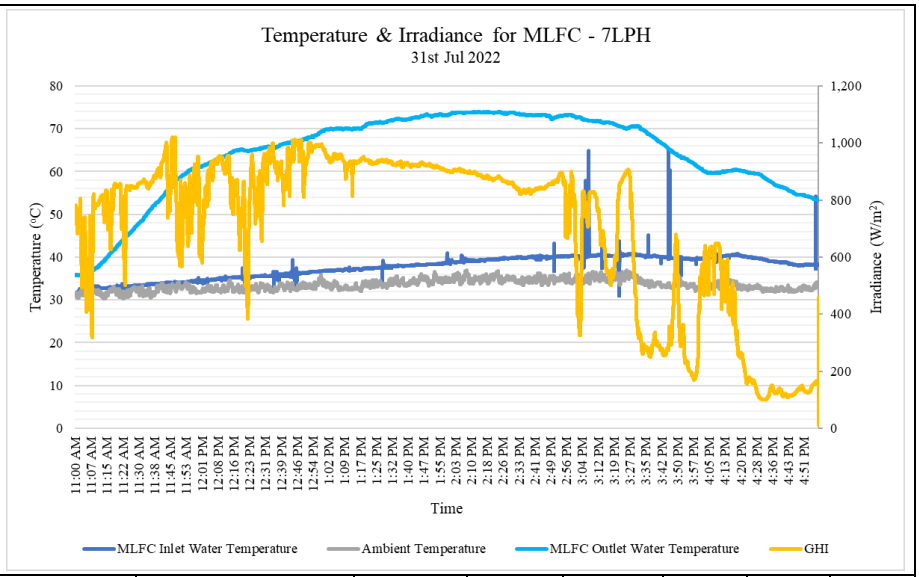

08-01	10:45 AM	11:15 AM	534.98	31.87	37.67	31.01	214	0.43
	11:15 AM	11:45 AM	647.04	32.71	48.40	31.53	623	1.25
	11:45 AM	12:15 PM	956.34	34.18	58.10	32.36	850	1.70
	12:15 PM	12:45 PM	765.22	34.95	63.02	32.39	895	1.79
	12:45 PM	1:15 PM	911.52	36.10	65.82	32.93	1045	2.09
	1:15 PM	1:45 PM	841.33	37.01	68.74	33.80	1174	2.35
	1:45 PM	2:15 PM	834.41	37.73	69.20	34.85	980	1.96
	2:15 PM	2:45 PM	891.69	38.84	71.84	35.44	537	1.07
	2:45 PM	3:15 PM	640.42	38.86	69.24	33.66	408	0.82
	3:15 PM	3:45 PM	479.88	38.98	64.28	34.15	592	1.18
	3:45 PM	4:15 PM	169.78	38.00	57.82	32.99	217	0.43

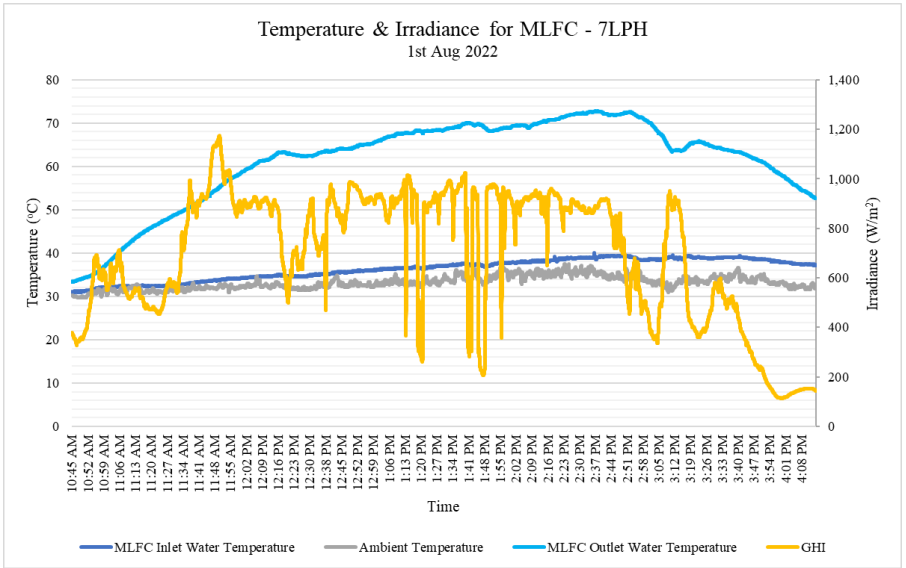

08-05	11:30 AM	12:00 PM	939.49	34.30	45.01	34.64	267	0.53
	12:00 PM	12:30 PM	869.65	34.61	52.51	33.06	455	0.91
	12:30 PM	1:00 PM	863.15	35.86	62.88	33.71	602	1.20
	1:00 PM	1:30 PM	897.12	37.16	67.61	34.65	731	1.46
	1:30 PM	2:00 PM	686.64	37.82	68.76	35.04	832	1.66
	2:00 PM	2:30 PM	564.89	37.80	64.57	34.43	534	1.07
	2:30 PM	3:00 PM	463.31	37.35	59.71	34.39	403	0.81
	3:00 PM	3:30 PM	481.32	37.50	57.70	33.87	327	0.65
	3:30 PM	4:00 PM	481.55	37.61	56.77	34.10	300	0.60
	4:00 PM	4:30 PM	328.48	37.42	55.31	33.61	236	0.47

	4:30 PM	5:00 PM	293.62	37.15	52.46	33.32	159	0.32
	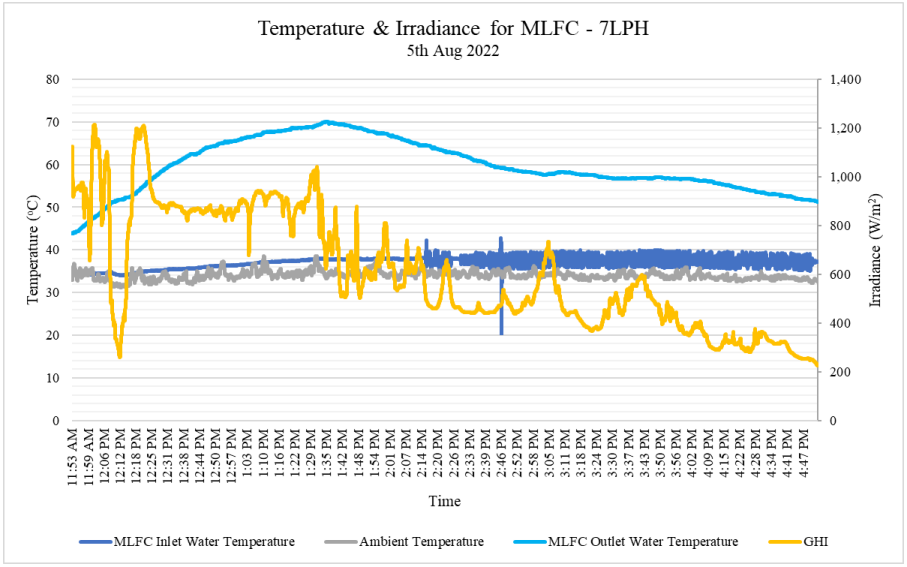						
09-16	11:30 AM	12:00 PM	901.96	35.57	60.35	33.82	660	1.32
	12:00 PM	12:30 PM	961.70	36.63	69.07	34.44	842	1.68
	12:30 PM	1:00 PM	764.38	37.12	70.67	34.70	582	1.16
	1:00 PM	1:30 PM	1,014.37	38.22	70.61	34.77	782	1.56
	1:30 PM	2:00 PM	977.64	39.10	74.03	36.79	760	1.52
	2:00 PM	2:30 PM	834.69	39.58	74.47	36.35	724	1.45
	2:30 PM	3:00 PM	240.88	38.39	65.35	33.63	280	0.56
	3:00 PM	3:30 PM	304.34	37.69	54.62	33.52	180	0.36
	3:30 PM	4:00 PM	356.00	37.79	51.94	33.91	240	0.48
	4:00 PM	4:30 PM	526.46	37.96	53.05	34.43	350	0.70
	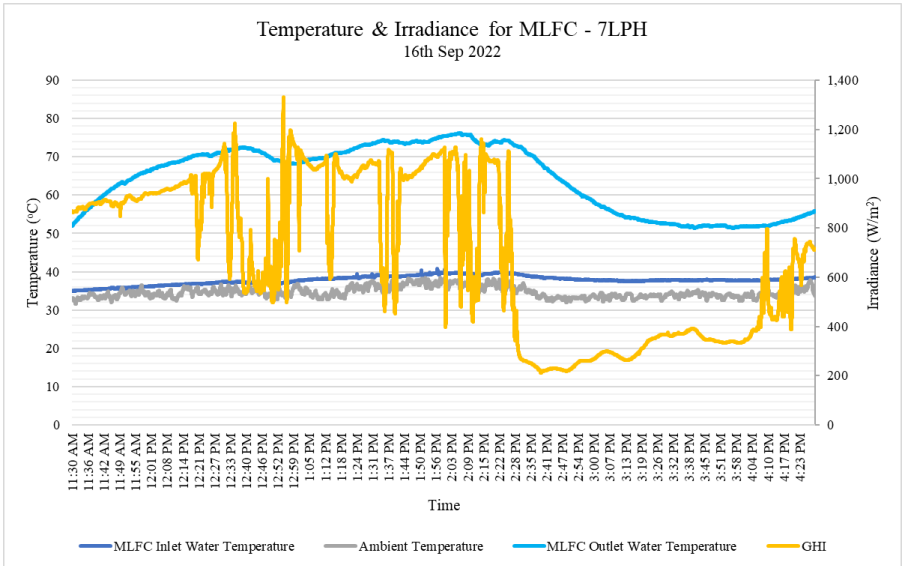						
09-22	11:45 AM	12:15 PM	770.44	32.20	48.05	31.34	390	0.78
	12:15 PM	12:45 PM	865.04	33.46	61.30	31.84	580	1.16
	12:45 PM	1:15 PM	1,093.06	34.96	68.30	32.47	804	1.61
	1:15 PM	1:45 PM	784.25	35.67	71.26	32.52	630	1.26
	1:45 PM	2:15 PM	957.35	36.33	69.51	33.75	702	1.40
	2:15 PM	2:45 PM	710.03	36.43	68.51	33.59	534	1.07
	2:45 PM	3:15 PM	921.01	37.48	69.61	34.58	652	1.30
	3:15 PM	3:45 PM	683.19	38.01	71.63	33.46	520	1.04
	3:45 PM	4:15 PM	492.32	37.79	65.78	33.46	368	0.74
	4:15 PM	4:45 PM	479.09	37.54	60.27	33.01	260	0.52

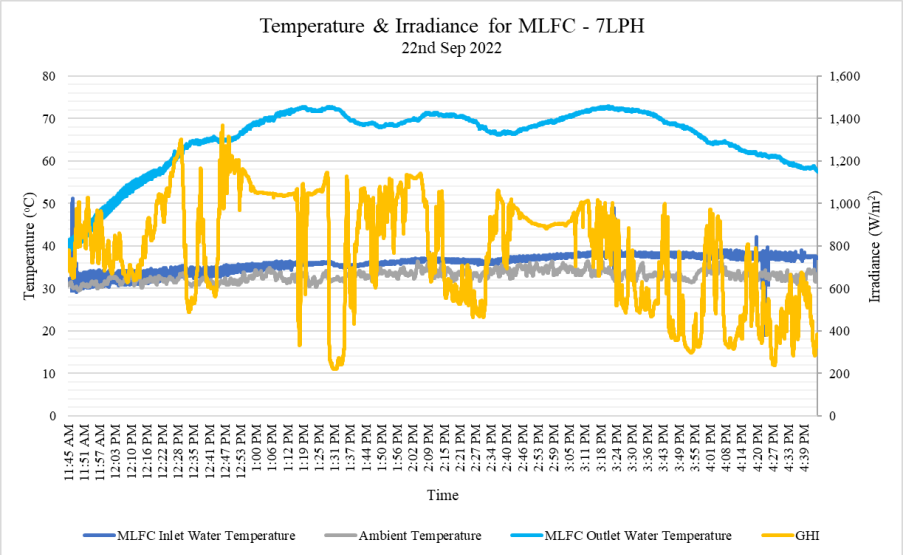

09-23	11:30 AM	12:00 PM	901.38	34.38	58.71	32.60	630	1.26
	12:00 PM	12:30 PM	814.47	35.16	65.83	33.32	674	1.35
	12:30 PM	1:00 PM	626.20	35.34	62.53	33.76	476	0.95
	1:00 PM	1:30 PM	760.36	36.37	63.10	34.00	586	1.17
	1:30 PM	2:00 PM	505.36	36.25	60.51	33.84	384	0.77
	2:00 PM	2:30 PM	839.84	37.15	61.88	35.11	566	1.13
	2:30 PM	3:00 PM	892.93	38.33	68.24	36.51	696	1.39
	3:00 PM	3:30 PM	707.29	38.55	68.35	33.32	442	0.88
	3:30 PM	4:00 PM	201.77	36.97	59.38	30.46	232	0.46

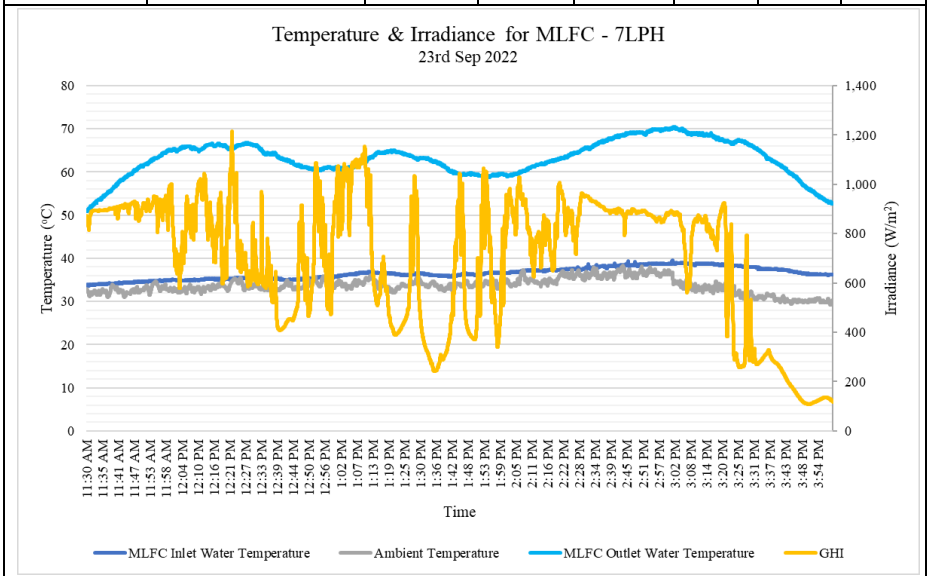

D. Flow Rate 9LPH

Date	Time Interval (30 mins)		GHI (W/m^2)	$T_{MLFC,i}$ (°C)	$T_{MLFC,o}$ (°C)	T_a (°C)	FWY (ml)	FWY (l/h)
09-07	11:30 AM	12:00 PM	702.13	34.00	54.80	33.17	438	0.88
	12:00 PM	12:30 PM	480.22	34.32	56.48	33.01	380	0.76
	12:30 PM	1:00 PM	452.60	34.44	51.91	33.07	300	0.60
	1:00 PM	1:30 PM	507.87	34.99	51.75	33.18	350	0.70
	1:30 PM	2:00 PM	780.26	35.84	55.38	34.67	520	1.04
	2:00 PM	2:30 PM	829.08	36.61	61.33	35.48	530	1.06
	2:30 PM	3:00 PM	807.98	37.49	65.13	36.13	610	1.22
	3:00 PM	3:30 PM	746.14	37.91	65.12	37.18	650	1.30

	3:30 PM	4:00 PM	646.95	38.09	63.05	36.49	494	0.99
	4:00 PM	4:30 PM	277.19	37.13	56.35	32.60	255	0.51

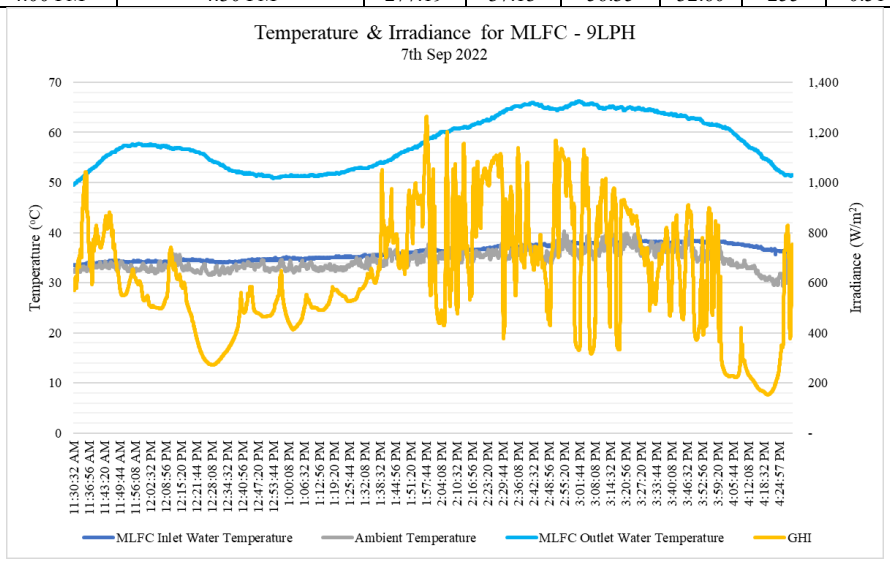

09-09	11:30 AM	12:00 PM	571.19	33.86	48.86	32.38	316	0.63
	12:00 PM	12:30 PM	397.28	34.04	51.62	32.96	310	0.62
	12:30 PM	1:00 PM	524.20	34.62	50.79	34.02	350	0.70
	1:00 PM	1:30 PM	626.30	35.29	54.44	34.22	422	0.84
	1:30 PM	2:00 PM	937.73	36.38	59.39	35.55	664	1.33
	2:00 PM	2:30 PM	824.17	37.60	68.09	35.75	794	1.59
	2:30 PM	3:00 PM	537.19	37.38	63.03	35.10	434	0.87
	3:00 PM	3:30 PM	458.93	37.29	57.01	34.54	350	0.70
	3:30 PM	4:00 PM	538.08	37.72	56.10	34.85	370	0.74
	4:00 PM	4:30 PM	375.60	38.06	56.59	34.84	290	0.58

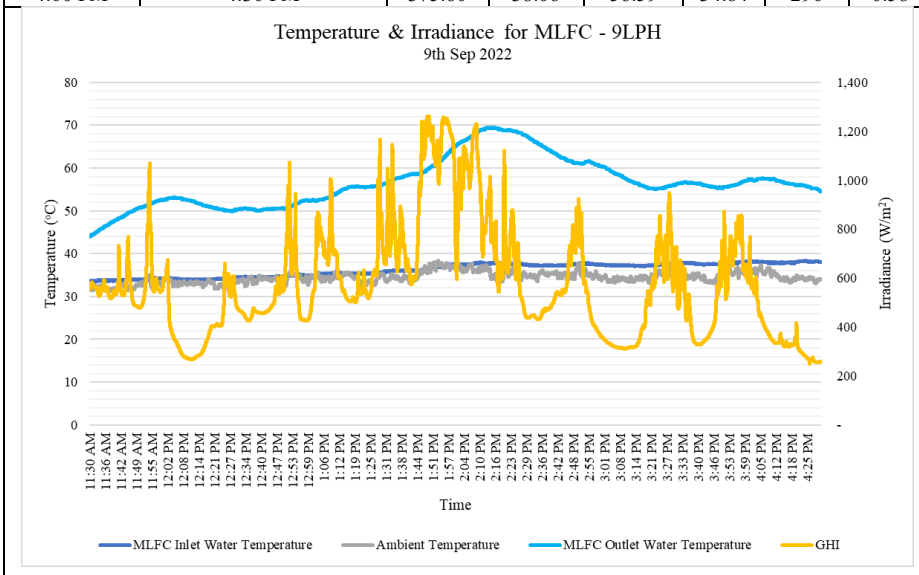

09-15	11:30 AM	12:00 PM	891.39	34.26	54.70	32.57	320	0.64
	12:00 PM	12:30 PM	596.85	34.66	61.01	32.67	440	0.88
	12:30 PM	1:00 PM	939.95	35.64	60.45	33.89	608	1.22
	1:00 PM	1:30 PM	951.77	36.93	67.51	34.52	756	1.51
	1:30 PM	2:00 PM	950.81	37.69	70.29	35.56	772	1.54
	2:00 PM	2:30 PM	798.91	38.06	69.98	34.79	672	1.34
	2:30 PM	3:00 PM	866.76	38.31	67.25	36.42	610	1.22
	3:00 PM	3:30 PM	538.42	38.48	65.54	36.40	480	0.96
	3:30 PM	4:00 PM	570.97	38.29	59.25	36.08	344	0.69
	4:00 PM	4:30 PM	495.77	38.40	58.28	36.28	330	0.66

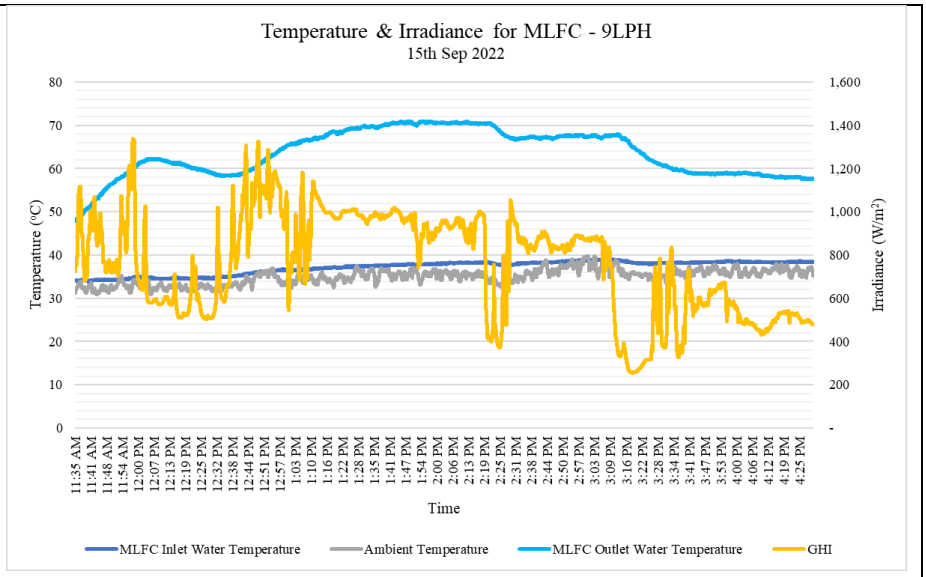
Temperature & Irradiance for MLFC - 9LPH
15th Sep 2022
Temperature (°C)
Irradiance (W/m²)
Time
MLFC Inlet Water Temperature
Ambient Temperature
MLFC Outlet Water Temperature
GHI

APPENDIX III – EXAMPLE OF SIMULATION PROCESS

																			Sum	5.49
14/7/2022	sec	kg/hr	W/m2	oC	K	oC	K	K	K	K	N/m2	N/m2	K	J/s	J/s	W/m2.oC	J/s	J/s	J/s	kg
Time	Interv	Flow Ra	G	Ta	Ta	Tw,i	Tw,i	Tpc	Tb	Tw	Ppc	Pw	Tsky	Q r,pc-s	Q c,pc-	h c,w-p	Q c,w-	Q evap,w-	Q r,w-p	m
11:45:00 AM	1	3	566.59	32.90	305.90	51.50	324.50	305.90	324.50	324.50	4,919.92	12,899.19	299.90	66.56	0.00	2.71	100.70	702.99	224.46	-
11:45:01 AM	1	3	567.18	32.90	305.90	51.50	324.50	306.60	324.79	324.48	5,113.15	12,883.89	299.90	74.61	8.15	2.68	95.64	676.63	216.37	0.00
11:45:02 AM	1	3	567.78	32.90	305.90	51.50	324.50	307.27	325.04	324.45	5,301.86	12,870.49	299.90	82.28	15.85	2.64	90.92	651.48	208.70	0.00
11:45:03 AM	1	3	567.78	32.80	305.80	51.50	324.50	307.89	325.27	324.44	5,485.75	12,858.77	299.80	90.63	24.28	2.61	86.52	627.50	201.43	0.00
11:45:04 AM	1	3	567.78	32.80	305.80	51.50	324.50	308.48	325.47	324.42	5,664.06	12,848.60	299.80	97.54	31.13	2.59	82.42	604.72	194.56	0.00
11:45:05 AM	1	3	568.37	32.90	305.90	51.60	324.60	309.04	325.66	324.41	5,837.08	12,839.84	299.90	103.01	36.44	2.56	78.61	583.05	188.06	0.00
11:45:06 AM	1	3	568.37	32.90	305.90	51.60	324.60	309.57	325.83	324.39	6,005.16	12,832.41	299.90	109.25	42.57	2.53	75.04	562.41	181.89	0.00
11:45:07 AM	1	3	568.97	32.90	305.90	51.60	324.60	310.07	325.98	324.38	6,167.68	12,826.17	299.90	115.16	48.35	2.50	71.72	542.82	176.05	0.00
11:45:08 AM	1	3	568.97	32.80	305.80	51.60	324.60	310.54	326.12	324.38	6,324.59	12,821.03	299.80	121.85	54.96	2.48	68.62	524.25	170.54	0.00
11:45:09 AM	1	3	568.97	32.80	305.80	51.60	324.60	310.98	326.25	324.37	6,475.31	12,816.91	299.80	127.14	60.09	2.46	65.74	506.72	165.34	0.00
11:45:10 AM	1	3	569.56	32.80	305.80	51.60	324.60	311.40	326.37	324.36	6,620.38	12,813.71	299.80	132.16	64.93	2.43	63.06	490.12	160.43	0.00
11:45:11 AM	1	3	569.56	32.80	305.80	51.60	324.60	311.79	326.47	324.36	6,759.86	12,811.36	299.80	136.91	69.49	2.41	60.56	474.43	155.80	0.00
11:45:12 AM	1	3	570.15	32.80	305.80	51.60	324.60	312.16	326.57	324.36	6,893.79	12,809.80	299.80	141.41	73.80	2.39	58.22	459.61	151.43	0.00
11:45:13 AM	1	3	570.15	32.90	305.90	51.60	324.60	312.51	326.65	324.36	7,022.25	12,808.96	299.90	144.59	76.70	2.37	56.05	445.60	147.30	0.00
11:45:14 AM	1	3	570.75	32.80	305.80	51.60	324.60	312.84	326.73	324.36	7,145.93	12,808.79	299.80	149.72	81.71	2.35	54.01	432.33	143.39	0.00
11:45:15 AM	1	3	571.34	32.80	305.80	51.60	324.60	313.16	326.81	324.36	7,263.77	12,809.22	299.80	153.53	85.32	2.33	52.12	419.87	139.72	0.00
11:45:16 AM	1	3	571.34	32.80	305.80	51.60	324.60	313.45	326.87	324.36	7,376.49	12,810.23	299.80	157.14	88.73	2.31	50.35	408.12	136.27	0.00
11:45:17 AM	1	3	571.94	32.90	305.90	51.70	324.70	313.73	326.93	324.36	7,484.22	12,811.75	299.90	159.47	90.79	2.29	48.70	397.05	133.01	0.00
11:45:18 AM	1	3	572.53	32.80	305.80	51.70	324.70	313.99	326.99	324.36	7,587.75	12,813.76	299.80	163.80	95.00	2.27	47.16	386.56	129.92	0.00
11:45:19 AM	1	3	572.53	32.80	305.80	51.70	324.70	314.24	327.04	324.37	7,685.97	12,816.22	299.80	166.85	97.86	2.26	45.72	376.75	127.03	0.00
11:45:20 AM	1	3	573.13	32.80	305.80	51.70	324.70	314.47	327.09	324.37	7,779.67	12,819.09	299.80	169.73	100.56	2.24	44.38	367.52	124.30	0.00
11:45:21 AM	1	3	573.72	32.70	305.70	51.70	324.70	314.69	327.14	324.38	7,869.01	12,822.33	299.70	173.54	104.27	2.23	43.13	358.83	121.74	0.00
11:45:22 AM	1	3	573.72	32.70	305.70	51.70	324.70	314.89	327.18	324.38	7,953.54	12,825.91	299.70	176.10	106.66	2.21	41.97	350.72	119.34	0.00
11:45:23 AM	1	3	573.72	32.70	305.70	51.70	324.70	315.09	327.22	324.39	8,034.06	12,829.82	299.70	178.52	108.91	2.20	40.89	343.10	117.08	0.00
11:45:24 AM	1	3	574.32	32.70	305.70	51.70	324.70	315.27	327.25	324.40	8,110.73	12,834.02	299.70	180.82	111.04	2.19	39.88	335.94	114.96	0.00
11:45:25 AM	1	3	574.32	32.70	305.70	51.70	324.70	315.45	327.28	324.40	8,183.74	12,838.49	299.70	182.99	113.05	2.17	38.93	329.21	112.96	0.00
11:45:26 AM	1	3	574.32	32.70	305.70	51.70	324.70	315.61	327.31	324.41	8,253.22	12,843.22	299.70	185.04	114.95	2.16	38.05	322.89	111.08	0.00